Geothermal Play Fairway Analysis of Low-Temperature Resources for Sedimentary Basin Geothermal Play Types: An Example in the Denver Basin

Estefanny Davalos-Elizondo, Nicole Taverna, Abra Gold, Karthik Menon, and Whitney Trainor-Guitton

National Renewable Energy Laboratory

NREL is a national laboratory of the U.S. Department of Energy
Office of Energy Efficiency & Renewable Energy
Operated by the Alliance for Sustainable Energy, LLC

This report is available at no cost from the National Renewable Energy Laboratory (NREL) at www.nrel.gov/publications.

Contract No. DE-AC36-08GO28308

Technical Report
NREL/TP-5700-91108
September 2024

Geothermal Play Fairway Analysis of Low-Temperature Resources for Sedimentary Basin Geothermal Play Types: An Example in the Denver Basin

Estefanny Davalos-Elizondo, Nicole Taverna, Abra Gold, Karthik Menon, and Whitney Trainor-Guitton

National Renewable Energy Laboratory

Suggested Citation
Davalos-Elizondo, Estefanny, Nicole Taverna, Abra Gold, Karthik Menon, and Whitney Trainor-Guitton. 2024. Geothermal Play Fairway Analysis of Low-Temperature Resources for Sedimentary Basin Geothermal Play Types: An Example in the Denver Basin. Golden, CO: National Renewable Energy Laboratory. NREL/TP-5700-91108.
https://www.nrel.gov/docs/fy24osti/91108.pdf

NREL is a national laboratory of the U.S. Department of Energy
Office of Energy Efficiency & Renewable Energy
Operated by the Alliance for Sustainable Energy, LLC

This report is available at no cost from the National Renewable Energy Laboratory (NREL) at www.nrel.gov/publications.

Contract No. DE-AC36-08GO28308

Technical Report
NREL/TP-5700-91108
September 2024

National Renewable Energy Laboratory
15013 Denver West Parkway
Golden, CO 80401
303-275-3000 • www.nrel.gov

NOTICE

This work was authored by the National Renewable Energy Laboratory, operated by Alliance for Sustainable Energy, LLC, for the U.S. Department of Energy (DOE) under Contract No. DE-AC36-08GO28308. Funding provided by the U.S. Department of Energy Office of Energy Efficiency and Renewable Energy Geothermal Technologies Office. The views expressed herein do not necessarily represent the views of the DOE or the U.S. Government.

Cover Photos by Dennis Schroeder: (clockwise, left to right) NREL 51934, NREL 45897, NREL 42160, NREL 45891, NREL 48097, NREL 46526.

Acknowledgments

This work was authored by the National Renewable Energy Laboratory, operated by Alliance for Sustainable Energy, LLC, for the U.S. Department of Energy (DOE) under Contract No. DE-AC36-08GO28308. Funding provided by the U.S. Department of Energy Office of Energy Efficiency and Renewable Energy Geothermal Technologies Office. The views expressed herein do not necessarily represent the views of the DOE or the U.S. Government.

List of Acronyms

BHT	bottom-hole temperature
CHP	combined heat and power
CRS	common risk segment
DOE	U.S. Department of Energy
EGS	enhanced geothermal systems
GDR	Geothermal Data Repository
GeoRePORT	Geothermal Resource Portfolio Optimization and Reporting Tool
GDU	geothermal direct use
GPT	geothermal play type
GTO	Geothermal Technologies Office
IDW	inverse distance weighted (or weighting)
LCOH	levelized cost of heat
NREL	National Renewable Energy Laboratory
PFA	play fairway analysis
SBGPT	sedimentary basin geothermal play type
SMU	Southern Methodist University
USGS	U.S. Geological Survey

Executive Summary

This project is part of a nationwide effort to highlight the advantages of incorporating low-temperature geothermal resource evaluation into the implementation of combined heat and power and geothermal direct use technologies (e.g., space heating and/or cooling). The initiative aims to hasten the nation's decarbonization process by exploring the potential for using low-temperature geothermal resources (<150°C) in selected sedimentary basins that have several population centers.

The play fairway analysis techniques were modified from earlier studies of sedimentary basin geothermal play types (SBGPTs) that assessed the viability of low-temperature resources. The decision-making process for leveraging low-temperature geothermal resources for geothermal direct use and combined heat and power applications is complex and considers a variety of factors, including geological, economic, and risk criteria. This study covers workflows, relevant datasets, Python code, and both common and composite maps used to create low-temperature geothermal resource favorability maps for the Denver Basin, which extends across Colorado, Nebraska, and Wyoming.

The replication of these methodologies in other SBGPTs can be used to evaluate the potential for low-temperature resources. The proposed geothermal play fairway analysis approach for low-temperature geothermal resources includes (1) identifying available relevant data and grouping datasets into play fairway analysis criteria (e.g., geological, economic, and risk criteria), (2) analyzing data gaps to enable future focalized exploration, (3) performing uncertainty quantification, (4) weighting relevant data, and (5) developing favorability and common risk maps for low-temperature geothermal resources to identify potential locations for focused data collection. This project will facilitate future deployment of combined heat and power and geothermal direct uses by providing data, tools, and a workflow applicable to low-temperature geothermal resources in sedimentary basins.

Table of Contents

List of Figures

List of Tables

1 Introduction

A sedimentary basin geothermal play type (SBGPT) is shaped by its historical evolution and the present tectonic and geological conditions (Davalos-Elizondo et al. 2023). Play fairway analysis (PFA) workflows and associated data should be customized for each type of geothermal play. In classifying SBGPTs, Davalos-Elizondo et al. (2023) utilized the classification proposed by Coleman and Cahan (2012) based on a straightforward geological framework (Figure 1): (1) intracratonic basins that occur within craton boundaries, (2) pericratonic basins located near or attached to craton edges, (3) intercratonic basins situated between cratons, extending onto oceanic crust, and (4) oceanic basins that developed separately from cratons, primarily on oceanic crust. For a more detailed classification scheme, refer to Davalos-Elizondo et al. (2023).

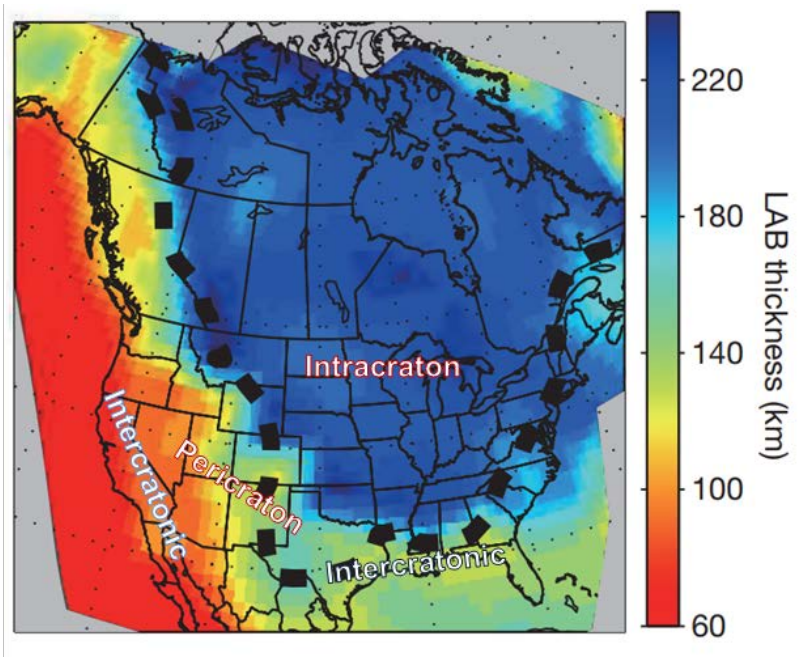

Figure 1. The current thickness of the lithospheric-asthenospheric boundary beneath the North American continent is illustrated; the thick, black dashed line marks the edges of the craton.

Image from Yuan and Romanowicz (2010)

This study focuses on applying a geothermal play fairway analysis (PFA) methodology from the hydrocarbon sector to low-temperature resources in SBGPTs, using the Denver Basin as a case study. The framework adopted from the hydrocarbon industry details crucial components of a sedimentary basin, correlates them with geological factors, and identifies relevant datasets that expand the geological criteria to include economic and risk criteria, essential for decision-making in low-temperature geothermal applications. The PFA method pinpoints areas that are promising for geothermal resources while avoiding larger regions with greater chances of failure, thus reducing risk in the resource identification process. The proposed workflow is informed by the *Geothermal Play Fairway Analysis Best Practices* report (Pauling et al. 2023) and the study assessing low-temperature geothermal play types (Davalos-Elizondo et al. 2023), which outlines a comprehensive geothermal PFA methodology (Figure 2).

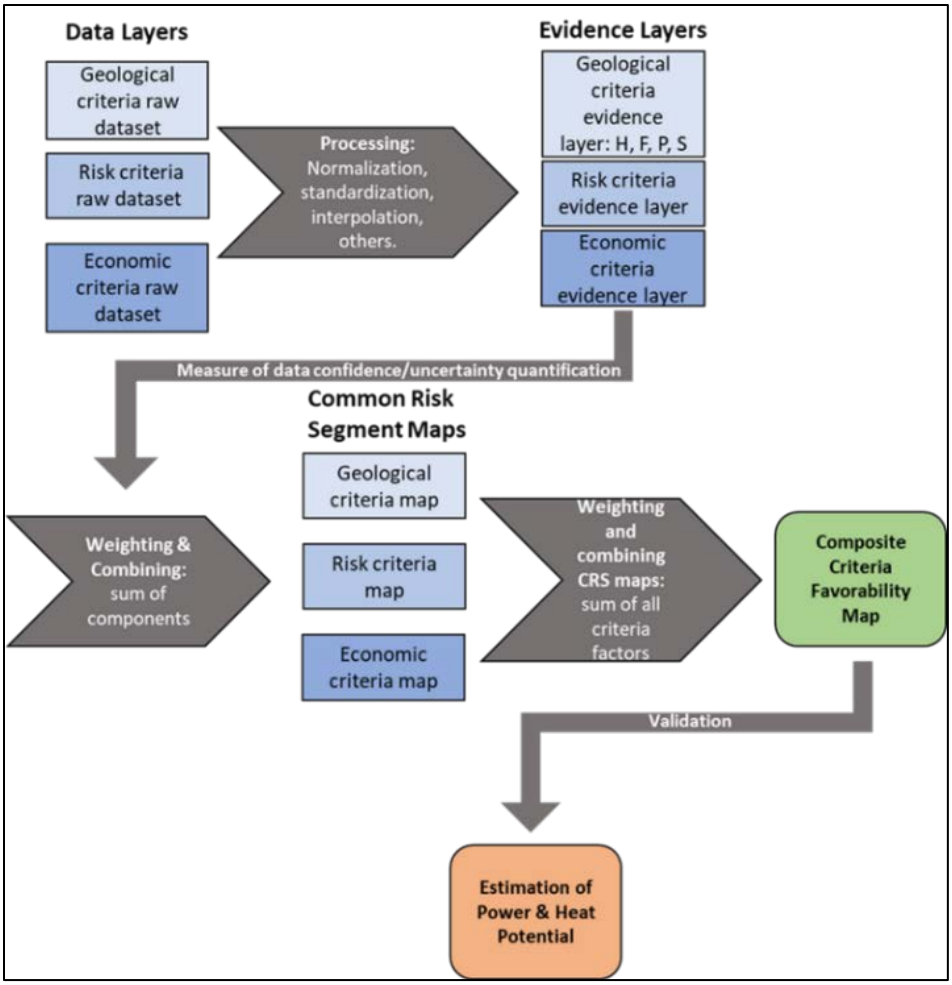

Figure 2. Flowchart for a generalized methodology for low-temperature assessment resources.

Modified from Pauling et al. (2023) by Davalos-Elizondo et al. (2023).

Sedimentary basins typically consist of various layers of highly porous rocks and may present increased secondary permeability from fractures formed by the influence of the stress conditions in the geological history of the basin. Fluids suitable for low-temperature geothermal applications (<150°C) gather in these naturally porous and fractured rocks located deep underground. Nearly half of the United States is situated over sedimentary basins that remain largely unexplored for their low-temperature geothermal potential (U.S. Geological Survey [USGS] 2022). Additionally, sedimentary basins linked to prolific oil and gas production present a valuable opportunity to leverage existing data, technologies, and abandoned petroleum sector wells for repurposing/retrofitting to enhance the development of geothermal resources (Johnston et al. 2020).

Hydrothermal systems primarily influenced by conduction in sedimentary basins are typically found in deep aquifers exhibiting a nearly normal geothermal gradient (Moeck 2014). The variations in porosity and permeability are determined by factors such as lithology, faulting, diagenetic processes, and stress fields (Wolfgramm et al. 2009; Hartmann, Beaumont, and Coalson 2000), all of which are significantly influenced by geological evolution, subsidence rates, and active tectonics. Past studies on geothermal resources in sedimentary formations have

highlighted the importance of either high porosity/high permeability (~100 millidarcy [mD]) for efficient convection (Augustine 2014) or high porosity/low permeability at higher temperature gradients, typically found below 3 km (Moeck 2014).

It is crucial to conduct additional research to assess the potential of low-temperature geothermal resources found in the permeable and porous rocks typical of SBGPTs. Past research has concentrated on fewer than 15 sedimentary basins (Figure 3, Porro et al. 2012), which possess high- to moderate-temperature power generation potential.

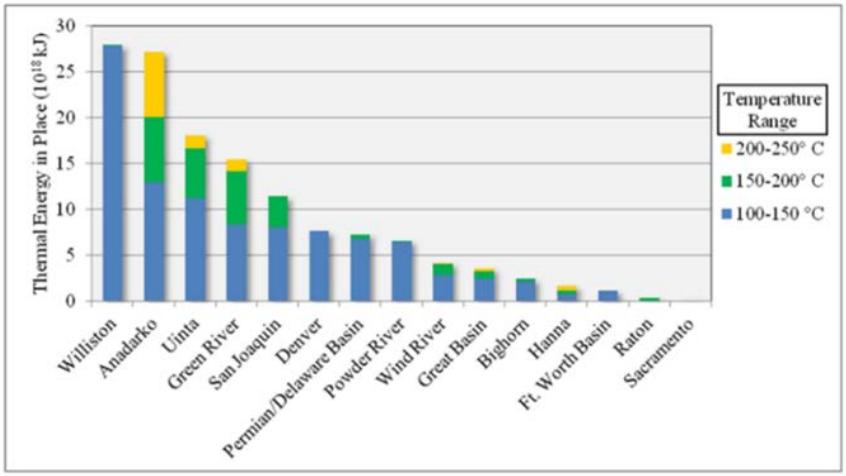

Figure 3. Total thermal energy in place for 15 selected sedimentary basins of the U.S.

From Porro et al. (2012)

The main controls in SBGPTs (as shown in Table 1) include heat flow (normal or anomalous), heat sources (magmatic or radiogenic), the chemistry and circulating geothermal fluids (whether natural or injected), the shape of the basin, faults and fractures, stress conditions, permeability and porosity, and stratigraphic sequences, storage properties (both natural and artificial), and sealing mechanisms (refer to Table 1). These features set SBGPTs apart from hydrocarbon play systems, which are defined by their source rock, reservoir traps, and sealing layers (Doughty et al. 2018). SBGTPs and hydrocarbon play systems can overlap where production fluids from petroleum sector wells exhibit elevated temperatures, and fault intersections are numerous. In exploring hydrothermal systems, Pauling et al. (2023) suggested four key elements for different geothermal play types:

1. Heat (H)
2. Accessible fluids (F)
3. Permeability/porosity (P)
4. Caprock or seal (S) (may or may not always be a present or essential component).

Table 1. Geothermal Main Controls of SBGPT Shaped by the Formation and Evolution History and/or the Present Time Geological and Tectonic Settings

H, F, P, and S denote available heat, accessible fluids, permeability, and caprock or seal, respectively

Geothermal Key Controls	Formation and Evolution	Present Time	Related PFA "Critical Component"
Heat Flow		x	H
Lithology/ Stratigraphy	x		H, F, P, S
Fluid Chemistry	x		F, S
Fluid Dynamics		x	F, S
Basin Geometry	x	x	P
Faults and Fractures	x	x	P
Stress State		x	P
Porosity	x	x	P

Identifying regions with low-temperature geothermal potential in SBGPTs involves a multicriteria geospatial decision-making process. We proposed three key criteria for assessing low-temperature resources (see Figure 2):

- Geologic criteria (e.g., heat availability, fluid accessibility, permeability, and sealing)
- Economic criteria (e.g., population density, infrastructure, demand for heating and cooling, and the levelized cost of heat)
- Risk criteria (e.g., exclusion environmental zones and areas prone to natural disasters).

We established a classification of the Denver Basin geothermal play type as a foreland basin to define our work's scope. The modified PFA workflow overlays multiple criteria data described above that facilitate the identification of regions with resource potential and feasibility for development.

To develop an assessment workflow, the following steps were taken:

1. Identify relevant and available data
2. Evaluate uncertainty for the heat component, as these data have greater uncertainty relative to other data

3. Conduct a gap analysis with the Geothermal Resource Portfolio Optimization and Reporting Tool (GeoRePORT) to inform lack of relevant data
4. Develop a Python library and script to integrate various available data into a PFA based on geological, economic, and risk criteria
5. Group and weight relevant datasets into PFA criteria
6. Create favorability maps to indicate regions suitable for combined heat and power (CHP) and geothermal direct use (GDU) technologies to conduct a more detail exploration assessment and collect new data.

The development of a Python library called "geoPFA" by the National Renewable Energy Laboratory (NREL) in this work facilitated the generation of common and composite maps (Section 5). The Python geoPFA library will be released as an open-source tool once sufficiently refined. QGIS, an open-source geographic information system produced by OSGeo, was also used in addition to the geoPFA library to combine and process (e.g., transform, standardize, interpolate) various geographic raw datasets related to geological, economic, and risk factors.

2 Background

The Denver Basin is a geothermal sedimentary foreland basin located on the eastern side of the Rocky Mountain orogenic belt (Figure 4) within a pericratonic area. Foreland basins, which are situated between an orogenic belt and a craton, are defined by their thick sedimentary layers and asymmetric structures. They arise from the weight of both the thickened crust and sediment accumulation, leading to downward bending of the lithosphere and the development of zones characterized by extension and normal faulting. The creation of these basins is influenced by factors such as horizontal compression, slab pull, lateral push from the asthenosphere, and the delamination of the retreating mantle lithosphere, while the rigidity of tectonic plates significantly affects their geometry and drainage patterns.

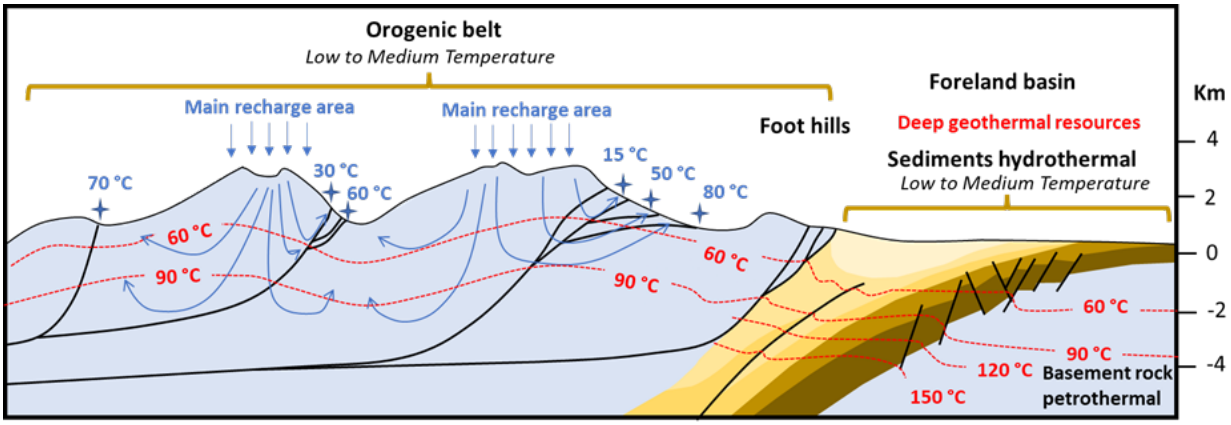

Figure 4. Orogenic Belt Geothermal Play Type and related SBGPT foreland basin.

Modified from Moeck (2014) by Davalos-Elizondo et al. (2023).

The Denver Basin has an asymmetrical structure, with presumed granite basement rocks lying beneath its sedimentary layers. It deepens significantly toward the Front Range to the west, reaching depths of about 3.5 km, while the eastern section measures approximately 1.6 km deep (Dixon 2002). The thickest sedimentary rocks are found along a north-south axis that generally coincides with the cities of Denver and Cheyenne (Fishman 2005). Spanning more than 70,000 mi^2, (180,000 km^2) the basin is mainly located in eastern Colorado, with smaller areas in southeastern Wyoming and southwestern Nebraska (Higley and Cox 2007). The basin is well known for prolific petroleum production, hosting thousands of wells for oil and gas extraction across various reservoir formations.

The stratigraphic column (Figure 5) displays the ages and designations of formations, highlighting those associated with oil and gas production and hydrocarbon source rocks (Fishman 2005). The Precambrian rocks, located at depths of up to 13,000 ft (4,000 m) beneath the Denver Basin, are approximately 1.6 billion years old (Weimer and Sonnenberg 1996). Around 70% of the overlying sedimentary rock thickness consists of Cretaceous-aged sandstones, shales, and limestones (144 to 67 million years old; Hemborg 1993a–d). Prominent ridges west of the basin axis consist of east-dipping layers, shaped by the Laramide orogeny, which took place approximately 67.5 to 50 million years ago (Tweto 1975). This key tectonic event folded the initially flat rocks, established the basin's current structure, and led to the uplift of the Rocky Mountains, with some areas, like Mount Blue Sky (formerly Mount Evans),

experiencing up to 25,600 ft (7,800 m) of uplift (Bryant and Naeser 1980). Between 1,000 ft (300 m) and 6,500 ft (1,910 m) of Paleogene and older layers were eroded in the central Front Range (Higley and Schmoker 1989; L.C. Price, oral commun. 1991), leaving Paleogene-Neogene aged rocks at the surface of the Denver Basin, which represent sediment that was eroded from the Rocky Mountains and redeposited in the subsiding basin.

Porro et al. (2012) suggested that the Denver Basin has reservoir temperatures around 100°C–150°C from a depth of 2.5 to 4 km (Figure 6). Additionally, Porro et al. (2012) identified thermal recovery factors in the Denver Basin, such as low vertical permeability, >20% net/gross interval carbonate and sandstone for horizontal permeability, moderate to low flow volume, and reservoir compartmentalization. Anderson (2013) reported average porosity and permeability values in two formations of the Denver Basin: Lyons Sandstone with an average porosity of 15% and permeability of 45 mD, and Ingleside formation with an average porosity of 19% and permeability 100 mD. This information was included in the GeoRePORT for the Gap Analysis in Section 4.

Anomalous bottom-hole temperatures (BHTs) in the western Denver Basin have been observed since the 1980s, according to exploration reports related to the Wattenberg gas field overlaying the observed thermal anomaly (Meyer and McGee 1985; Higley and Gautier 1988). This thermal anomaly has been attributed by Fishman (2005) to plutonic intrusions, similar to the intrusions beneath fault structures of the Colorado mineral belt in basement rock in the northern Denver Basin (Weimer and Sonnenberg 1996; Myer and McGee 1985); however, there is no evidence to support this assertion. The wrench fault structures that vertically cut through the Wattenberg field could be facilitating deep thermal recharge of fluid (Figure 7). This vertical wrench fault system may also intersect deep diffuse reverse faults, as indicated in a seismic cross section of the Rocky Flats, released by Weimer and Davis (1996). A recent study by Mibei et al. (2024) found that BHTs in the Wattenberg region of the Denver Basin are approximately 160°C, corresponding to a thermal gradient of 62°C/km. Additionally, reservoir temperature estimates indicate values exceeding 200°C below depths of 3 km.

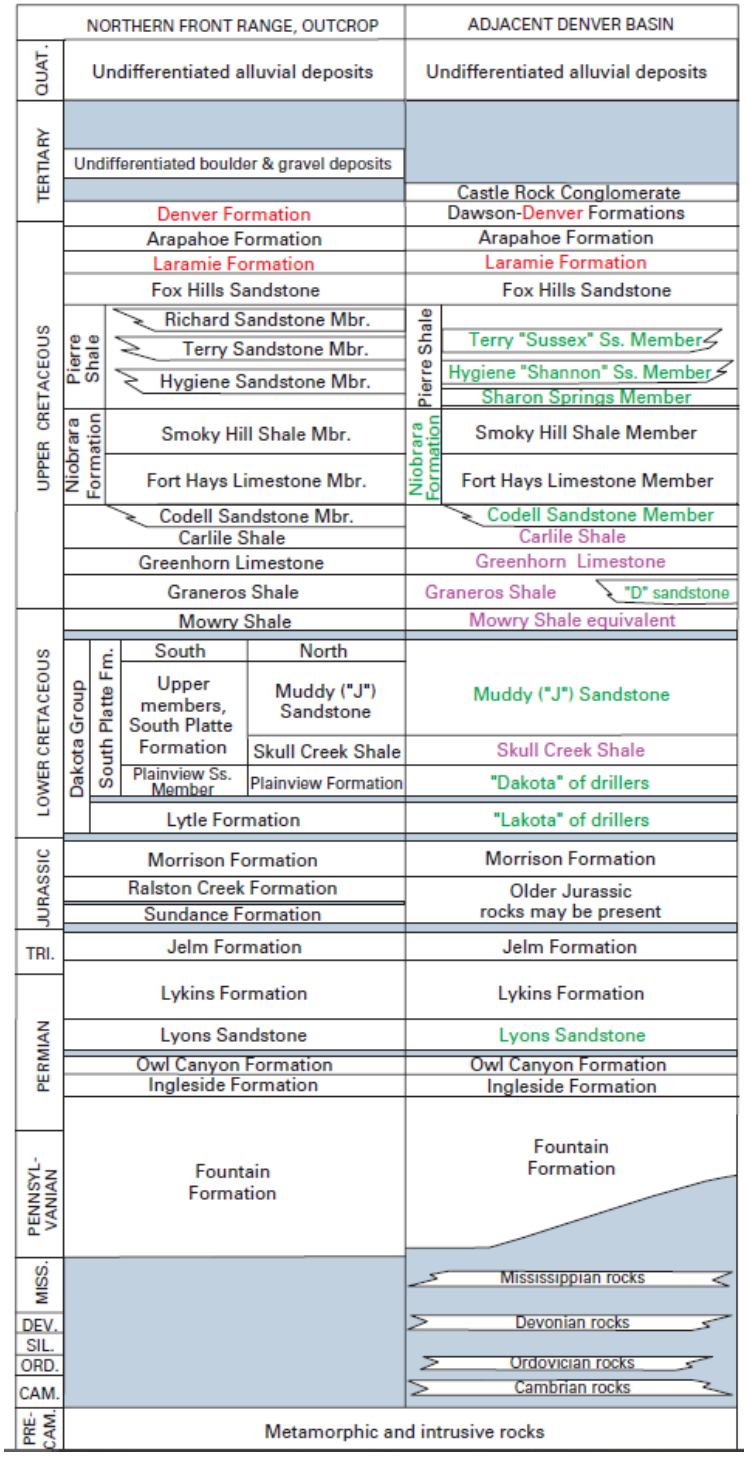

Figure 5. The stratigraphic section of rock units nearby Denver Basin, with light blue areas indicating periods of erosion or nondeposition. Formations that generate oil and/or gas are highlighted in green text, while potential coal-bed methane formations are noted in red. Hydrocarbon source rocks are indicated by purple text.

This information is derived from Hoyt (1963), Momper (1963), Irwin (1977), Sonnenberg and Weimer (1981), Higley and Schmoker (1989), Hjellming (1993), MacLachlan et al. (1996), and Fishman (2005).

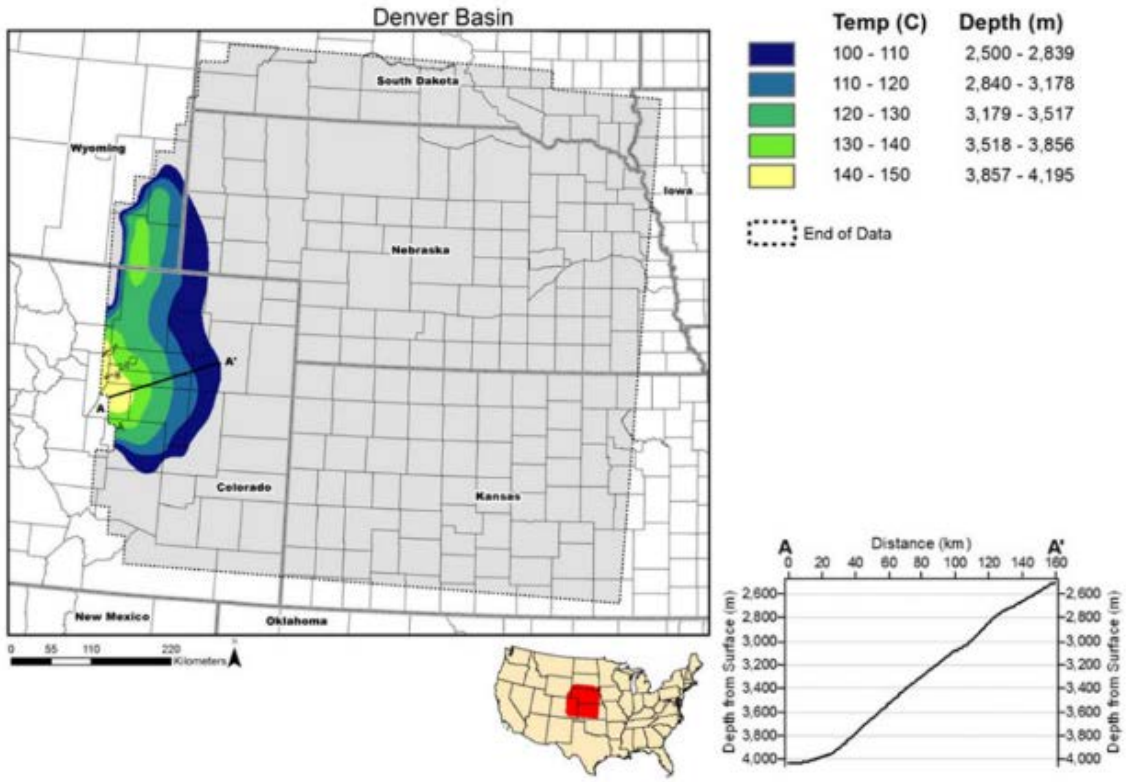

Figure 6. Denver Basin map showing regions with temperatures greater than 100°C, delineated by 10°C increments.

From Porro et al. (2012)

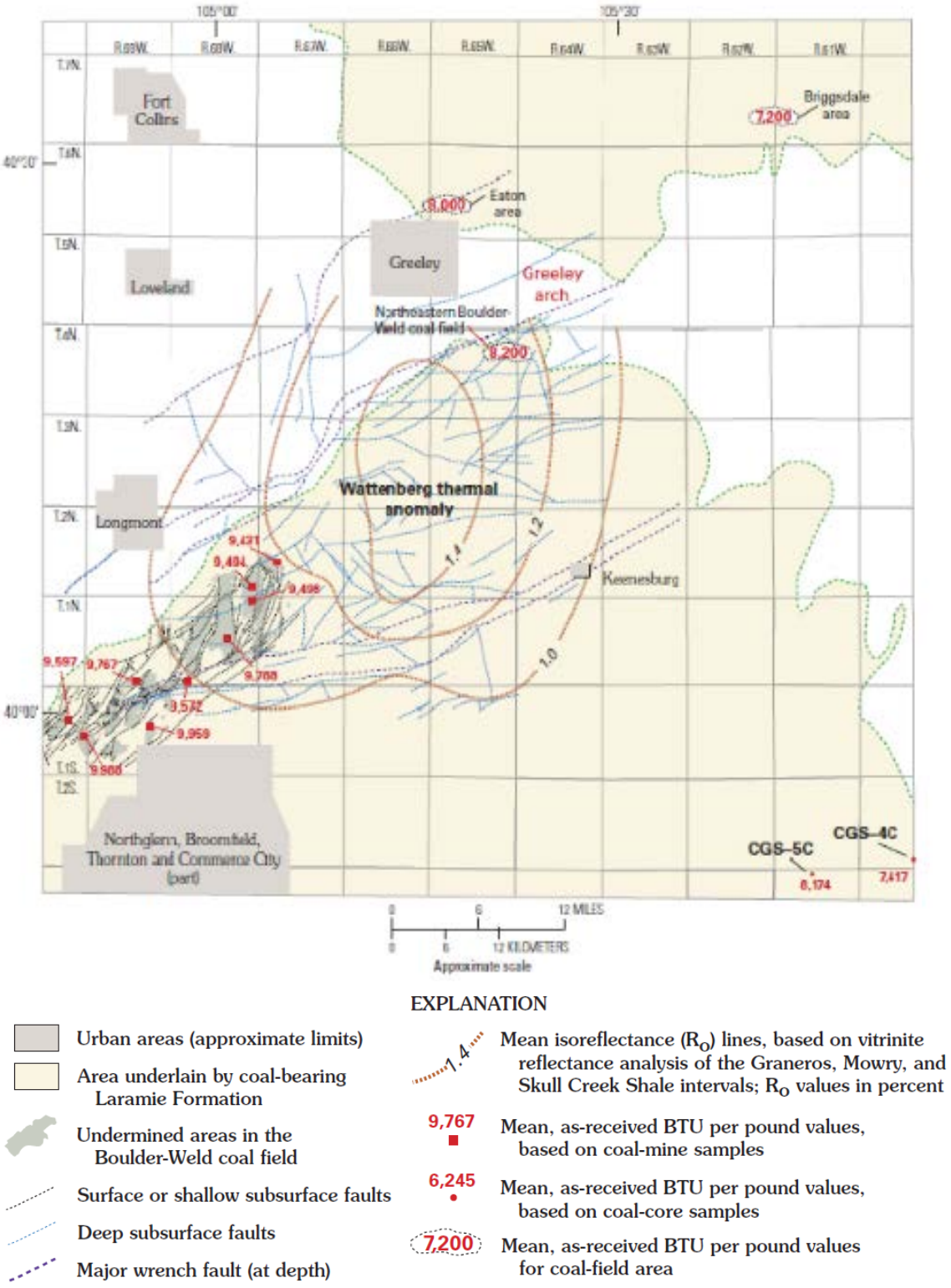

Figure 7. Regional structural map. These thrust faults and associated buried structures could be influencing the thermal anomaly observed in the Wattenberg area.

From Fishman (2005)

3 Relevant Data

Determining optimal locations for low-temperature geothermal heating applications and GDU involves the consideration of multiple factors, such as geological, economic, and risk criteria. Combining these criteria into favorability maps suggests areas for low-temperature geothermal resource utilization.

The relevant data for this PFA workflow are outlined in Table 2. Data applicability may vary depending on geothermal play type (GPT), availability, and new data collection.

Table 2. Relevant Data Suggested for PFA of Low-Temperature Geothermal Resources in the Denver Basin

GPT and Combination Method	Criteria		Component	Data
Pericratonic Foreland Basin Modified Voter-Veto	Geological		Heat	Bottom-Hole Temperatures
				Gradient Temperatures
				Thermal Conductivity
				Heat Flow
			Accessible Fluid	Hot Springs
				Coproduction Water (*BBL) per Year
				Groundwater Wells
			Permeability	Faults and Shear Zone
				Earthquake Data
	Economic		Demand	Population
				Infrastructure
				Heat and Cooling Demand
			Site accessibility	Roads
	Risk	Safety	Natural Disaster	Flood Areas
		Exclusion Areas	Environmental Protected Areas	National Park Services, Conservation Lands, Habitats, etc.

* BBL: stands for barrel, a unit of volume used to measure crude oil and other petroleum products defined as exactly 42 US gallons, approximately 159 liters, or 35 imperial gallons.

3.1 Geological Criteria

We assessed the suitability of sites based on geological criteria related to geothermal resources available in the Denver Basin. One of the project's aims was to use geological and thermophysical data to identify low-temperature geothermal resource potential. The three geological components we used to characterize the Denver Basin were heat, accessible fluid, and permeability (Table 2).

We collected BHT datasets and thermal conductivity data for the heat component, which allowed us to estimate geothermal gradient temperatures and heat flow. This research also utilized hot springs, groundwater wells, and coproduction from oil and gas wells to evaluate the accessible fluid component. For the permeability component, we focused solely on secondary permeability: specifically, faults, shear zones, and earthquake data. These data were used to substitute porosity datasets, which were unavailable, in the Denver Basin.

3.1.1 Heat Component Analysis

According to Spicer (1964) and Whealton (2015, 2016), the analysis of BHTs in oil and gas wells, despite uncertainty in dataset accuracy, is essential for assessing geothermal resources. Our assessment aims to estimate temperature gradients and heat flows across the Denver Basin, pinpointing areas with anomalous temperatures that may host low-temperature geothermal resources. Decades of oil and gas production have provided extensive temperature data, particularly in the western and central parts of the Denver Basin. These data form the foundation of our evaluation, because BHT datasets are indicators of subsurface temperature trends.

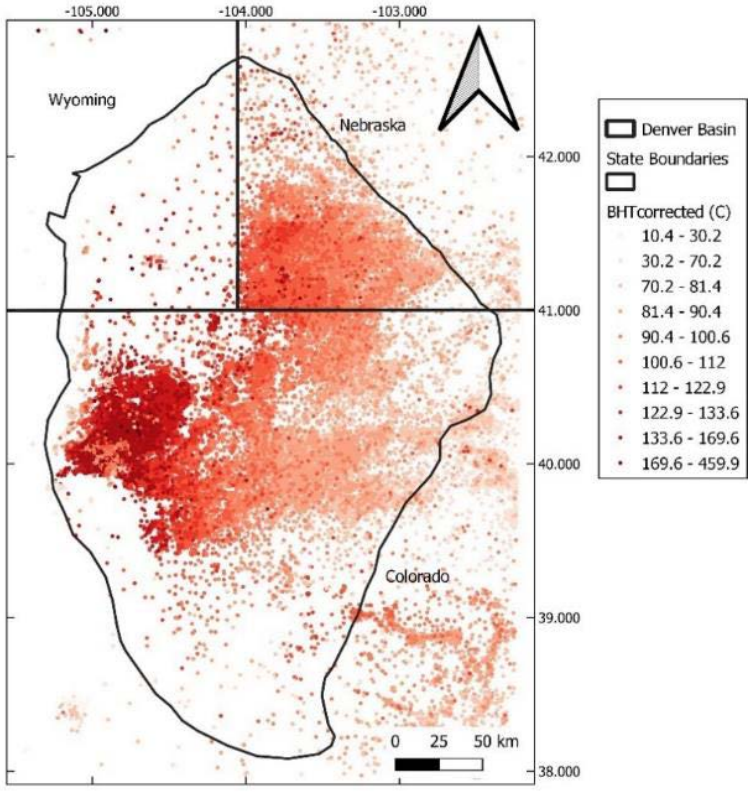

Figure 8. Bottom-hole temperatures (BHTs) of oil and gas wells from three different datasets: Southern Methodist University (SMU), Association of American State Geologists (AASG), and Colorado Geological Survey (CGS). BHTs were corrected by a Förster equation tailored to the Denver Basin.

All report figures by NREL, unless otherwise noted.

We identified three datasets of BHTs in our study area (Figure 8): (1) Southern Methodist University (SMU); (2) Association of American State Geologists (AASG); and (3) Colorado Geological Survey (CGS). BHT data from Wyoming, Nebraska, and Colorado were gathered and narrowed down to the Denver Basin region. Initially, data from all three sources were combined into a comprehensive dataset. Our uncertainty analysis (see Section 3.1.2) of the combined data illuminated that using multiple diverse datasets introduced variance and additional uncertainty into the results. Therefore, the primary dataset utilized was the AASG dataset for Colorado and Nebraska. The SMU data were included as the secondary dataset for Wyoming, where the AASG data points were sparse. Using only the primary and secondary datasets improved the visible trends in temperature gradient interpolations and made the uncertainty modeling of the temperature gradient data more meaningful (see Section 3.1.2).

Although there is a wealth of BHT data, temperature alterations from drilling (i.e., mud circulation in the wellbore inducing artificial lowering BHTs) and inaccuracies in data collection can lead to distorted measurements. For example, BHT data obtained from a survey a week after drilling may show a spuriously low reading due to mud circulation, in contrast to readings taken from a thermally stable shut-in well. Various correction techniques have been developed to approximate equilibrium conditions for BHTs within sedimentary basins (e.g., Harrison et al. 1983; Förster et al. 1996; Blackwell and Richards, 2004).

This project corrected BHT data points from the SMU, AASG, and CGS datasets. A generalized correction scheme was required. If a prior BHT correction scheme had been applied to the constituent datasets, that correction was reversed to obtain the original uncorrected BHT data points (i.e., AASG). We used the Förster correction to unify the datasets. The Förster correction has been suggested as the best correction scheme tailored for the Denver Basin based on equilibrium data by Crowell, Ochsner, and Gosnold (2012):

$$Tcf = 0.0124\ x + 7.8825 \quad (1)$$

where Tcf is the temperature correction factor, and x is the depth at which the BHT measurement was reported. It is important to mention that this correction formula is only suitable for the Denver Basin and potentially other basins that have comparable stratigraphy (Crowell, Ochsner, and Gosnold 2012). For this reason, the Förster equation was applied to the Wyoming portion of the Denver Basin to the limited BHT data points in that region, as the stratigraphy is not drastically different from the Colorado and Nebraska portions (for which the Förster correction scheme had been applied previously in Crowell, Ochsner, and Gosnold [2012]). The BHT data from SMU, AASGS and CGS were corrected with the Förster equilibrium factor. Overall, the AASG dataset combined with SMU data on Wyoming offered a more comprehensive evaluation of BHTs, reducing uncertainty (see Section 3.1.2) and navigating potential errors in the datasets via a tailored Förster correction scheme for the Denver Basin (Figure 9). This partial integration of AASG and SMU BHT data will be available in the Geothermal Data Repository.

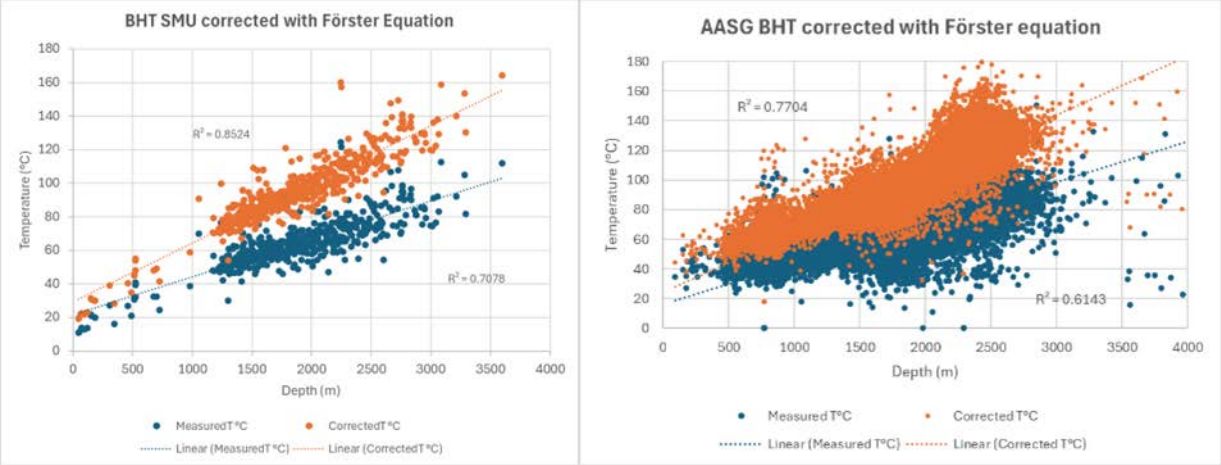

Figure 9. Bottom-hole temperature data of AASG and SMU corrected with the Förster equilibrium factor suggested by Crowell, Ochsner, and Gosnold (2012) in the Denver Basin

Heat transfer is a crucial aspect in locating geothermal resources because the heat discharge data associated with the Earth's heat flow serves as a key indicator of resource potential within a region or nation (Blackwell, Negraru, and Richards 2007). The geothermal gradient is significant in assessing heat flow. Consequently, the integrated and corrected AASG and (partial) SMU BHT dataset was used to estimate a temperature-depth profile based on the equilibrium model developed by Crowell, Ochsner, and Gosnold (2012). We calculated the geothermal gradient (Figure 10) using the following equation:

$$dT/dZ = [\text{corrected BHT data point} - \text{Surface temperature}] / \text{depth} \quad (2)$$

where dT/dZ is the geothermal gradient (°C/km).

Understanding the thermal conductivity of numerous boreholes was crucial for estimating heat flow and temperature distribution at depth. This process entailed categorizing lithologic units, determining unit thicknesses, and assigning thermal conductivities from the surface to the basement for each borehole with BHT data included in the analysis. We referenced the lithology charts and thermal conductivity values from the SMU data provided by the American Association of Petroleum Geologists Correlation of Stratigraphic Units of North America in the Denver Basin. To accomplish this, we conducted a nearest-neighbor inverse distance weighted (IDW) interpolation, which estimated the thermal conductivity distribution across the basin (Figure 11). The southwest Denver Basin displayed higher thermal conductivities while the northeast region maintained a nearly constant thermal conductivity of 1.6 W/m/K.

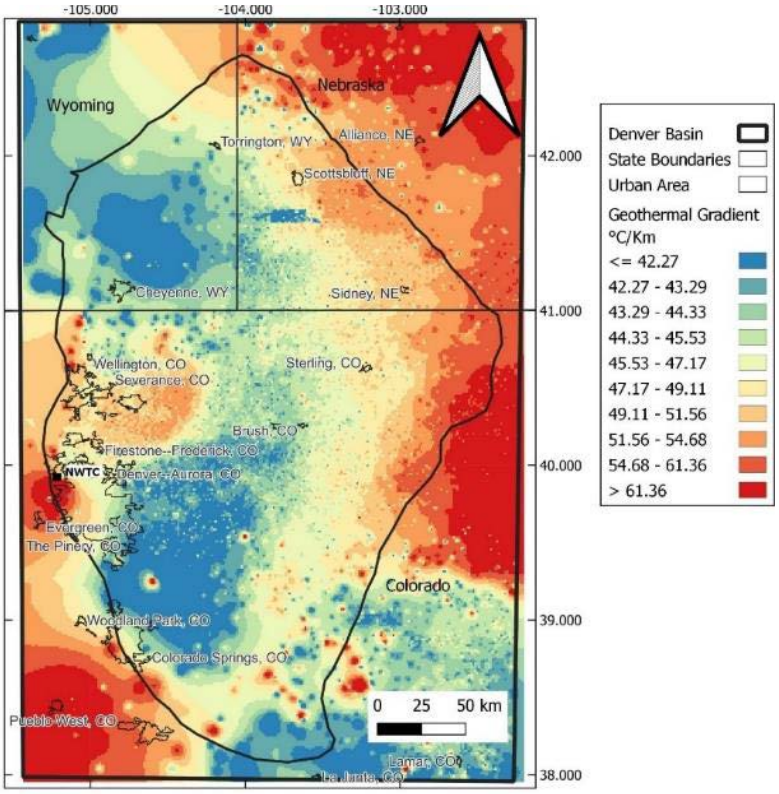

Figure 10. Geothermal gradient estimated from BHT data at 1 km from AASG dataset and SMU data in Wyoming. The average gradient temperature in the Denver Basin ranges around 42–61°C/km.

NWTC: National Wind Technology Center (NREL)

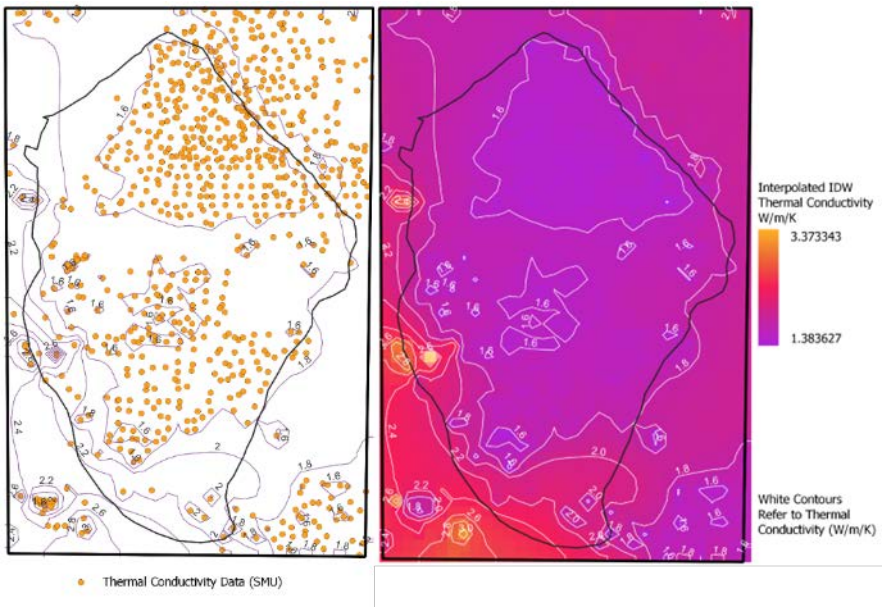

Figure 11. Nearest-neighbor IDW interpolation of thermal conductivities from SMU dataset of rock across the Denver Basin

We calculated heat flow (mW/m^2; Figure 12) using the previous estimation of geothermal gradient (Eq. 2; Figure 10). The BHT dataset created in this study (by combining AASG BHT data in Nebraska and Colorado with partial SMU BHT data from Wyoming) is required to estimate a geothermal gradient in conjunction with the lithology-dependent thermal conductivity. The following equation was used to estimate the heat flow:

$$Q = dT/dz * K \quad (3)$$

where Q is the heat flow (mW/m^2), dT/dz is the geothermal gradient (°C/km), and K is thermal conductivity (W/m/K).

The one-dimensional heat flow model contains the following input assumptions and simplifications:

1. The model assumes that the generation of radiogenic heat is consistent and evenly spread throughout sedimentary rocks.
2. Input data were spatially interpolated to estimate the average and standard error of the average data values for the resource, producing maps depicting thermal quality in a GeoTIFF format (Figure 12).

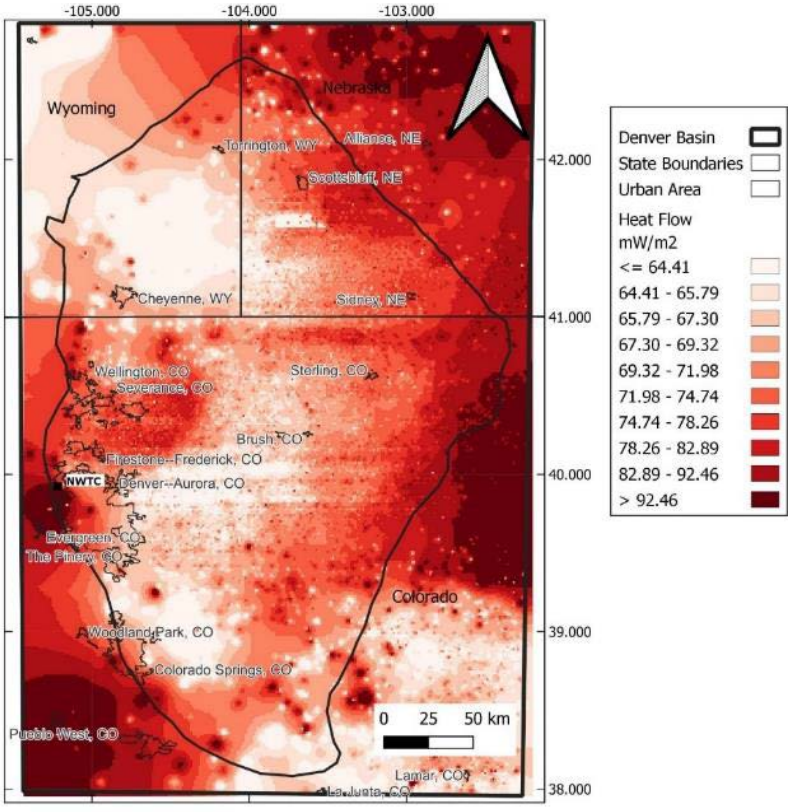

Figure 12. IDW interpolated heat flow map of the Denver Basin. Interpolation calculated from geothermal gradient and thermal conductivities from SMU data. The heat flow map shows an average around 64–92 mW/m^2.

NWTC: National Wind Technology Center (NREL)

In the Denver Basin, BHT data are concentrated in regions containing oil and gas reserves, such as central Colorado. BHT data are sparse in less explored areas, such as southeastern Wyoming and southern Colorado. Sparsity of data in areas of the basin necessitates interpolation algorithms that can accurately predict nonexistent data points in both sparse and clustered datasets. However, the interpolation process could add uncertainty to the results, as discussed in Section 3.1.2 regarding uncertainty in temperature gradient measurements. The spatial IDW interpolation method predicts cell values by averaging the values of surrounding sample data points, with those closer to the center of the cell receiving more weight in the calculation. However, different interpolation methods were also applied for the geoPFA Python Library, as detailed in Section 5.

3.1.2 Uncertainty Analysis: Heat Component

Quantifying the uncertainty in temperature gradient measurements across the Denver Basin is vital for informed decision-making, particularly in locating where new information is needed or new wells should be drilled. There exist multiple uncertainty quantification methods and variogram methods, such as simple kriging (Krige 1951), ordinary kriging or co-kriging (Isaac and Srivastava 1989) are often easy to implement and can be used to "smooth" an uncertainty map, as it tends to overestimate the small values and underestimate the large values (Yamamoto 2005). Sequential Gaussian simulation (SGS; Deutsch and Journel 1998) is another method that utilizes kriging in its workflow (described below). The major advantages SGS has over kriging methods are that the uncertainty profile is not as smooth, and SGS is a relatively simple and flexible method. The workflow is as follows (Deutsch and Journel 1998):

1. Choose a fixed domain where the data lies and convert them all into Gaussian space using the standard normal distribution.
2. Obtain a random path to visit all nodes within the simulation.
3. At each location, use nearby data (within a given radius) and previously simulated values to (1) estimate the conditional distribution at that node, and (2) perform a Monte Carlo simulation to sample a single value from this distribution. The value is then assigned to the node.
4. The above steps are repeated until each node is visited.
5. The simulated data is then transformed back into its original space.

To simplify the process, we made use of AASG dataset and SMU data (particularly from Wyoming, where there is a gap in the AASG dataset), for temperature gradients, and partitioned it by depths: 0–1,000 m, 1,000–1,500 m, 1,500–2,000 m, 2,000–2,500 m, and 2,500–3,000 m. SGS with ordinary kriging (which estimates the mean locally) was used to generate 35 realizations for each depth, with each realization containing a grid of 200 × 200 nodes, simulated using the open-source Python package geostatspy (Pyrcz 2024; Pyrcz et al. 2021). The plots for conditional standard deviation for each case are presented in Figures 13–17, where the plots on the left showcase the spatial uncertainty distribution within the region of interest without the data points, and the plots on the right showcase the SGS grid used with the corresponding data points. The conditional standard deviation at each point is calculated using the simulated values from each of the 35 realizations. The variogram used was an isotropic variogram with major range and minor range equal to 30 km, and an azimuth angle of 45°. The other constraints used in the modeling process include a radius of 30 km with the maximum number of points set as 20.

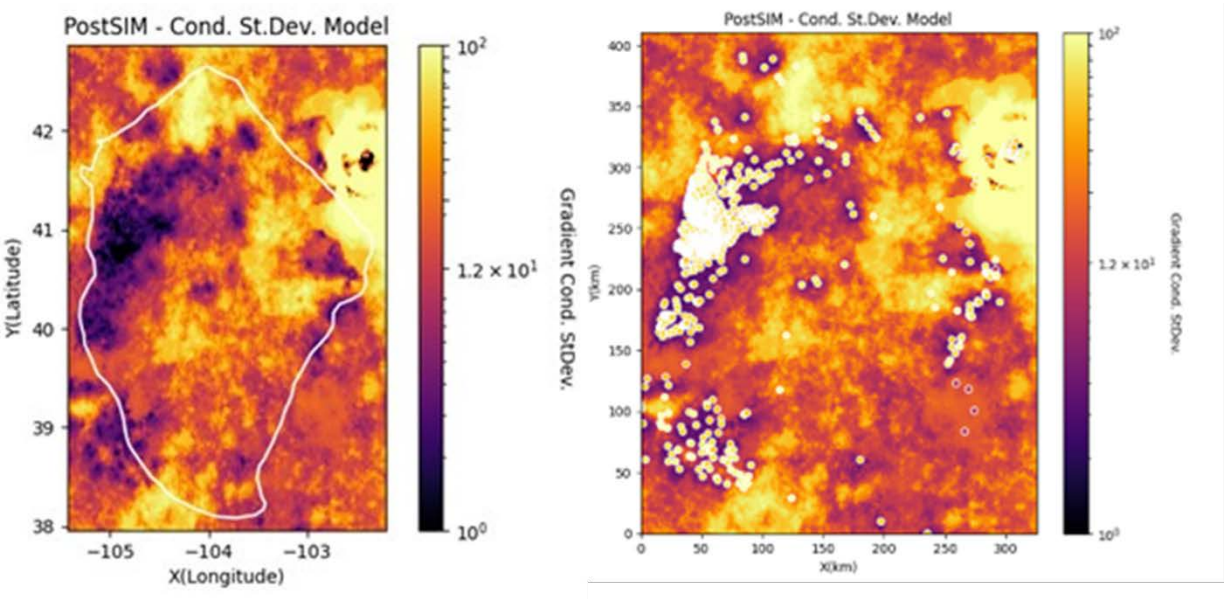

Figure 13. Temperature gradient uncertainty plot for depths 0–1 km

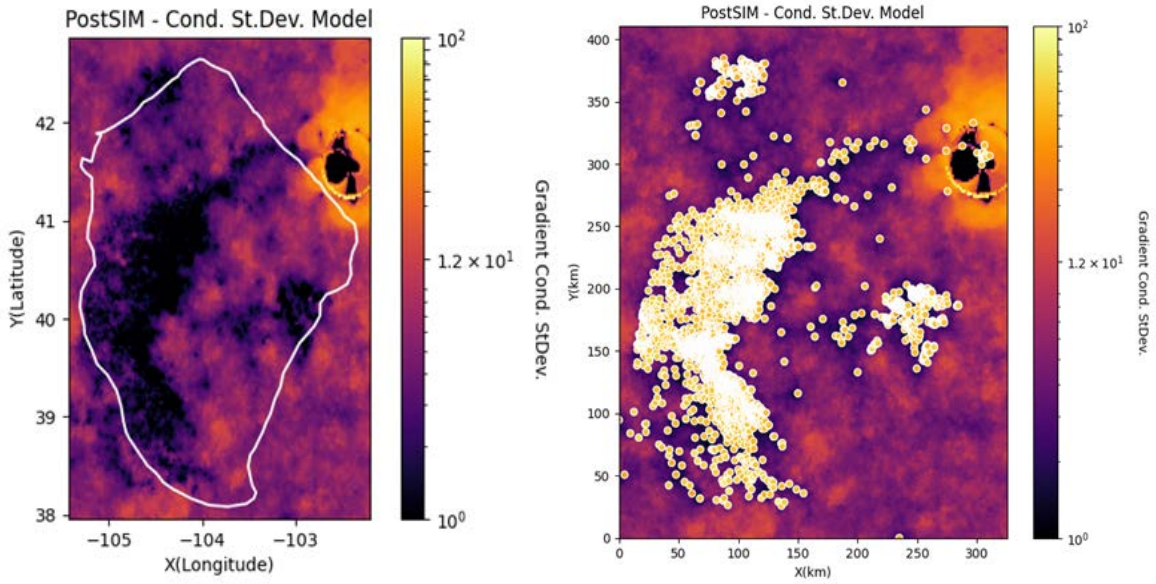

Figure 14. Temperature gradient uncertainty plot for depths 1–1.5 km

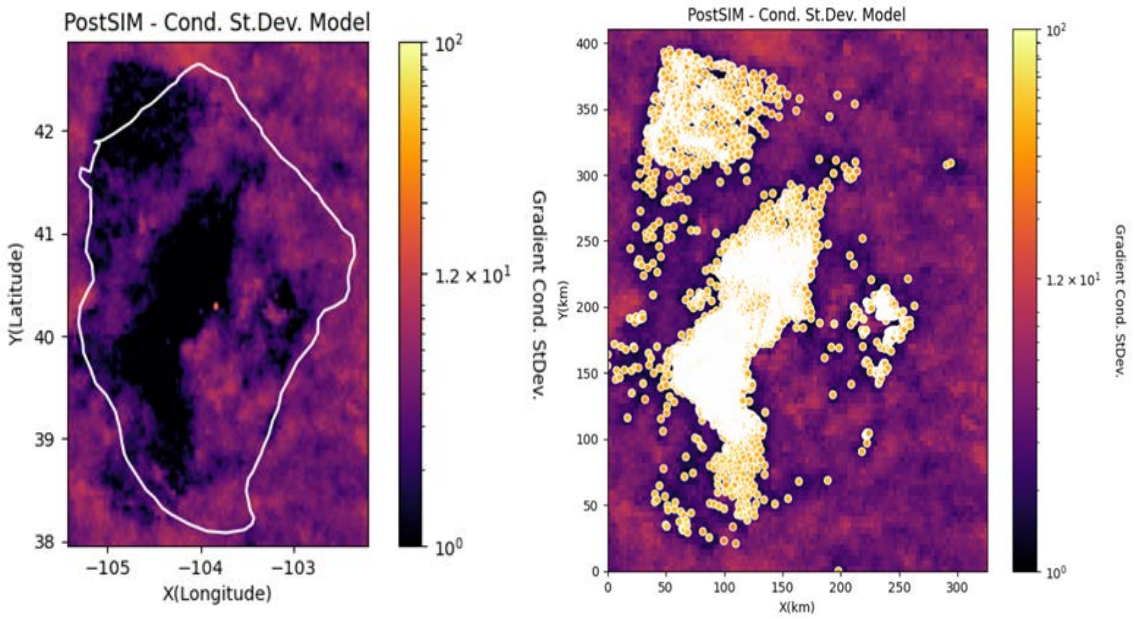

Figure 15. Temperature gradient uncertainty plot for depths 1.5–2 km

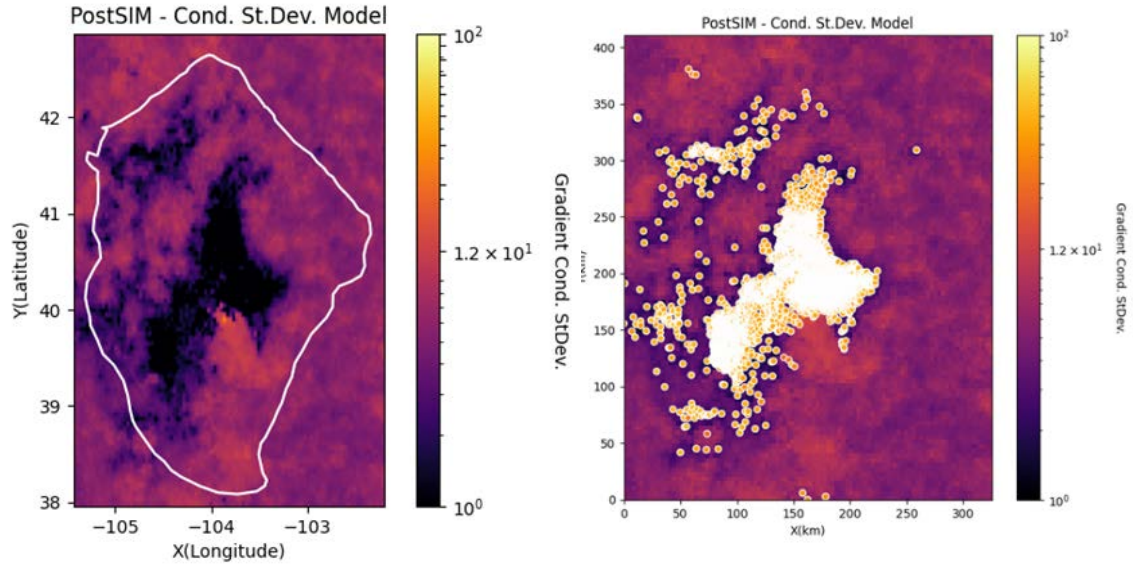

Figure 16. Temperature gradient uncertainty plot for depths 2–2.5 km

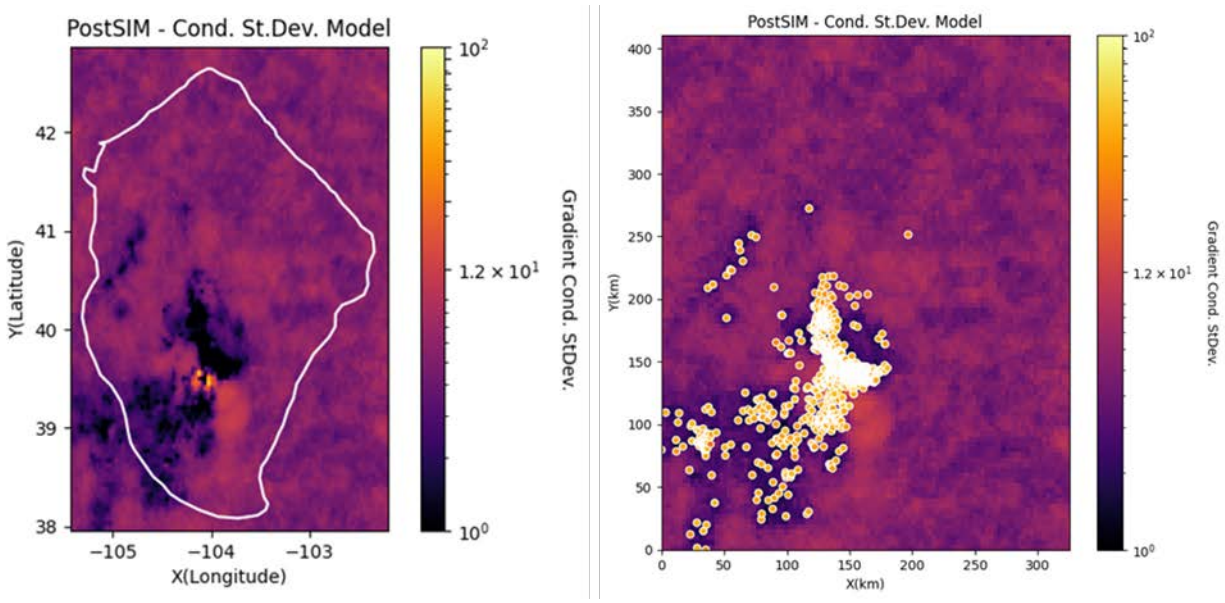

Figure 17. Temperature gradient uncertainty plot for depths 2.5–3 km

3.1.3 Fluid Component Analysis

The fluid component analysis required a few simplifying assumptions due to lack of data availability in the Denver Basin. The initial analysis concentrated on the occurrence of coproduced water in oil and gas wells. Data on water production can reveal the locations of flowing water within the basin and serve as an indirect indicator of the permeability of aquifers or geothermal reservoirs, which is crucial for evaluating potential hydrothermal resources and direct use applications. This information reflects the reservoir quality of rocks by demonstrating their ability to sustain the fluid flow rates required for heat extraction.

The main source for water coproduction data from oil and gas wells in the Denver Basin is the USGS database that collates drilling and production records in the United States. The USGS dataset offers a comprehensive summary of the production records of U.S. wells spanning 1817 to 2020. It was constructed using information gathered by IHS Markit, a commercial database provider. The production figures are consolidated in increments ranging from 2 to 10 m^2 for the cumulative output of oil, gas, and water volumes. In this study we used water production aggregated in 2 mi^2 that sum production per year in barrels reported between different years from 2000 to 2020 to determine accessible fluid in the area (BBL; Figure 18).

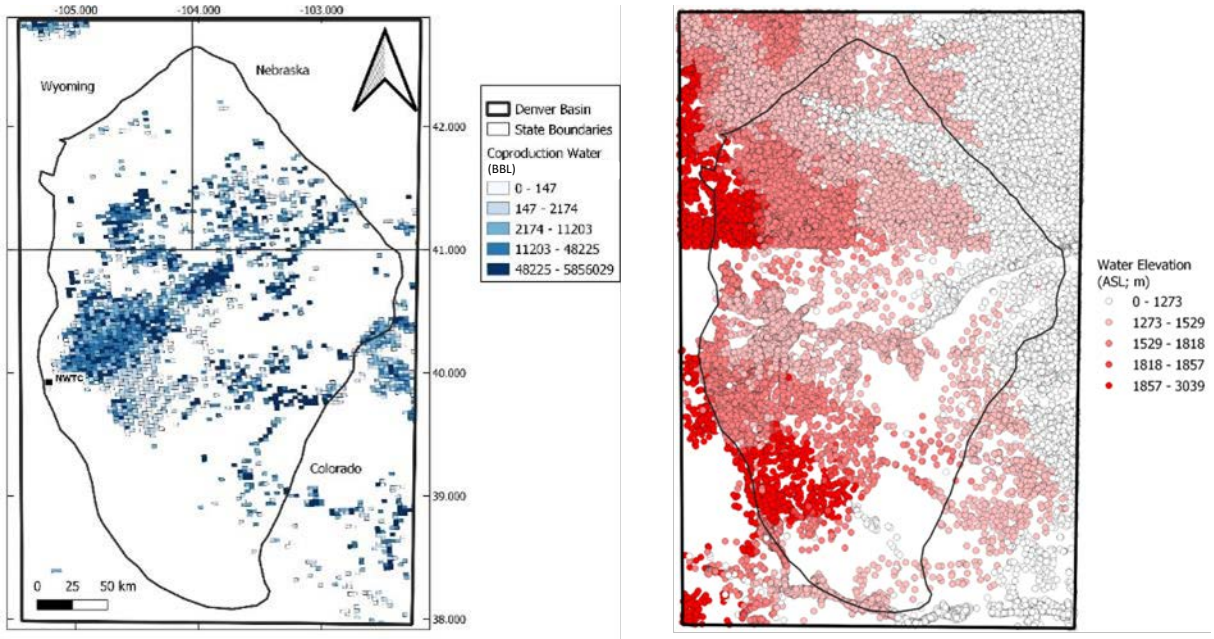

Figure 18. Water coproduction volumes (BBL) per year from oil and gas wells in the Denver Basin (left). Well groundwater levels for Colorado, Nebraska, and Wyoming (right).

The data quality information in the USGS database mentioned that comparing the annual production numbers with the total production figures revealed a discrepancy likely stemming from wells with unspecified production years. To ensure accuracy, the consistency between the original and processed total production values was verified. Moreover, a cross-check of well counts in various categories was performed to confirm alignment, with the disparity between annual and total figures attributed to wells lacking spud dates.

Deeper reservoirs in the Denver Basin are well explored; however, more than 8,000 wells have been drilled across the basin into the top of the Terry ("Sussex") sandstone alone (Fishman 2005). Depths to the top of the Terry ("Sussex") range from about 4,400 to 5,200 ft (1,300 to 1,600 m). When investigating potential for direct use geothermal energy (range of 50 m to 2,000 m vertical depth, minimum 30°C), grasping the potential volume of fluid available in shallower reservoirs is crucial.

To achieve an estimation of shallow fluid availability, the elevation of static water level for all available groundwater wells in the Denver Basin area was calculated using:

$$WL = GL - SWL \quad (4)$$

where WL (ft) is the water elevation in the well above sea level, GL (ft) is the ground surface elevation, and SWL (ft) is the reported static water level measured in the well.

The datasets used to create an estimated water elevation in the Denver Basin were (1) Wyoming State Engineer's Office groundwater wells for Wyoming (Wyoming Water Development Commission 2024), (2) Colorado's Decision Support System groundwater wells for Colorado, and (3) Department of Natural Resources groundwater wells for Nebraska. The ground elevation

was obtained from USGS digital elevation model files in instances where no ground elevation data were reported. Well water elevation availability is visualized in Figure 18.

Figure 19 shows the hot springs located in or near the Denver Basin: Douglas Hot Spring, Warm Spring, El Dorado Spring, and Canon City Hot Spring. The Denver Basin geothermal potential is evident in the western part, where numerous thermal springs and warm wells have been found, with temperatures ranging from 20°C to a peak of 83°C (Barrett and Pearl 1978). The flow rates of these hydrothermal features vary greatly; for instance, the Big Spring in Glenwood Springs, Colorado (a hot spring outside of our study area), was reported to vary from less than one gallon per minute to over 2,263 gallons per minute (Barrett and Pearl 1978).

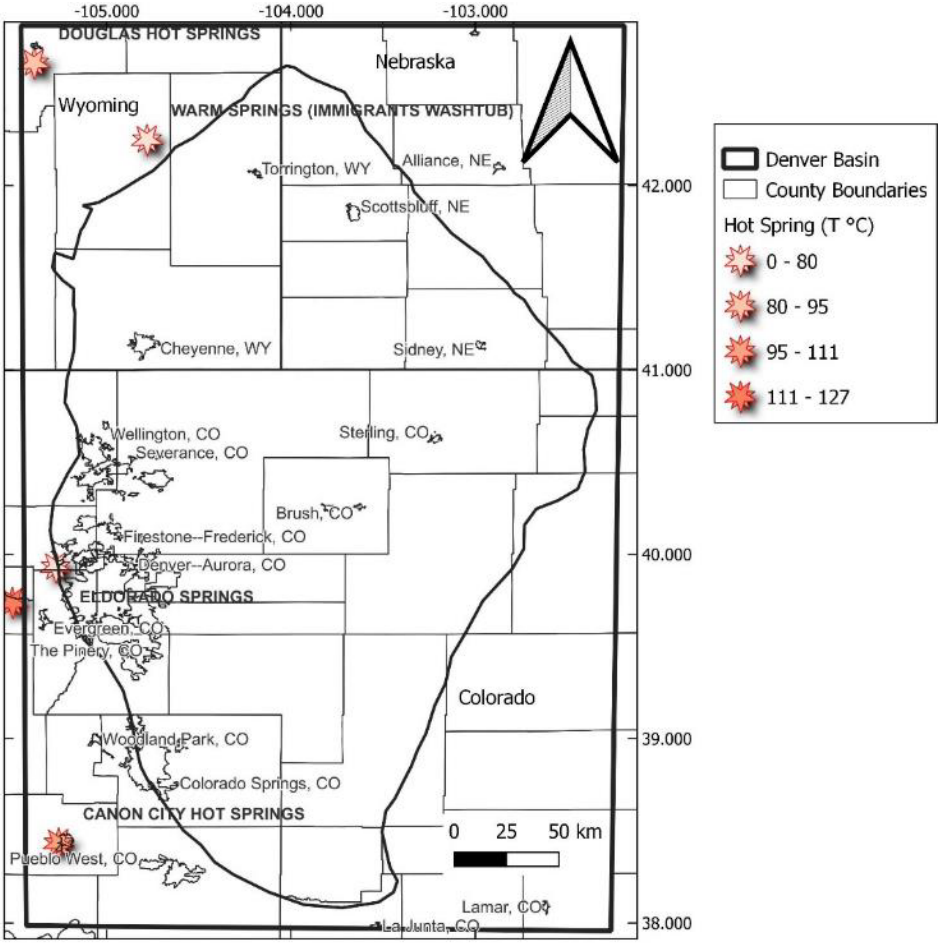

Figure 19. Hot springs located near the Denver Basin

Douglas Hot Spring is located south of the city of Douglas in Wyoming. Water surface temperatures are 30°C, while geothermometers estimated reservoir temperatures of 86°C. Warm Springs in the eastern part of Platte County, Wyoming, exhibits surface temperatures of 21°C, and geothermometers estimated reservoir temperatures of 70°C. The Haystack Well, an oil test hole drilled in 1920 between Boulder and Longmont in Colorado, reaches a depth of 2,932 ft but was abandoned due to significant water influx. The brine discharge from the well is primarily sodium bicarbonate. Positioned at the southern end of a faulted anticline, its waters likely stem from the Dakota Formation and may be replenished by the western mountain front. The heat

source may relate to Paleogene igneous features near the mountain front (Barrett and Pearl 1978).

In Eldorado Springs, Colorado, situated south of Boulder at the eastern edge of the Front Range, water temperatures range from 24°C to 26°C, with total dissolved solids between 84 and 101 mg/L, and reservoir temperatures are estimated with a geothermometer at around 80°C (Table 3). These waters, classified as calcium sulfate type, emerge from alluvial deposits along South Boulder Creek, which overlies the Fountain and Lyons Formations. It is thought that the water comes from deep circulation through fault and fracture zones in the basement rocks to the west, with subsurface temperatures estimated between 26°C and 40°C (Barrett and Pearl 1978). The Cañon City Hot Spring, situated near Cañon City, Colorado, presented a surface temperature around 40°C, and geothermometers estimated reservoir temperatures around 104°C (Table 3). The Cañon City spring presents high chloride content, above 180 mg/L (Table 3).

Table 3. Fluid Chemistry Data and Geothermometer (Na-K and Na-K-Ca) Estimations for Hot Springs and Wells Located Near Denver Basin in Colorado (Barrett and Pearl 1978)

Name	pH	TDS (mg/L)	T (°C)	Flow (L/m)	*Na	*K	*Ca	*Mg	*HCO_3	*SiO_2	*B	*Cl	Na-K (°C)	Na-K-Ca (°C)
Canon City	6.2	1,220	40	4-19	180	20	180	58	867	23	0.20	186	187	68-72
Eldorado A	6.9	101	24	45	7	3	15	5	63	16	0.02	1	314	80
Eldorado B	6.7	86	25	45	9	3	11	3	45	15	0.02	2	254-320	45-57
Haystack	8	1200	24	15	510	1	3	0.7	1250	29	0.74	30	52	62

*Data reported in mg/L

3.1.4 Permeability Component Analysis

The permeability component analysis was simplified using secondary permeability due to a lack of datasets and a short time frame to find, collect, and organize porosity, thickness, and other primary permeability data for reservoir rock in the Denver Basin. Secondary permeability in the Denver Basin was assessed by the presence and density of geologic structures and earthquakes.

The permeability component analysis used structures visible from the surface in Colorado and Wyoming and buried structures in Nebraska (Figure 20). High-angle reverse faults that trend northwest and dip northeast, as documented by Erslev and Selvig (1997), as well as a series of large-scale wrench faults as documented by Fishman (2005) are predominant in the western Denver Basin. For this reason, it is likely that the western Denver Basin currently experiences compressive stress with the highest horizontal stress oriented toward the north-northwest, as noted by Heidbach et al. (2018). Within the Wattenberg area north of Denver, smaller yet significant structural characteristics emerge, including east-northeast-trending wrench strike-slip faults and related listric normal faults with north-northeast, north, and north-northwest trends, as highlighted by Fishman (2005) and Weimer and Sonnenberg (1996). Research suggests the existence of five significant wrench faults in the Denver Basin exhibiting right-lateral movement along vertical planes, extending from the basement to the sedimentary cover (Fishman 2005; Weimer and Sonnenberg 1996; Weimer and Davis 1996). No update regarding formation permeability was available because released data concerning these factors are scarce. Colorado structures were obtained from the USGS Geologic Map Database (USGS 2005).

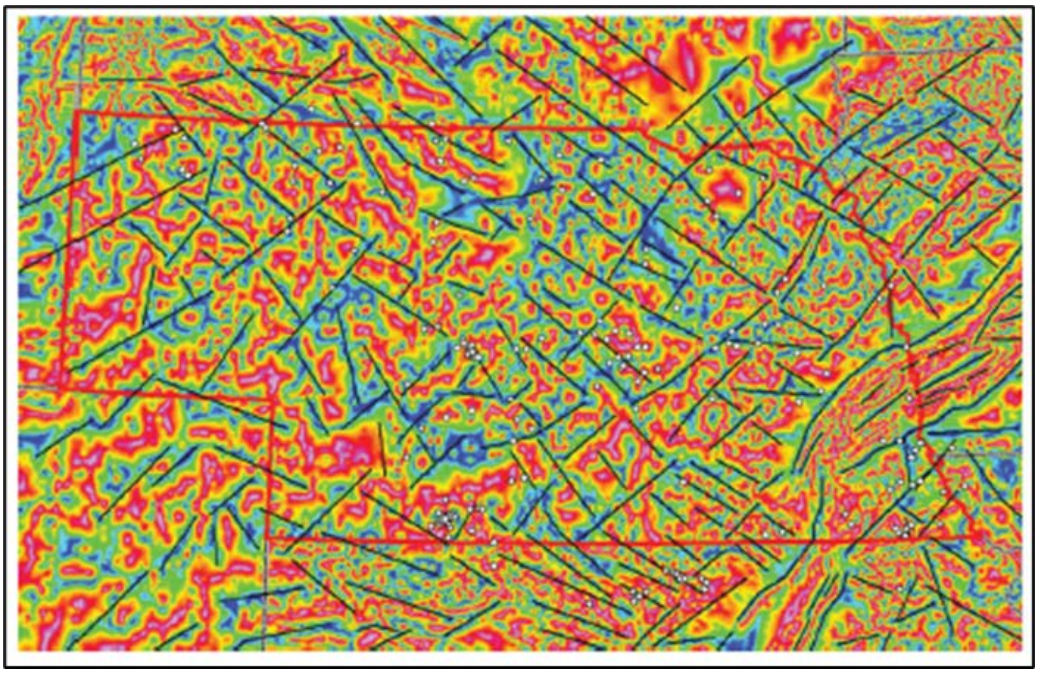

Figure 20. Filtered magnetic field of buried lineaments and structures, with earthquakes as gray points for Nebraska. The figure displays a tilt derivative of reduced pole to magnetic field; basement faults were picked from lows and abrupt changes in pattern.

From Filina et al. (2018)

In a study conducted by Filina et al. (2018), basement structures in Nebraska were interpreted from gravity and filtered magnetics. The structures identified in the study were digitized and included in the assessment of Denver Basin secondary permeability (Figure 18). According to Filina et al. (2018), principal extensional stress is oriented north-south, which reactivates northwest-southeast trending basement faults.

In the lower southeast corner of Wyoming, the boundary between the Wyoming craton and the Colorado orogen is the northeast-trending mylonitic shear zone called the Cheyenne belt (Sims et al. 2001). This belt is collisional in nature, containing thrust faults, likely having occurred in 1.78 to 1.76 Ga (Sims et al. 2001). Figure 21 shows the structures evident in the Denver Basin. The structures identified in the study were digitized and included in the assessment of Denver Basin secondary permeability. Colorado structures were obtained from the USGS Geologic Map Database, and Wyoming structures were obtained from the Wyoming State Geological Survey (WSGS 2014). Primary permeability data of aquifers and rock formations were not accessible.

To project secondary permeability of active faults, earthquake data from the 1950s to present day with magnitude between 2 to 5.5 was obtained from the USGS earthquake database presented in Figure 21 to identify quaternary faults and permeability of fluid pathways.

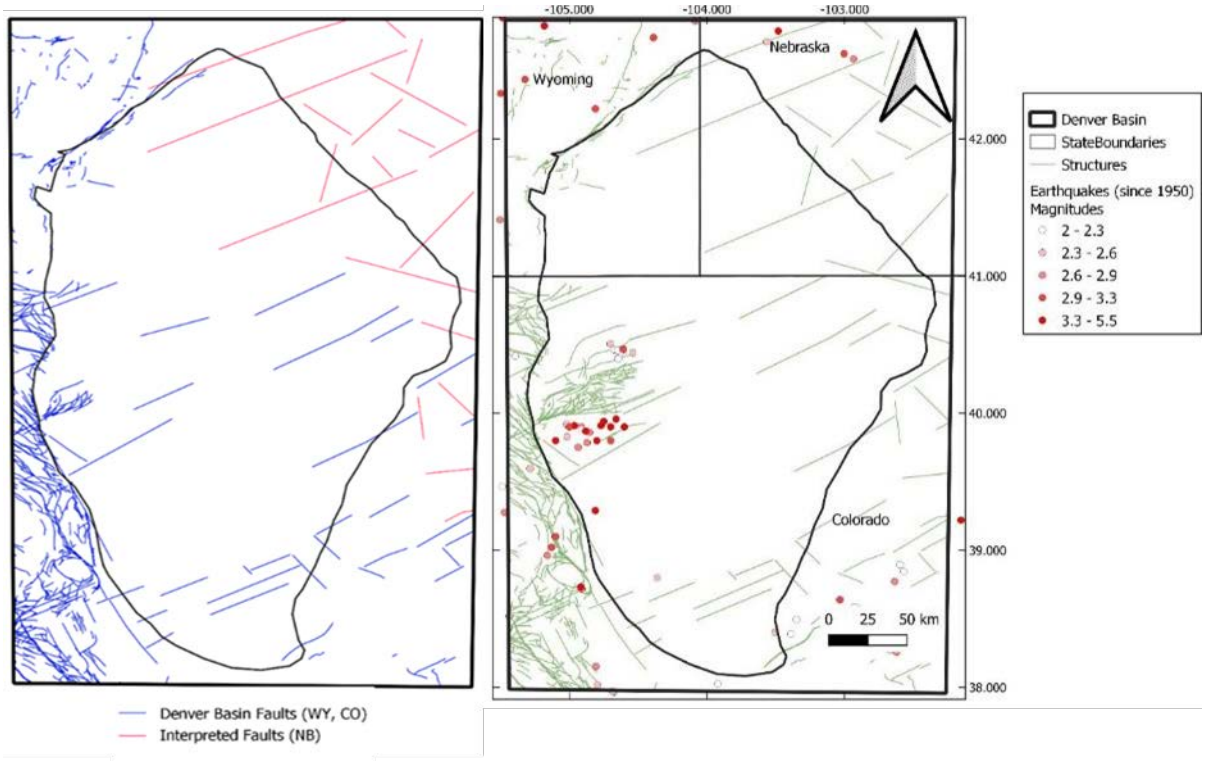

Figure 21. Faults, filtered magnetic lineaments, and other structures in the Denver Basin area (left). Earthquakes since 1950 in the Denver Basin from USGS earthquake catalog (right).

3.2 Economic Criteria

Economically viable projects that utilize geothermal heat at low temperatures need to be situated near the hot water source to minimize heat loss and pumping costs. As a key for socioeconomic factors in assessing the utilization risk, we primarily focused on demand and population density as a regional indicator. Furthermore, we include other important layers such as infrastructure and a component of site accessibility that includes a layer with roads in the region.

3.2.1 Energy Demand Component Analysis

The energy demand component is divided into the following input layers: population, and infrastructure. We identified a database containing 2020 decennial census data at the block level for all states, which includes redistricting areas total population. This data was filtered to reflect only the Denver Basin region (Figure 22) and a minimum population threshold of 4,000 residents was applied to justify the initial capital investment associated with district heating systems.

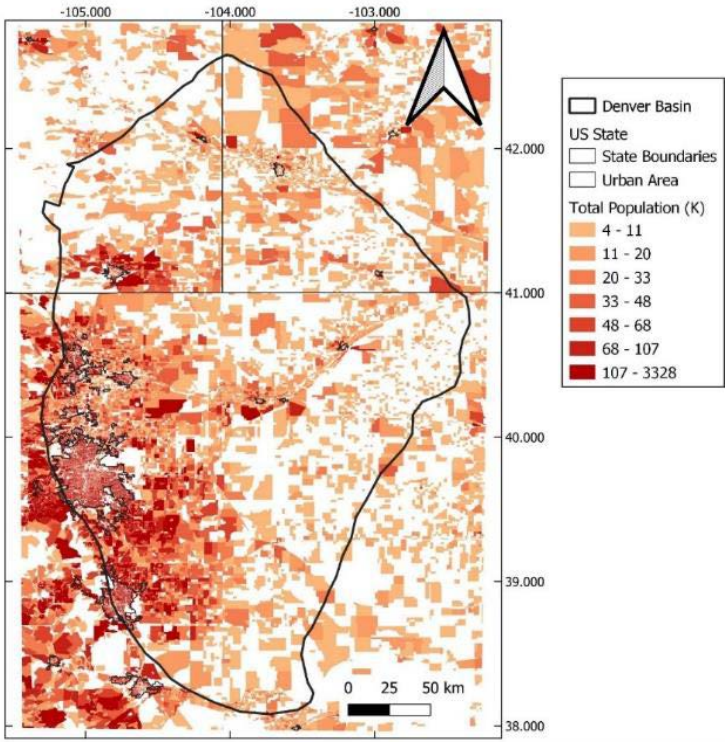

Figure 22. Total Population for redistricting areas.

From 2020 decennial census data (arcgis.com 2021)

Additionally, we used thermal demand data of residential, commercial, and manufacturing sectors (Oh and Beckers 2023) to compare with population centers and identify the higher energy demand by county in the Denver Basin region (Figure 23).

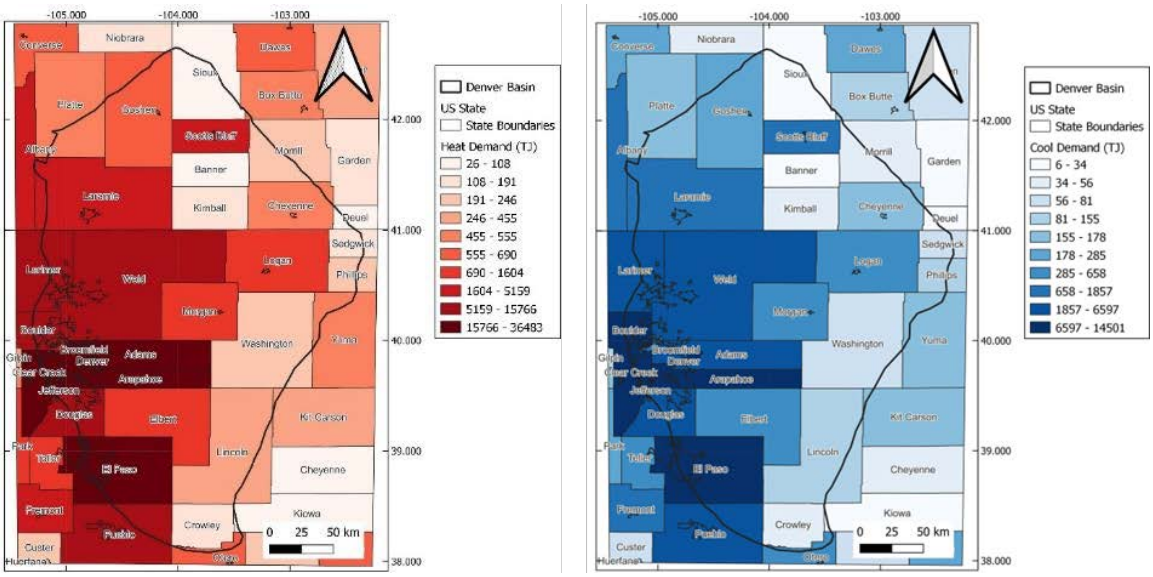

Figure 23. Heating (left) and cooling (right) demand for residential, commercial, and manufacturing in the Denver Basin region by county.

From Oh and Beckers (2023)

An infrastructure layer was added to the PFA analysis that identifies the density of buildings, residential areas, and other types of infrastructure (Figure 24) necessary for heating and cooling and/or other direct use applications. These datasets were combined for Colorado, Nebraska, and Wyoming from the USGS database (USGS n.d.) that shows various private and public manmade structures and installations. The purpose of this dataset is to document the spatial location of buildings for general cartographic representation purposes on USGS mapping products.

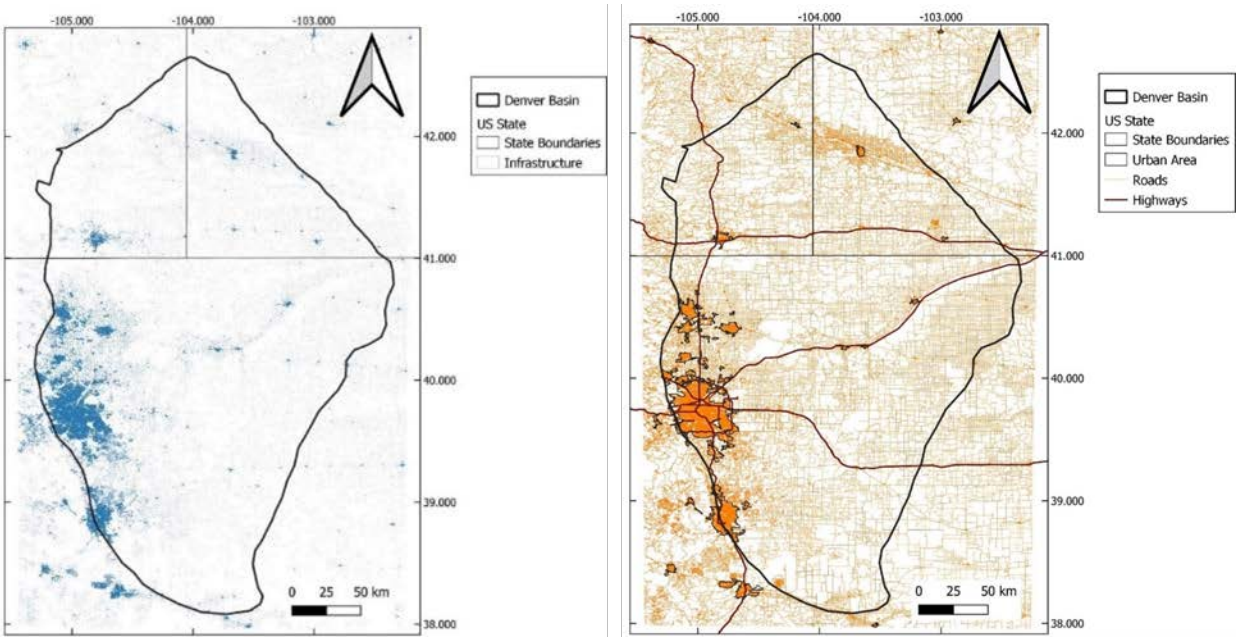

Figure 24. Infrastructure (left) and roads (right) in the Denver Basin.

From USGS (n.d.) and U.S. Census Bureau (2021)

3.2.2 Site Accessibility Component Analysis

We combined a road dataset for the Denver Basin (Figure 24) to identify sites geothermal projects that do not need new roads to be built. This is to avoid the costs and logistical challenges of constructing new roads, which would make the development of low-temperature geothermal projects unfeasible. Furthermore, the total length of roads could be used as a method to estimate the required piping length to service a given location (Reber 2013). Different road datasets were downloaded from the Topologically Integrated Geographic Encoding and Referencing (TIGER) dataset (U.S. Census Bureau 2021) and then combined to cover the Denver Basin region.

3.3 Risk Criteria

The risk criteria were divided into safety and exclusion area factors. The safety factor is named as the inverse of hazard because we are looking for the absence of hazard, or the presence of safety. This is more in line with the way we are viewing other components (i.e., presence of heat, fluid, permeability). The safety criteria consist of natural disaster components, and the exclusion component comprises environmental protected areas. For the natural disaster component, we identified and combined flood plain datasets for Colorado, Nebraska, and Wyoming (Figure 25) from the Purdue University Research Repository (Sangwan and Merwade 2015).

Furthermore, to avoid environmental protection lands, we identified exclusion layers such as National Park Service, environmental habitats, and protected areas (Figure 26). We did not exclude military, government, and Bureau of Land Management due to the possible interest in developing geothermal projects from government agencies.

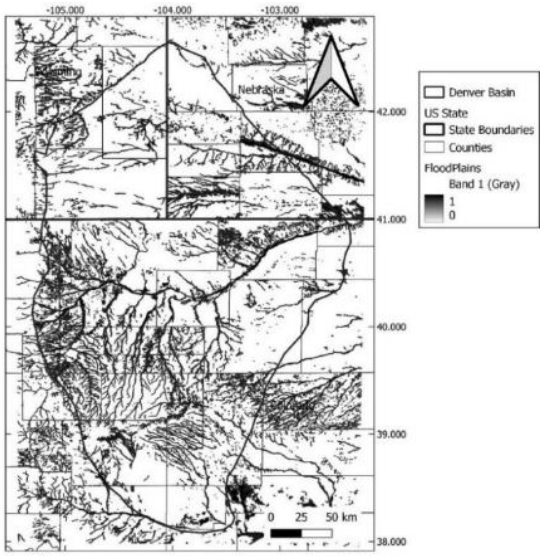

Figure 25. Flood plain areas located in Colorado, Nebraska, and Wyoming

From Sangwan and Merwade (2015)

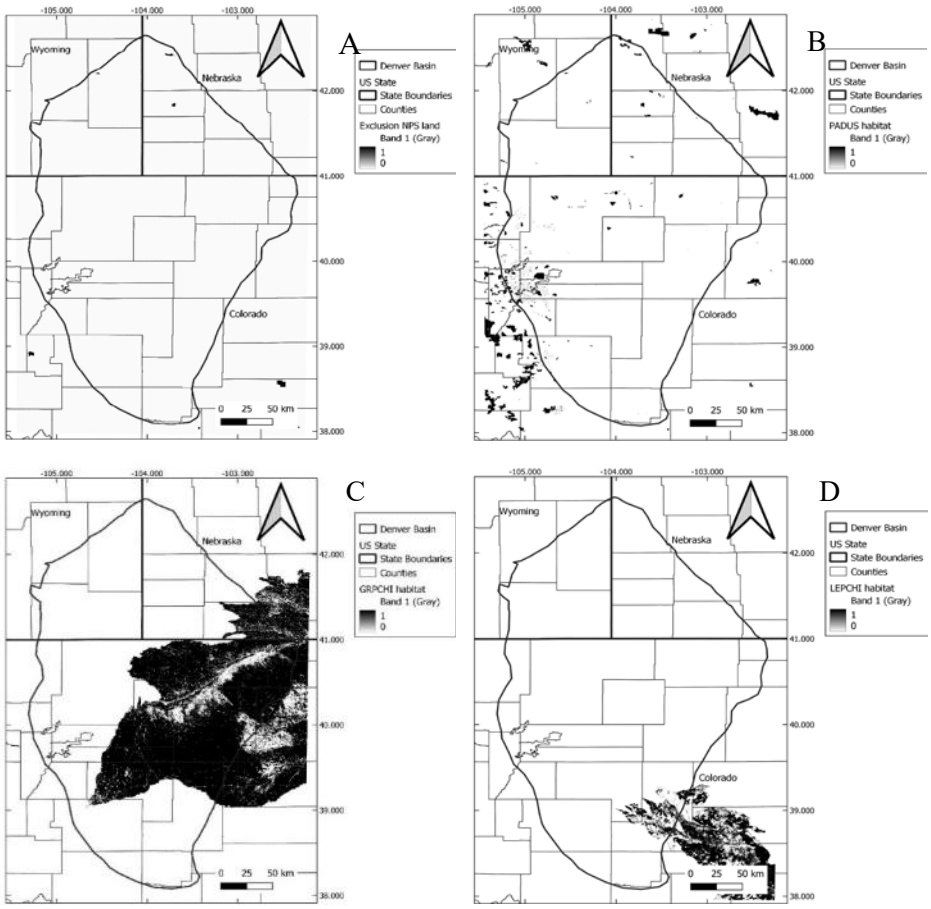

Figure 26. Environmental protection areas. (A) National Park Service (NPS), (B) Protected Areas Data of U.S. (PADUS), (C) greater prairie chicken habitat (GRPCHI), and (D) lesser prairie chicken habitat (LEPCHI).

4 Gap Analysis

Relevant data were gathered from our regional study and entered into NREL's GeoRePORT to help monitor the transition from exploration Phase I to future exploration (Phase II) of geothermal projects for CHP and GDU applications in the Denver Basin. Phase I involves preliminary studies, including geological, geochemical, and geophysical assessments, to evaluate the viability of potential geothermal sites and inform decisions on further subsurface exploration (Phase II) and drilling exploratory geothermal wells (Phase III).

This tool was created by NREL in collaboration with a significant group of industry stakeholders to assist the U.S. Department of Energy's Geothermal Technologies Office in tracking and evaluating the long-term effects of its research, development, demonstration, and deployment funding on geothermal projects (Pauling et al. 2023). It is important to highlight that this gap analysis was performed regionally, but site evaluations are needed for specific geothermal project development in the Denver Basin.

GeoRePORT aims to establish standardized assessment criteria for both scientists and nonexperts. The tool outlines a detailed and quantitative approach for reporting on two key aspects: (1) the inherent features of geothermal sites (project grade) and (2) the level of development maturity (project readiness). Since the feasibility of geothermal projects is influenced by multiple factors (such as temperature, permeability, and permitting), evaluations are based on 12 attributes related to geological, technical, or socioeconomic aspects for geothermal resource quality and project readiness as initiatives move from exploration to development (Kolker et al. 2019). It is intended to ensure consistency in reporting among users rather than serve as a guideline for exploration and development or an evaluation on project viability. To learn more about the GeoRePORT spreadsheet tool and its user protocol, refer to OpenEI Geothermal Resource Reporting (n.d.).

4.1 Resource Grades

Resource grade is illustrated using a rose diagram divided into three sections—geological, technical, and socioeconomic—each of which contains four to five attributes. The tool evaluates these attributes according to user feedback, using a grading scale from A (best) to E (worst). Additionally, GeoRePORT considers the activities performed to grade each attribute and the reliability of the collected data. Geological attributes such as temperature, volume, permeability, and fluid chemistry are assessed, with specific activity and execution indices created to manage uncertainties in the reported information (for an extensive overview of the geological assessment protocol, refer to Rubin et al. [2022a]).

Figure 27 shows the GeoRePORT resource grade totals for CHP uses in the Denver Basin. In general, our study of PFA in the Denver Basin displays attributes generally favorable to continue Phase II of exploration for CHP applications in localized areas with some geological, technical, and socioeconomic attributes scoring between A and D grades (i.e., "ideal conditions," "favorable conditions," "barriers are present," "difficult conditions," for A, B, C, and D, respectively). For the geological attribute, the Denver Basin was graded D in temperature, meaning "difficult conditions" in the region for CHP development due to the maximum average temperature of 150°C at depths > 2 km (Porro et al. 2013) for power generation. Although our study shows that there are some limited areas with higher temperature (≥150°C) that could be

suitable for power generation in the Denver Basin. The permeability and fluid chemistry were graded B, meaning the area has "favorable conditions" for CHP. We used general information such as pH (i.e., 6 to 7) and total dissolved solid content (<1,000 ppm) from hot springs in the eastern part of the Denver Basin. However, there are some unknown permeability attributes such as fracture spacing, aperture, and mineralization; silica and calcite saturation; and gas content in the fluid chemistry. Information about volume and flow rate is unknown until exploration in a focused area of the Denver Basin takes place.

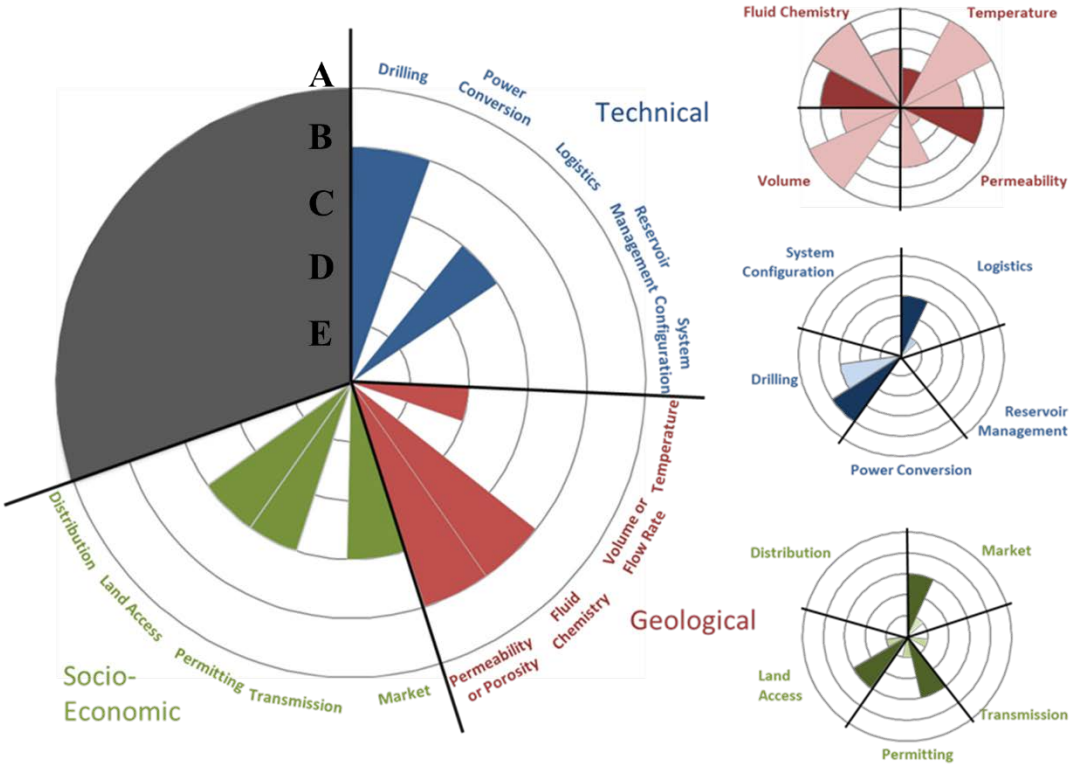

Figure 27. GeoRePORT grade (A – E) overview for CHP applications in the Denver Basin. Left: Character grade totals by geological, socioeconomic, and technical attributes. Right: Attribute grades broken down into subattributes.

In the technical attribute (Figure 27), the Denver Basin region has not been investigated in this project scope for power conversion, reservoir management, and system configuration because these data have not been tested, and they are not available for Phase I exploration of geothermal assessment in the region. Still, logistics shows a C grade, meaning that "logistic barriers are present" due to unknown information such as landslide hazards, wildfire hazards, topography slopes, and severe weather events. All those unknown data could be addressed in Phase II of the Denver Basin exploration using public maps or remote sensing tools. The logistical data included in this Phase I study displayed a degree of isolation in accessing resources and areas within reach of existing infrastructure and roads (Figure 24), as well as volcanic hazard, earthquake hazard, and flood plain areas (Figure 21 and 25). For the drilling attribute, a B grade, meaning "favorable drilling conditions," was evaluated due to the presence of thousands of oil and gas wells and BHT data in the basin with average depths between 1 and 2 km.

The socioeconomic section of Figure 27 shows the transmission and distribution attribute as unavailable because this information was not collected as part of Phase I study. The land access attribute was graded with a C, meaning "acceptable land access" exists in the Denver Basin area; for instance, our study identified environmentally sensitive areas (Figure 26). Market attribute was graded C as well, meaning that "acceptable market conditions" are present in the Denver Basin. We know that there is a long-term demand for power and heat in the region (Figure 23; see Section 3.2.1 for more information), and local incentives are present in the region to offset geothermal project costs and reduce risk. Permitting was graded C, meaning that "manageable permitting barriers" exist in the region; for instance, the state of Colorado has good regulations and permits for geothermal development, but Wyoming and Nebraska do not. This attribute was not part of this Phase I study; nevertheless, for help finding the required permits of each site, refer to OpenEI RAPID (n.d.).

Figure 28 shows the GeoRePORT resource grade totals for GDU applications in the Denver Basin. In general, our study of PFA in the Denver Basin displays attributes generally indicating ideal conditions for GDU applications in localized areas with some geological, technical, and socio-economic attributes scoring between A to C grades. The main difference between CHP and GDU uses in the region, is that for the geological attribute temperature avg. of ≤150 °C in the Denver basin is graded A as "ideal conditions" for GDU applications. As well as drilling attribute is graded A for GDU uses, meaning "ideal drilling conditions" are presented in the basin. The rest of the attributed are keeping the same for both CHP and GDU applications.

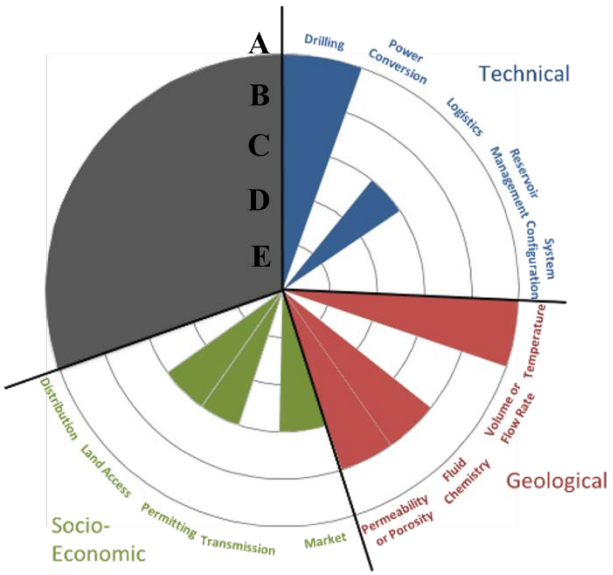

Figure 28. GeoRePORT grade (A – E) overview for GDU applications in the Denver Basin. Attribute grades broken down into subattributes.

4.2 Project Readiness

To assess project readiness, the following scoring has been assigned to the project attributes: G4, T2, and S2 (which stand for "tested," "potential," and "feasible," respectively). Thousands of oil and gas wells have been drilled in the Denver Basin, and BHT data were available to estimate

gradient temperature and heat flow in the region that gave a geological readiness score of G4 in the Denver Basin (Figure 29); still, flow tests need to be performed in future exploration in this region. Technical readiness was given a score of T2 due to the reservoir temperature provided by BHT data in the region, but fluid flow is unknown in some areas of the basin. The socioeconomic readiness score was S2 (Figure 29). Our analysis of population density, heat and energy demand, and site accessibility gave a general view of the economic potential in the region (see Section 3.2 for more information).

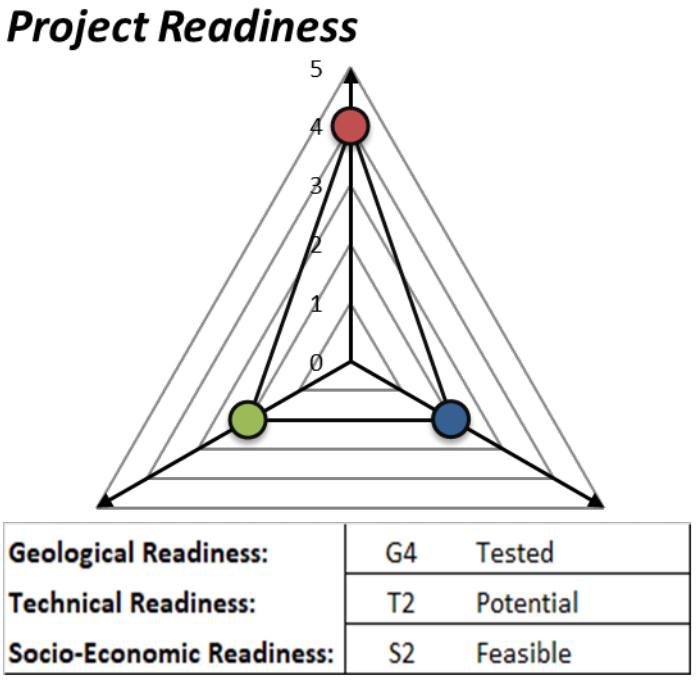

Figure 29. Denver Basin geothermal region's total project readiness score, demonstrating G4 ("tested") geological readiness, S2 ("feasible") socioeconomic readiness, and T2 ("potential") technical readiness.

5 PFA Methodology

The geothermal PFA best practice report by Pauling et al. (2023) suggested a uniform terminology for PFA projects based on the Snake River Plan PFA project by Shervais et al. (2017). These terms apply to all data types and allow communication between various domain experts. Pauling et al. (2023) define these layers as (Figure 30):

- **Data layers**: unprocessed raw data, which can include points, lines, or polygons, all requiring geographic coordinates
- **Evidence layers**: generated by applying geostatistical methods to data layers, typically involving a density function that assesses object occurrences in a specific area or an interpolation function to derive values from a limited set of data points
- **Confidence layers:** reflect data uncertainties, which are often assessed using a combination of approaches (e.g., fuzzy logic and kriging standard error)
- **Common risk segment (CRS) maps:** formed by the weighted sum of several confidence and evidence layers for a particular play component, resulting in a CRS map for each characteristic observed in the project
- **Composite CRS map**: the weighted product of multiple CRS maps, each corresponding to individual play components (like permeability and heat), emphasizing regions where the necessary characteristics for a sustainable geothermal resource are found.

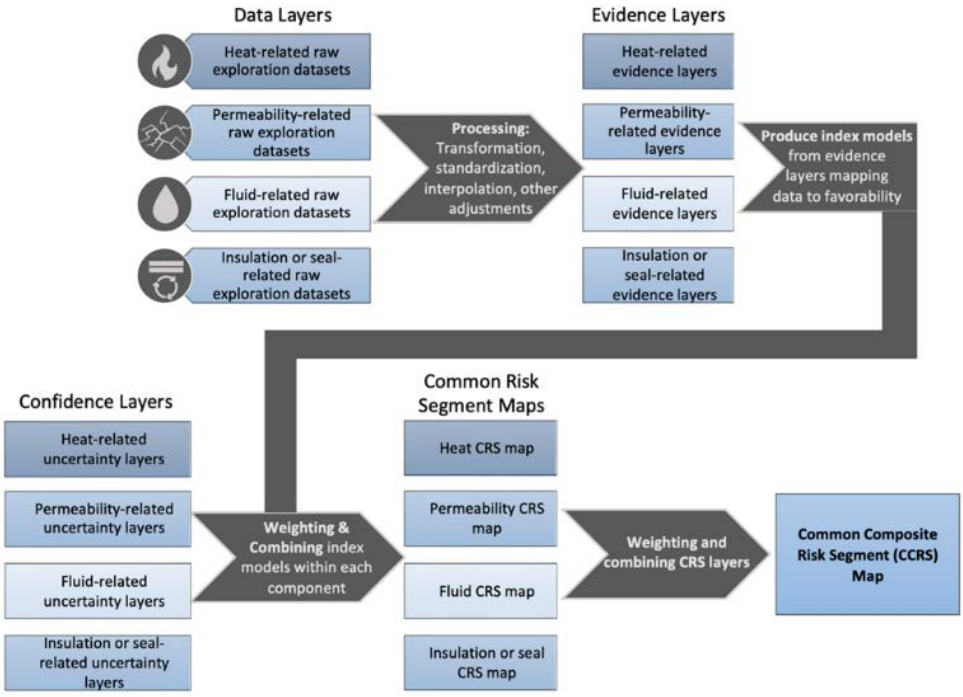

Figure 30. A flowchart depicting a generalized hydrothermal PFA method that integrates elements from other projects' methods.

From Pauling et al. (2023)

The Python library named "geoPFA" was created and employed to establish a process for generating both common and composite CRS maps. The geoPFA was built with extensibility and reusability in mind, in the hopes that it may eventually be developed further and released as an

open-source Python library. It is technologically agnostic and is modeled after the workflows described in the PFA best practices report (Figure 30). The library includes tools for:

- Reading in geospatial data in various formats (i.e., shapefile, TIFF, CSV)
- Cleaning the data (i.e., projecting onto the same coordinate reference system and grid, changing geometry type)
- Processing the data (i.e., distance function, various interpolation methods)
- Transforming the data (i.e., standardization, various methods for going from data values/data layers to favorability values/evidence layers)
- Weighting and combining the evidence layers (i.e., Voter-Veto method)
- Adding exclusion areas
- Plotting the data and outputs.

Throughout this section, examples of how the geoPFA Python library can be used to conduct PFA are provided. The geoPFA is expected to be released as an open-source toolset in the future.

5.1 Configuration

There are several required inputs for criteria and each component in the PFA process. These include component weights, component prior probabilities, evidence layer weights, and data layer transformation methods. In the full PFA, we also add in criteria weights since there are multiple criteria.

Component weights and component prior probabilities were assigned using expert opinion. Transformation methods were assigned based on a simple understanding of the relative relationships between data values and favorability (e.g., high values are more favorable = No transformation; vice-versa = Negate). This could also be done more intelligently in the next PFA iteration. Evidence layer weights were also assigned using expert opinion and are set to 1.0 when there is only one evidence layer within a component (i.e., heat). Table 4 lists these parameters.

The geoPFA library is built to be extensible to any possible combination of criteria, associated components, and data layers. It achieves this by requiring a configuration file that specifies the relationship between the data layers, respective components, and respective criteria. It also specifies the weights, units, data column names, and required transformation method for each data layer, and the prior probabilities associated with each component. Figure A.1 in Appendix A shows the configuration file for this PFA, in json format, compiling the information from Table 4 into a machine-readable format. Note that additional criteria and components may be added to the configuration file and formatted in a similar way.

Table 4: Table of criteria, component and evidence layer weights.

This table provides the basis for the configuration file shown in Figure A.1 in Appendix A.

Criteria	Criteria Weight	Component	Component Weight	Component Prior Probability	Evidence Layer Name	Evidence Layer Weight*	Transformation Method
Geologic	0.35	Heat	0.40	0.85 (low temp)	Temperature Gradient	1.0	None
Geologic	0.35	Permeability	0.30	0.50	Structures (Faults)	0.50	Negate
Geologic	0.35	Permeability	0.30	0.50	Earthquakes	0.25	None
Geologic	0.35	Fluid	0.30	0.50	Hot Springs	0.5	Negate
Geologic	0.35	Fluid	0.30	0.50	Groundwater	0.2	Negate
Geologic	0.35	Fluid	0.30	0.50	Coproduced Fluid	0.3	None
Economic	0.50	Demand	0.85	0.50	Population	0.50	None
Economic	0.50	Demand	0.85	0.50	Infrastructure Density	0.50	None
Safety	0.05	Natural Disaster	1.0	0.15	Distance from Flood Plains	1.0	Negate

*Note that the data layer weights are set to 1 when there is only one layer associated with a component.

It is also important that the data directory follows this same structure: there is a directory for criteria, which contains subdirectories for each component, which each contain their respective data layers. The temperature gradient shapefile is named as described in the configuration file. Everything is also named as it is in the configuration file. This structure is demonstrated in Figure A.2 in Appendix A.

The configuration file is read into a Jupyter Notebook and stored as a Python dictionary named "pfa." This pfa dictionary is updated throughout the process so that the entire PFA process is stored in a single data structure. This allows users to reference different parts of the PFA process throughout the workflow, for example, by comparing the original data layer to the final resulting favorability map or comparing the component favorability maps to the criteria favorability map.

5.2 Read in Data

The configuration and setup make it straightforward to read in the data. Figure A.3 in Appendix A shows a screenshot of the code, which uses the gather_data function from the GeospatialData class in the geoPFA Python library. In this code snippet, we limit the data gathering only to shapefiles, but this can be adjusted to other formats, or all compatible geospatial data formats (currently: shapefile, raster, csv, tiff). You can see from the text output that three data layers were read in, one for each component of criteria.

We can plot the raw data layers and see that they include various geometries (e.g., point, line, and polygon), different coordinate reference systems, and different data spacing. The data need to be converted into point geometries, interpolated and/or processed to represent a feature of interest (e.g., distance from faults instead of fault traces), and projected onto the same coordinate reference system and the same grid (Figures 31, 32, and 33). They also require some cleaning of outliers to show the trends more clearly in the data. These raw data layers are stored in Pandas

GeoDataFrames (a type of dataframe that stores geospatial metadata and geometry) and added to "data" keys within their associated layer/component/criteria path within the pfa dictionary so that they can be plotted at any point throughout the process.

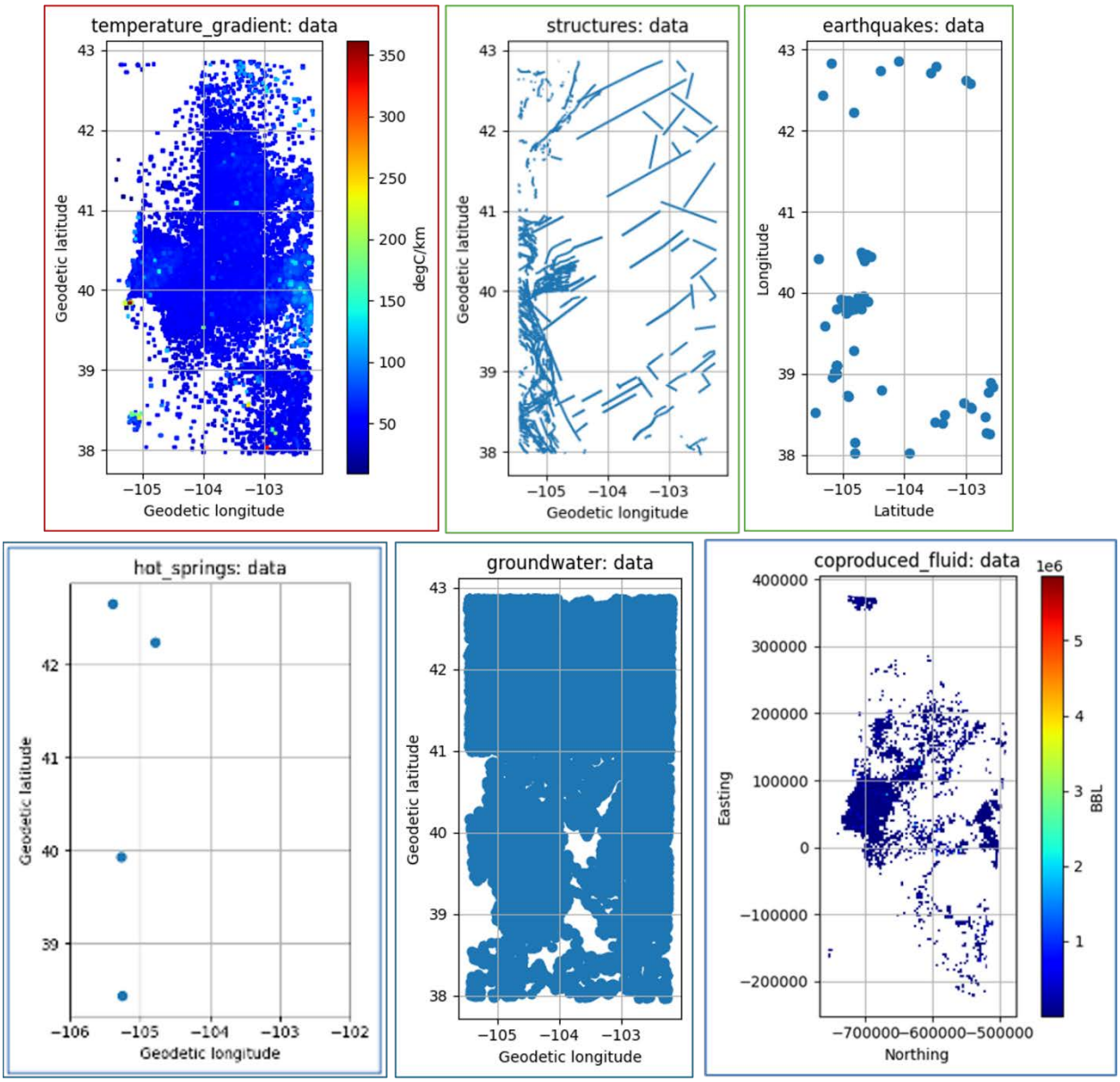

Figure 31. Raw data layers input into geoPFA for geologic criteria favorability mapping, including layers associated with the heat (red border), permeability (green border), and fluid (blue border) components

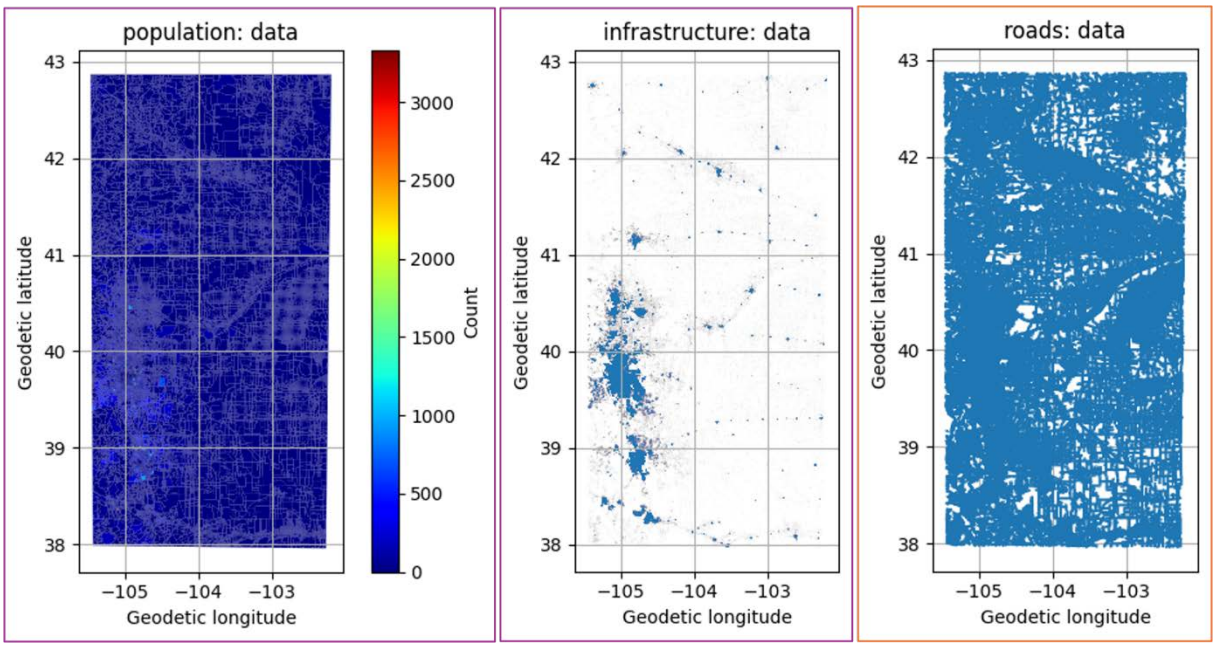

Figure 32. Raw data layers input into geoPFA for economic criteria favorability mapping, including layers associated with demand (purple border) and site accessibility (orange border) components.

Note that while the roads map is included here, it was excluded from the final favorability mapping because it significantly slowed down computational time without providing much benefit (i.e., there are roads everywhere).

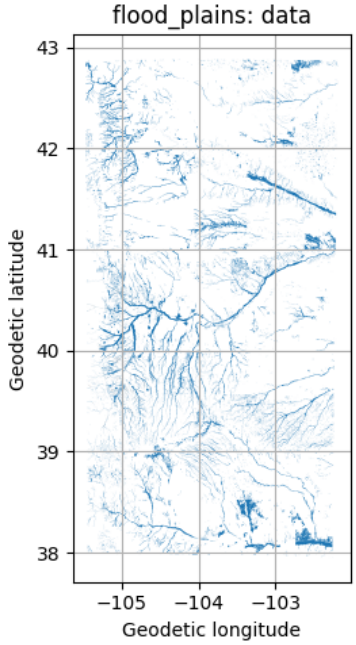

Figure 33. Raw data layers input into geoPFA for safety criteria favorability mapping, including the flood plains layer associated with natural disaster component

5.3 Cleaning and Processing

Cleaning is done in just a few lines of code (Appendix A, Figure A.4). This includes projecting everything onto the same coordinate reference system and filtering out outliers in some datasets by setting everything above the 0.9 quantile to the value associated with the 0.9 quantile. Particularly, the coproduced fluid and temperature gradient datasets included anomalously high values that masked the trends in the data. Outliers above the 90th percentile were filtered out and set to the value at the 90th percentile. Next, all the datasets were projected onto the same coordinate reference system. WGS 84 (EPSG:3857) was used because it is a common projected coordinate system. A projected coordinate system is a requirement for the interpolation and distance function to be accurate.

Cleaning is performed with functions provided by the Cleaners class in geoPFA. Currently, the code requires somewhat manual cleaning of the data, but this could be automated in the future through allowing the user to specify cleaning methods for each layer within the configuration file.

The data layers are interpolated/processed into maps (Appendix A, Figure A.5). This process also puts all the layers onto the same grid through setting the nx, ny, and extent variables. In addition, since the interpolate_points function in the geoPFA Processing class requires point geometry, the polygon geometry of the produced fluid data layer is converted to point geometry by calculating the centroid of each grid square and applying the values for each grid square to its associated centroid. We have built this functionality into the interpolate_points function. Currently, this function includes options for linear, cubic, or nearest-neighbor interpolation, and the linear option is selected. Linear interpolation is applied to temperature gradient and coproduced fluid data to produce two-dimensional maps from these point datasets. In a future iteration, functionality will be added for IDW to improve the interpolations (as was applied to produce the maps above in QGIS).

The fault location data is easily converted into a distance from faults map using the distance_from_lines function, and the hot springs and groundwater datasets are converted into distance from hot springs and distance from groundwater observations maps using the distance_from_points function. The earthquake location data are converted into an earthquake density map using the point_density function. All three of these functions are in the Processing class of geoPFA.

The block population dataset is converted to a point representation using the polygons_to_points function so that it matches the grid and format of the other maps. The infrastructure data is converted into an infrastructure density map using the polygon_density function. And lastly, natural disaster risk areas such as flood plains have buffers created around them at a specified distance of 1,000 m to represent incrementally decreasing natural disaster risk with distance from the safety area. These buffers are produced using the mark_buffer_areas function. All of these functions are in the Processing class of the geoPFA Python library. Currently, the code requires somewhat manual processing of the data, but we are in the process of automating this step by allowing the user to specify processing methods for each layer within the configuration file.

The resulting maps are added to map keys within their associated layer/component/criteria path within the pfa dictionary so that they can be plotted at any point throughout the process. Figures

34, 35, and 36 show the resulting maps produced from the processed data layers from geological, economic and safety criteria, respectively.

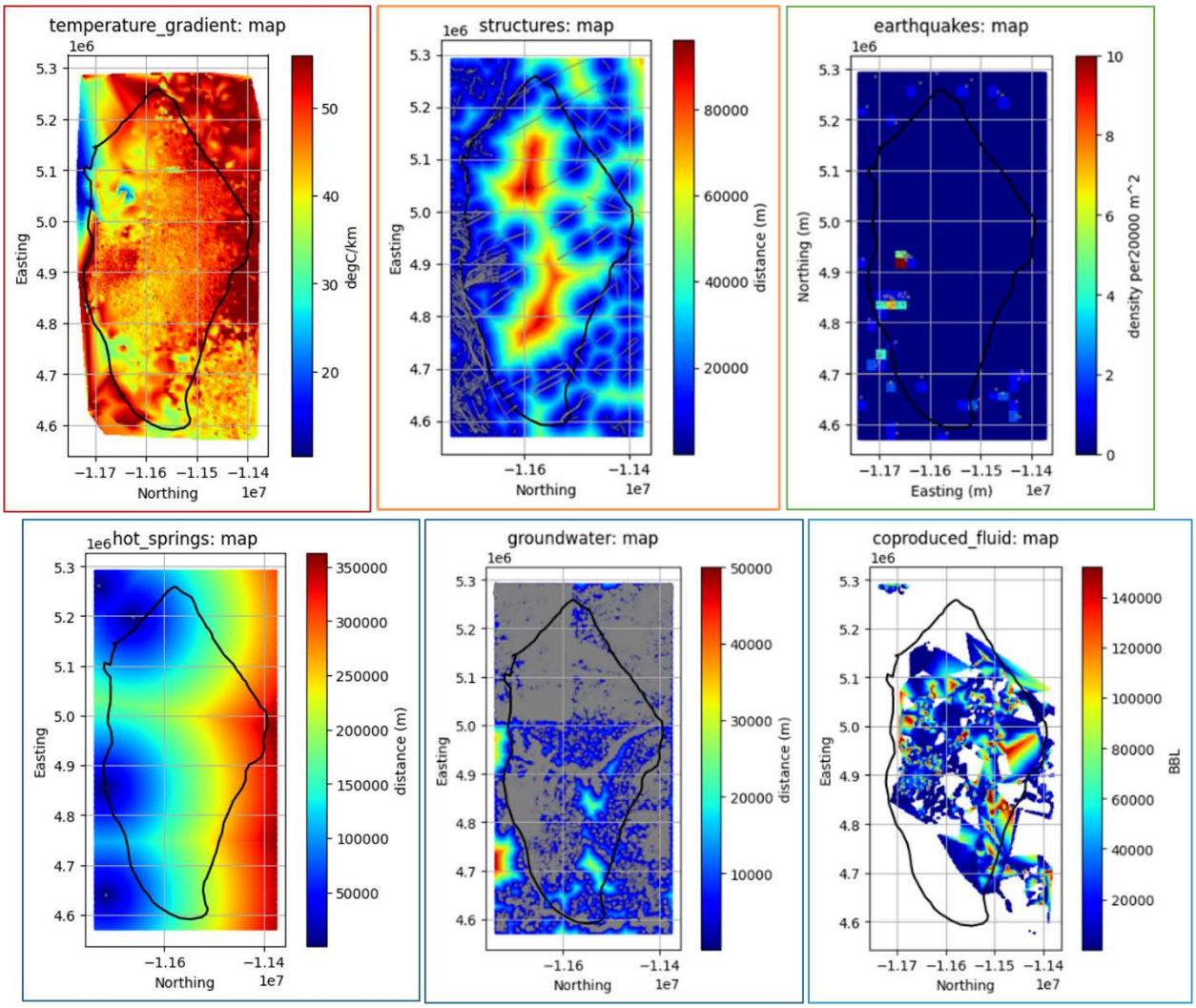

Figure 34. Processed data layers (or maps) input into geoPFA for geologic criteria favorability mapping, including layers associated with the heat (red border), permeability (orange border), and fluid (blue border) components

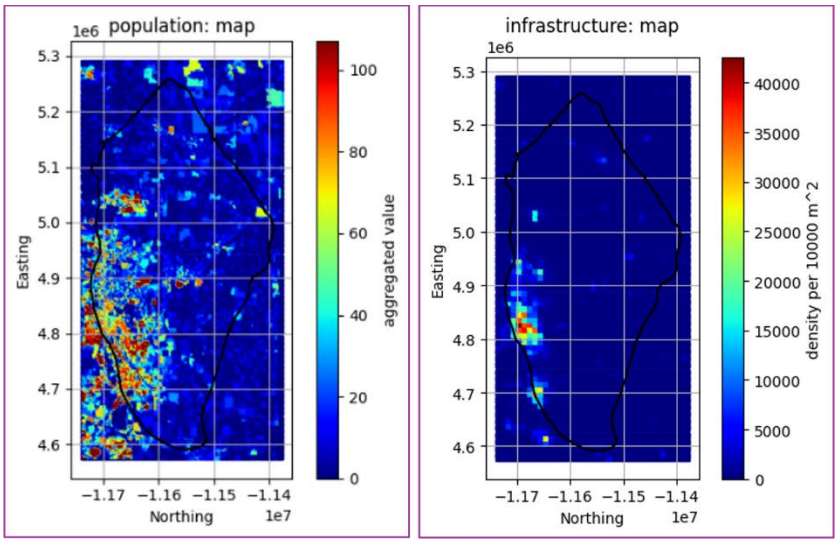

Figure 35. Processed data layers (or maps) input into geoPFA for economic criteria favorability mapping, including layers associated with the economic (purple border)

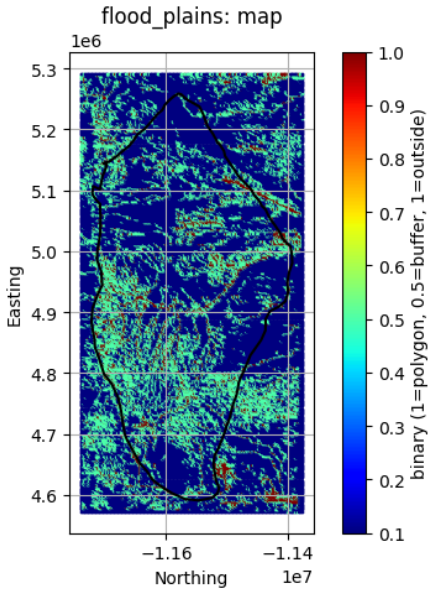

Figure 36. Processed data layers (or maps) input into geoPFA for safety criteria favorability mapping, including the flood plain layer associated with the natural disaster component

5.4 Transformation and Layer Combination

Next, all the data layers need to be converted into evidence layers. This involves normalizing and transforming (mapping data values to favorability values) each of the data layers. The evidence layers are then weighted and combined using the Voter-Veto method (Ito et al. 2017).

These steps are all built into the do_voter_veto function in the VoterVeto class because transformation methods are specific to a given layer combination method. Transformation

methods are additionally specific to a given data layer and are therefore specified in the configuration file for each data layer (Appendix A, Figure A.6). For example, lower distance from faults is more favorable than higher distance from faults, so the evidence layer is produced by multiplying the fault distance map by –1 ("negate" method). No transformation methods are applied to the temperature gradient and coproduced fluids data layers because higher values are more favorable. In the future, transformation methods will be improved to better represent probability distributions associated with data layers as they pertain to their respective components and criteria. This will enable mapping of probabilities rather than just relative favorability.

Each data layer is normalized using min-max normalization. This puts all datasets on the same, positive scale so that datasets with higher magnitudes do not dominate the results. Normalization may be done using either min-max or mean absolute deviation.

Figure A.6 in Appendix A shows that we are able to normalize, transform, weight, and combine all of the data layers using just one line of code and the information (i.e., prior probabilities, transformation methods) stored in the configuration file. This uses the do_voter_veto function from the VoterVeto class in geoPFA.

The do_voter_veto function is written to complete the following steps:

1. Converts the data from a Pandas GeoDataFrame into a rasterized array to allow linear algebra/matrix math
2. Transforms the data layers (map) into evidence layers (pr) using the transformation method specified for each data layer in the configuration file (if any) and then normalizing
3. Weights and combines evidence layers into component favorability maps using the Voter method with the evidence layer weights in the configuration file
4. Combines component favorability maps using the Veto method
5. Combines criteria favorability maps using the Veto method
6. Converts the rasterized favorability maps back into Pandas GeoDataFrames with the original geometry.

In other words, the weights and prior probabilities described in Table 4 are used in a modified version of the Voter-Veto equation (Ito et al. 2017). Within the Voter-Veto method proposed by Ito et al. (2017), the Voter method (generalized linear model) is used to combine data layers into component favorability maps. Then, the modified Veto equation (element-wise multiplication) is used to combine component favorability maps into a geologic criteria favorability map and to combine criteria maps into combined overall favorability maps, vetoing areas where any component criteria have a favorability value of 0. The original equations for this methodology are described in Section 2.1 of Ito et al. (2017), and our modified version of the Veto equation is as follows:

$$\Pr(R) = \frac{\sum^{c} w_c \Pr(X_c)}{\max[\sum^{c} w_c \Pr(X_c)]} \times \max[\prod^{c} \Pr(X_c)] \quad (5)$$

where Pr(R) is the probability of a resource, w_c is the weight of a given component or criteria, and Pr(X_c) is the probability of a given component or criteria. In written language, the equation produces a weighted some of the components or criteria, depending on which level the probability mapping is occurring on, normalizes by dividing by the maximum value, and scales using the product of the individual component or criteria probability maps to ensure that the resulting probability map represents a valid probability distribution. The veto portion of the equation is optional, but when desired, resulting indices in Pr(R) are set to zero if the associated indices in any Pr(X_c) are zero. In the methodology presented here, the veto option is used when combining criteria, but not when combining components.

The resulting evidence layers and component favorability maps are added to fav keys within their associated criteria/component/layer and criteria/component paths, respectively, within the pfa dictionary so that they can be plotted at any point throughout the process. The resulting component favorability maps are shown in Figures 37, 38, and 39. Note that since we only are inputting one data layer to map the heat component, the temperature gradient evidence layer is equivalent to heat component favorability map, but typically this is not the case.

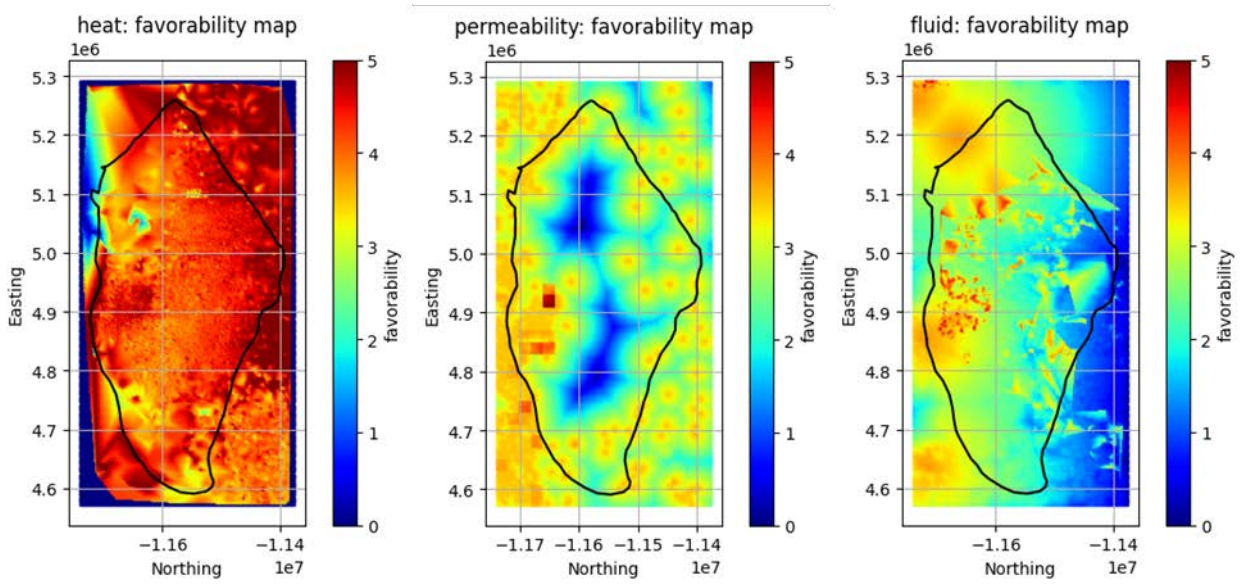

Figure 37. Geologic criteria component favorability maps, including heat, permeability, and fluid components, are produced using geoPFA

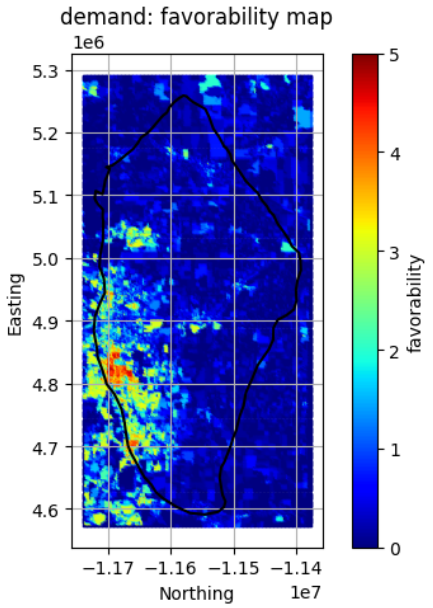

Figure 38. Economic criteria component favorability map, including demand and site accessibility components, produced using geoPFA

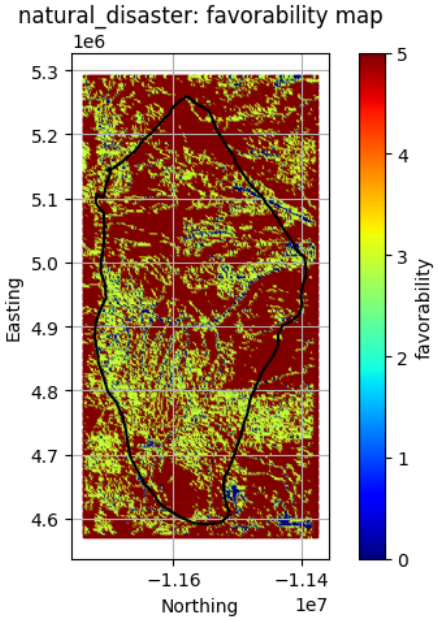

Figure 39. Safety criteria component favorability map, which currently only includes natural disaster favorability map based only on the flood plains layer, produced using geoPFA

The resulting criteria favorability maps are added to fav keys within their associated criteria paths (in this case, geologic) within the pfa dictionary, and the resulting combined favorability map (not yet generated) is stored under a fav key at the top level of the pfa dictionary. The draft criteria favorability maps produced by geoPFA are shown in Figure 40. Currently, the resulting probability maps are normalized onto a favorability scale due to unrealistic probability outputs.

In the future, more robust data transformation methods will be implemented to more realistically map data values to probability values.

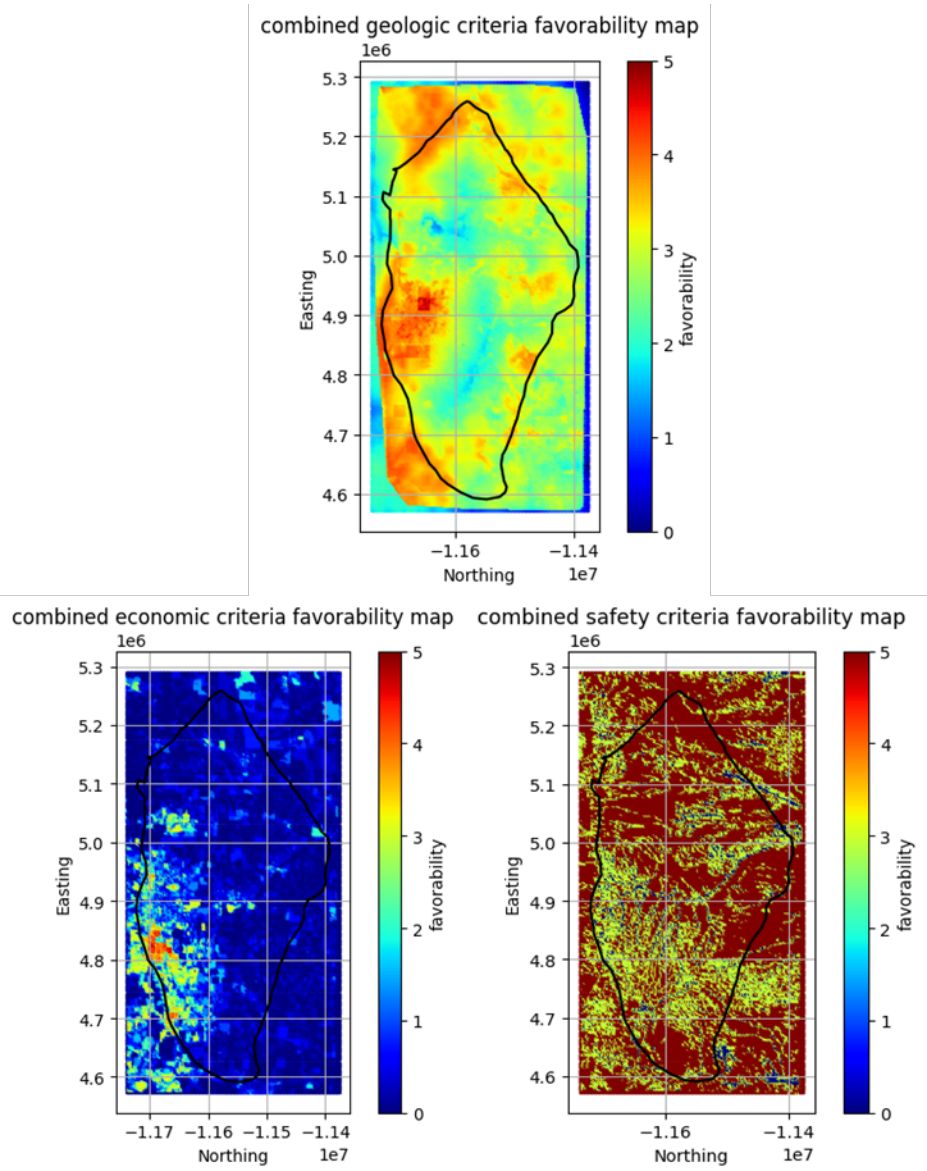

Figure 40. Combined criteria favorability maps of the Denver Basin produced using geoPFA, for geologic criteria (top), economic criteria (bottom left), and safety criteria (bottom right)

The draft combined favorability map, based on geologic, economic, and safety criteria, produced by geoPFA, is shown in Figure 41.

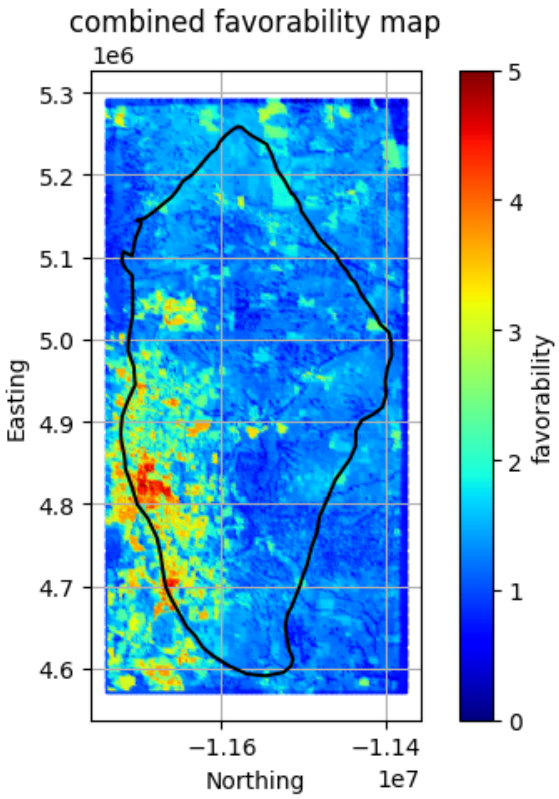

Figure 41. A combined overall favorability map of the Denver Basin, produced using geoPFA, based on geologic, economic, and safety criteria

5.5 Exclusion Layers

Lastly, exclusion areas are added to the combined favorability maps to display areas where development is not possible. To do so in geoPFA, the exclusion areas are read in using GeospatialDataReaders.read_shapefile. The resulting datasets are shown in Figure 42, including environmental habitat areas for lesser prairie chicken habitat, greater prairie chicken habitat, and protected areas data of the U.S., as well as National Park Service land.

Each exclusion area is masked using one line of code as shown in the screenshot of Figure A.7 in Appendix A. The code for masking exclusion areas is not as streamlined as the other code but will be improved in the future.

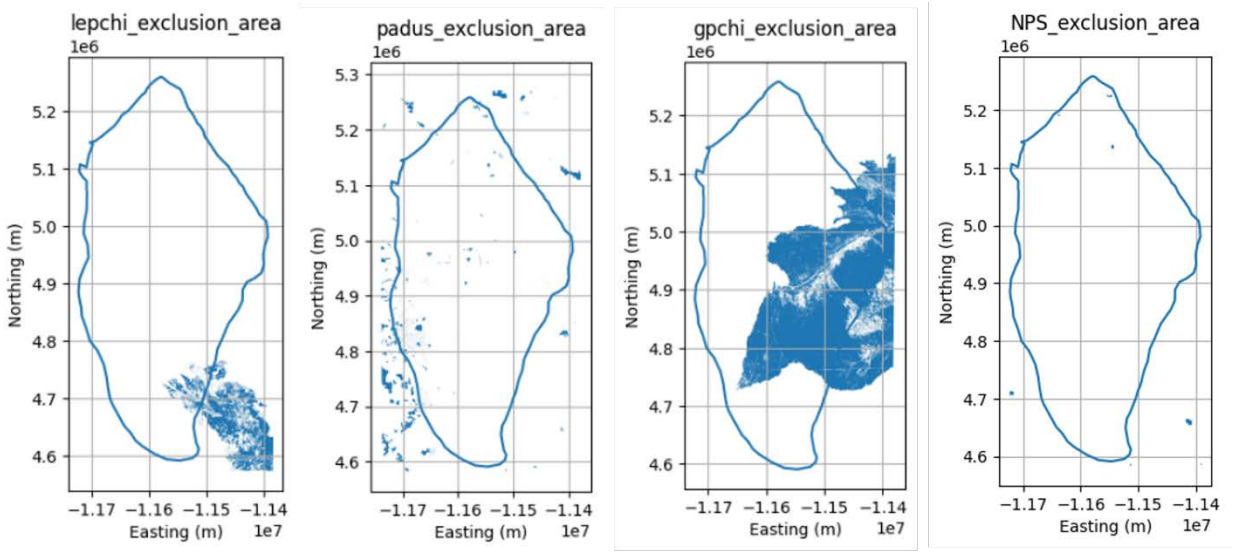

Figure 42. Raw data layers input into geoPFA for exclusion area mapping, including the environmental habitat areas (lesser prairie chicken habitat [LEPCHI], Protected Areas Data of U.S. [PADUS], greater prairie chicken habitat [GRPCHI]) and National Park Service (NPS) land

The final output is two combined favorability maps where grid squares within exclusion areas have zero favorability. An example is shown in Figure 43. Normalizing the outputs has improved this iteration by better highlighting the contrast in areas outside of the exclusion areas.

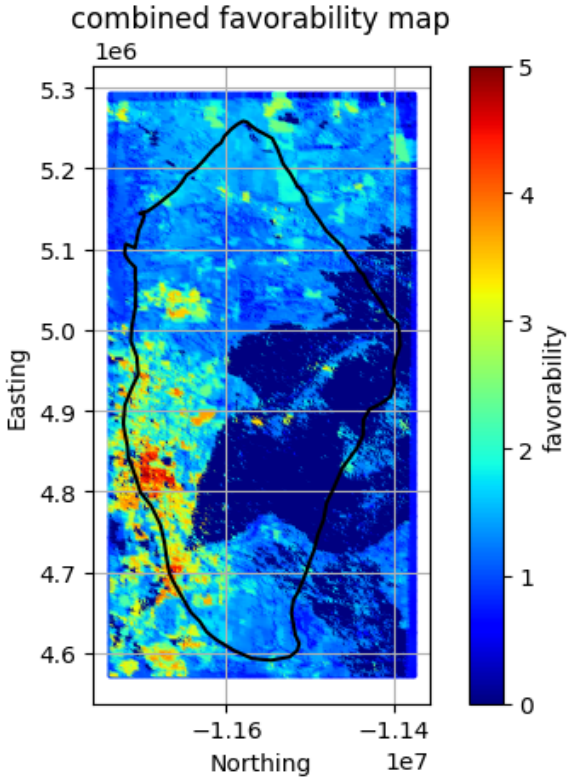

Figure 43. A combined overall favorability map of the Denver Basin, produced using geoPFA, based on geologic, economic, and safety criteria including data layers for exclusion areas: the environmental habitat areas and National Park Service land.

6 Results

6.1 Combined Criteria Favorability Map

The final resulting combined favorability maps are shown in Figure 44. The combined favorability maps appear to validate the methodology thus far. The maps highlight two areas to the west end of the Denver Basin where there appears to be geological favorability with the intersection between faults, some seismic activity, elevated temperature gradient values, ground water presence, hot springs, and relatively high volumes of coproduced fluids; economic favorability where high population and dense infrastructure is present (e.g., Denver metro area and Colorado Springs); and risk favorability where there are no hazard areas or the presence of exclusion environmental protected areas.

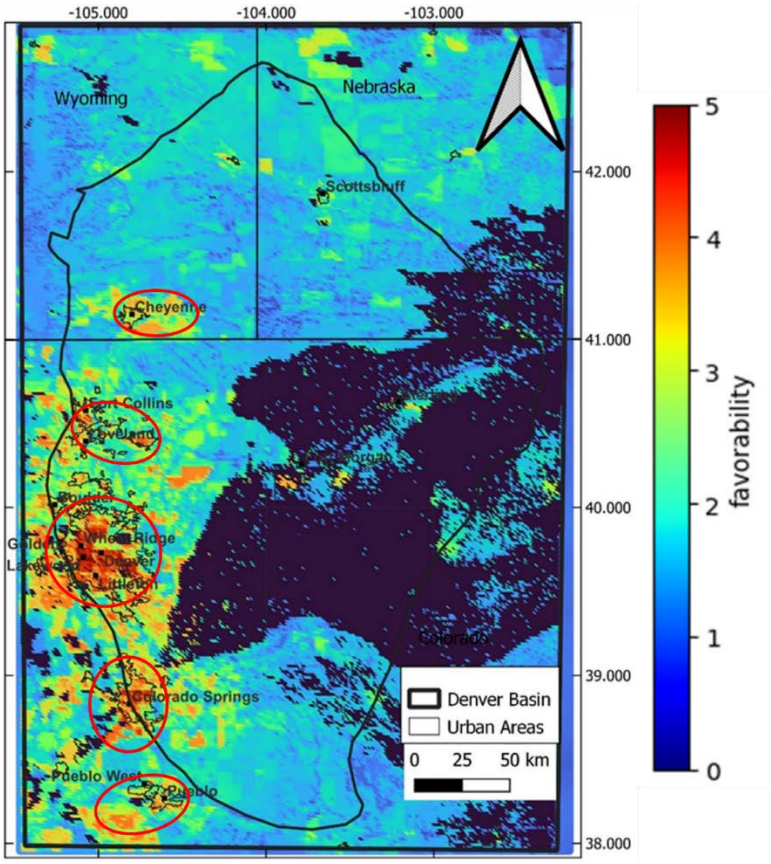

Figure 44. Combined criteria favorability map that includes geological, economic, and risk criteria for low- to high-temperature resources, along with five favorability areas (red circles) that indicate geothermal resource potential

The combined favorability map also highlights three less obvious areas to the human eye: southeastern Wyoming, where Cheyenne is located; northwestern Colorado, where Fort Collins and Loveland are found; and the southwestern region of the Denver Basin, where Pueblo West is situated.

6.2 Denver Metro Area Zoom-Ins

From the Denver Basin favorability maps, we can see that the Denver metro area is an area of significant favorability. To examine this area more closely, we can zoom in on the Denver metro area, as shown in Figures 45–48. The relevant maps (geologic criteria and combined favorability) are produced for a low to high temperature requirement (>30 °C) with potential localities for different GDU and CHP applications (see Section 6.3).

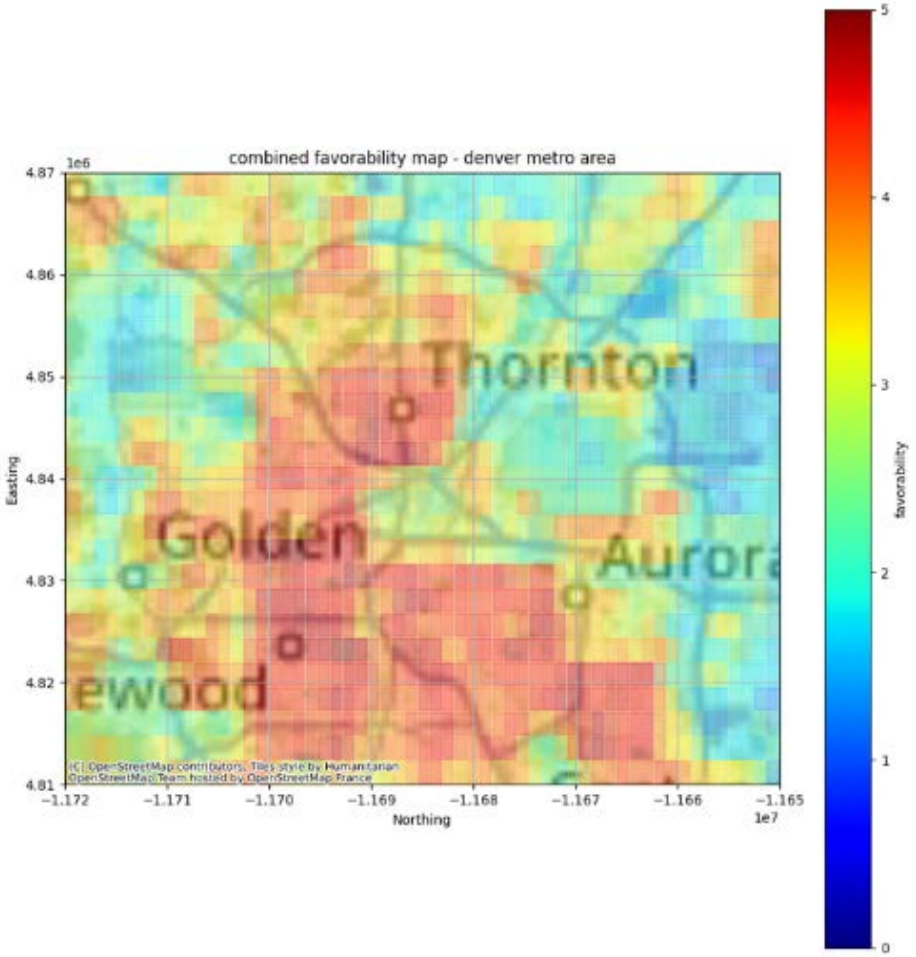

Figure 45. Combined favorability maps (geologic, economical, and risk criteria) for the Denver metro area for a low to high temperature requirement (>30°C)

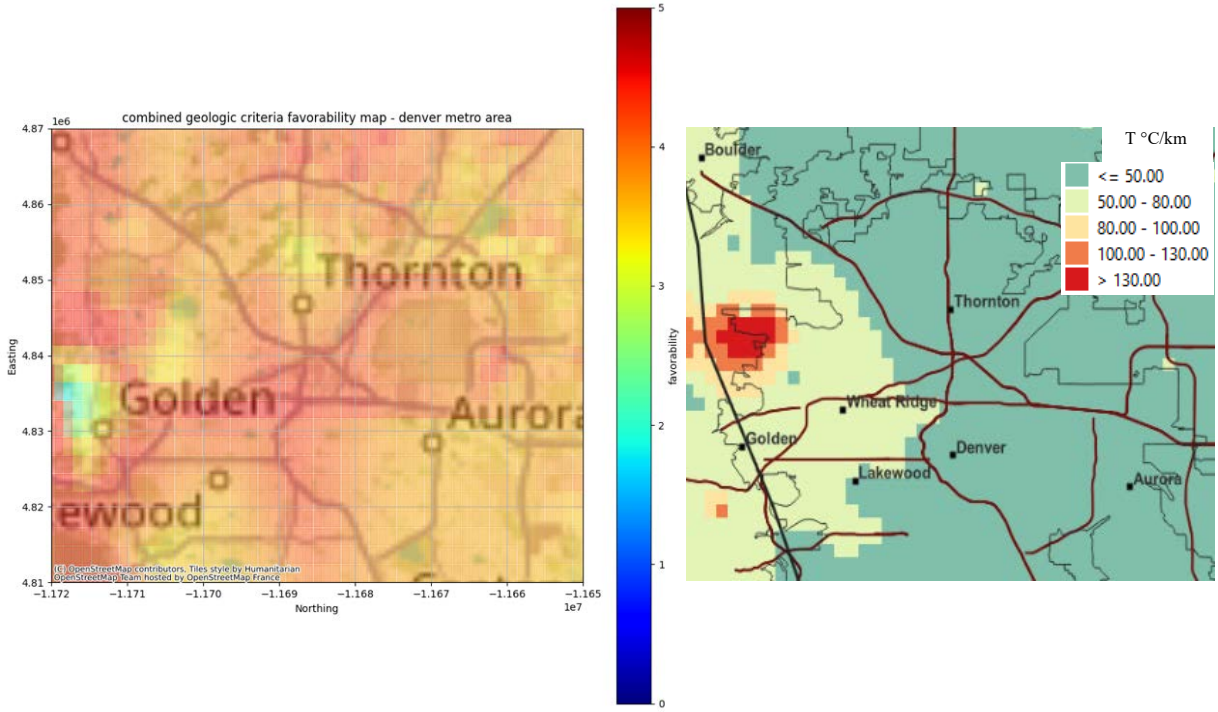

Figure 46. Geologic favorability maps for the Denver metro area for a low to high temperature requirement (left) and gradient temperature ranged from <50°C to >130°C at 1 km depth (right)

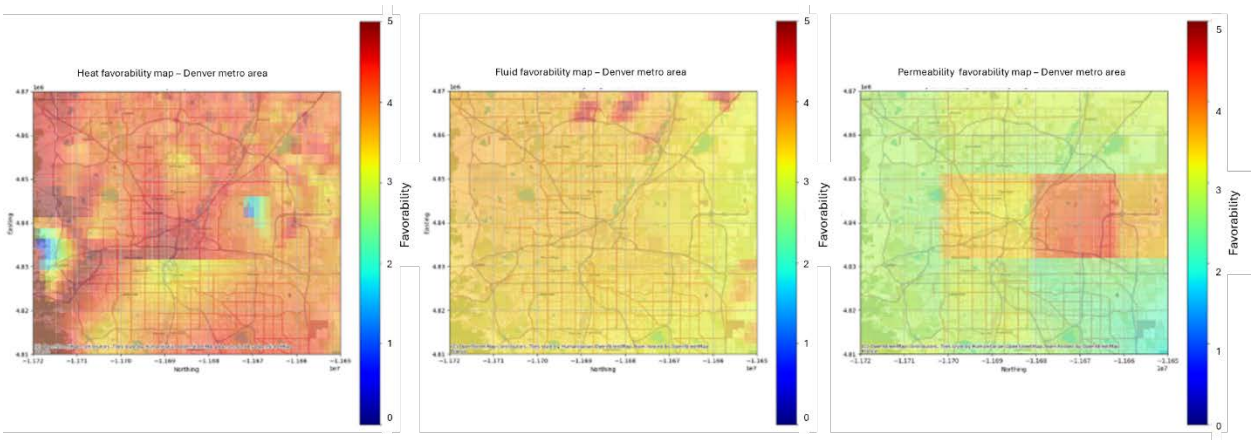

Figure 47. Heat (left), fluid (center), and permeability (right) favorability maps for the Denver metro area

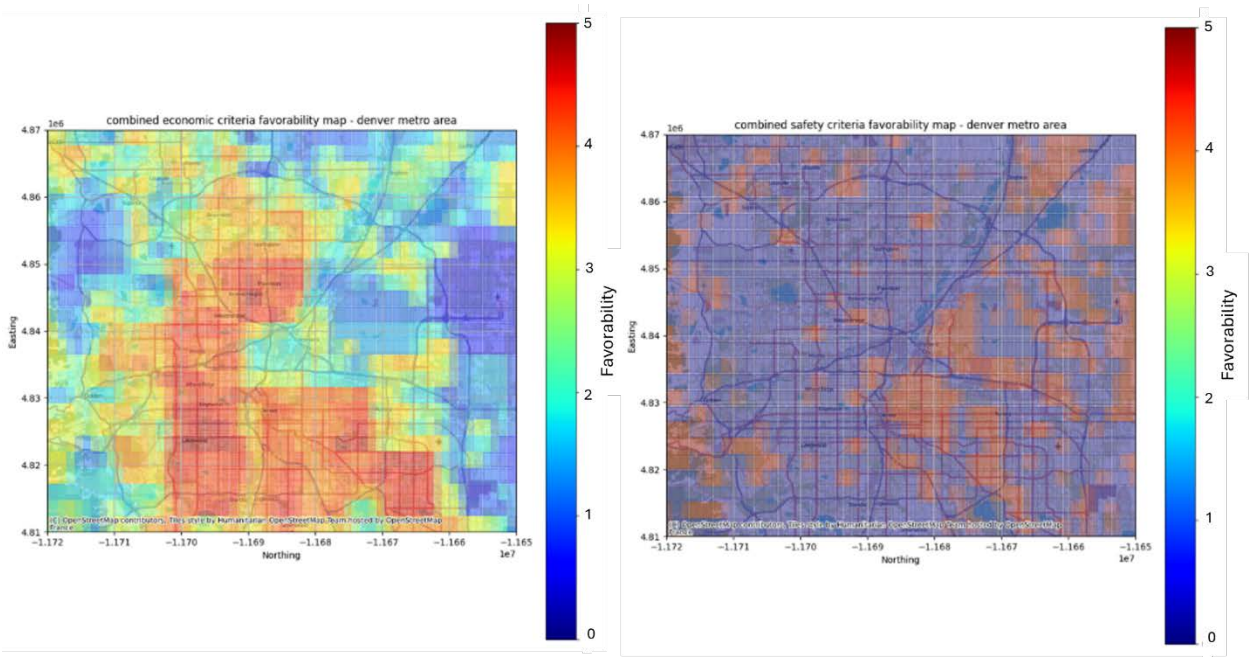

Figure 48. Economic (left) and safety (right) favorability maps for the Denver metro area

6.3 Gradient Temperature and Applications

The intended gradient temperature maps were created to identify potential locations that could support GDU (<150°C) and CHP (>150°C) at specific depth ranges depending on the application and compared to the uncertainty analysis maps.

Figure 49 shows a 30°C gradient temperature map at 0–1 km depth compared to the uncertainty analysis map at the same depth. This map illustrates low geothermal resources potential areas that could be utilized for GDU applications, such as fish farming, green houses, and heating buildings. Figure 50 shows a gradient temperature map of 60°C at depths between 500 m and 1.5 km compared to the uncertainty map at 1 to 1.5 km. Figure 51 shows a gradient temperature map of 90°C at depths between 1 km and 2 km compared to the uncertainty map at 1 to 1.5 km. The GDU applications for this temperature range between 60°C to 90°C could be green housing, food processing, industry process, such as concrete block drying, pulp and paper processing, and building heating. Lastly, Figure 52 shows a gradient temperature map of 150°C at 1.5 to 3 km depth that could identify potential areas for CHP applications in the Denver Basin.

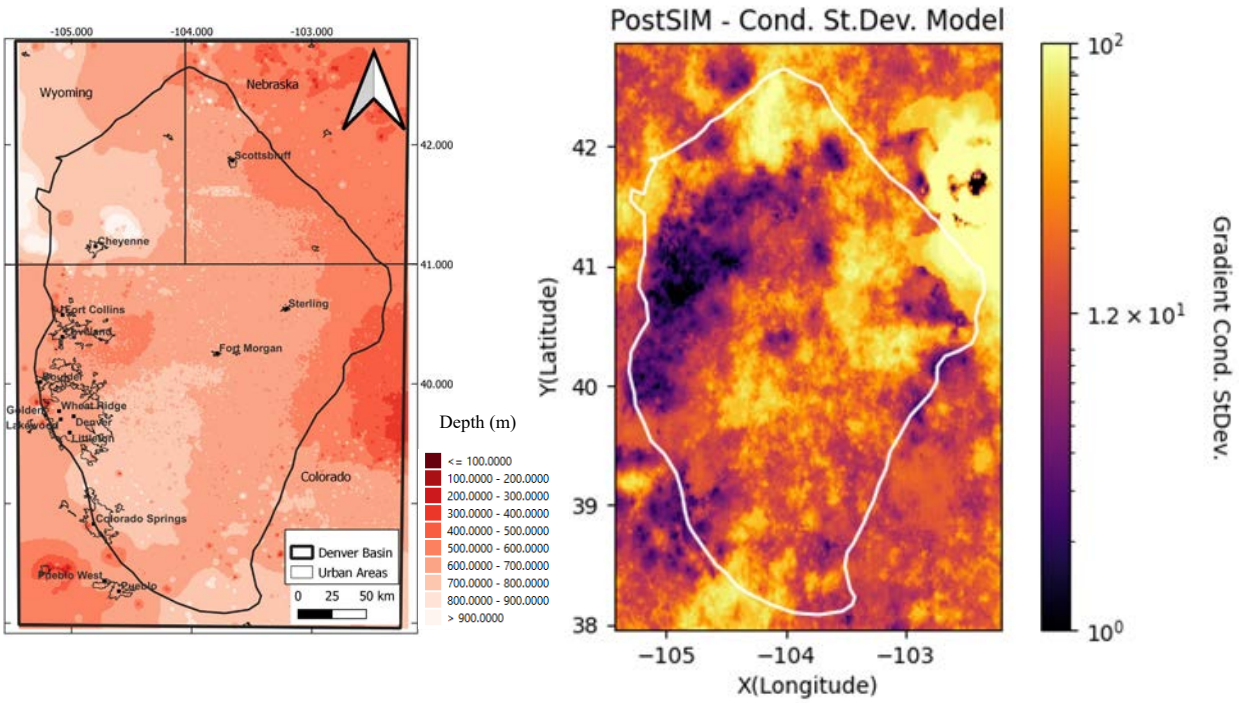

Figure 49. Gradient temperature at 30°C for depths 0–1 km (left). Temperature gradient uncertainty plot for depths 0–1 km (right).

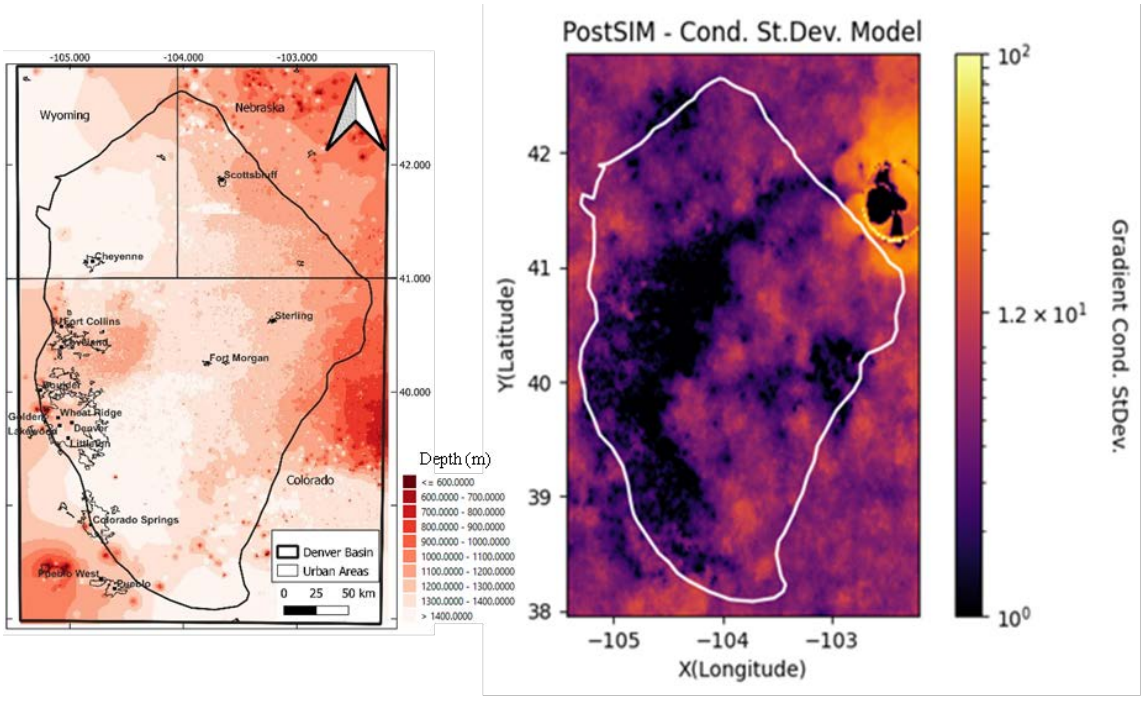

Figure 50. Gradient temperature at 60°C for depths 0.5–1.5 km (left). Temperature gradient uncertainty plot for depths 1–1.5 km (right).

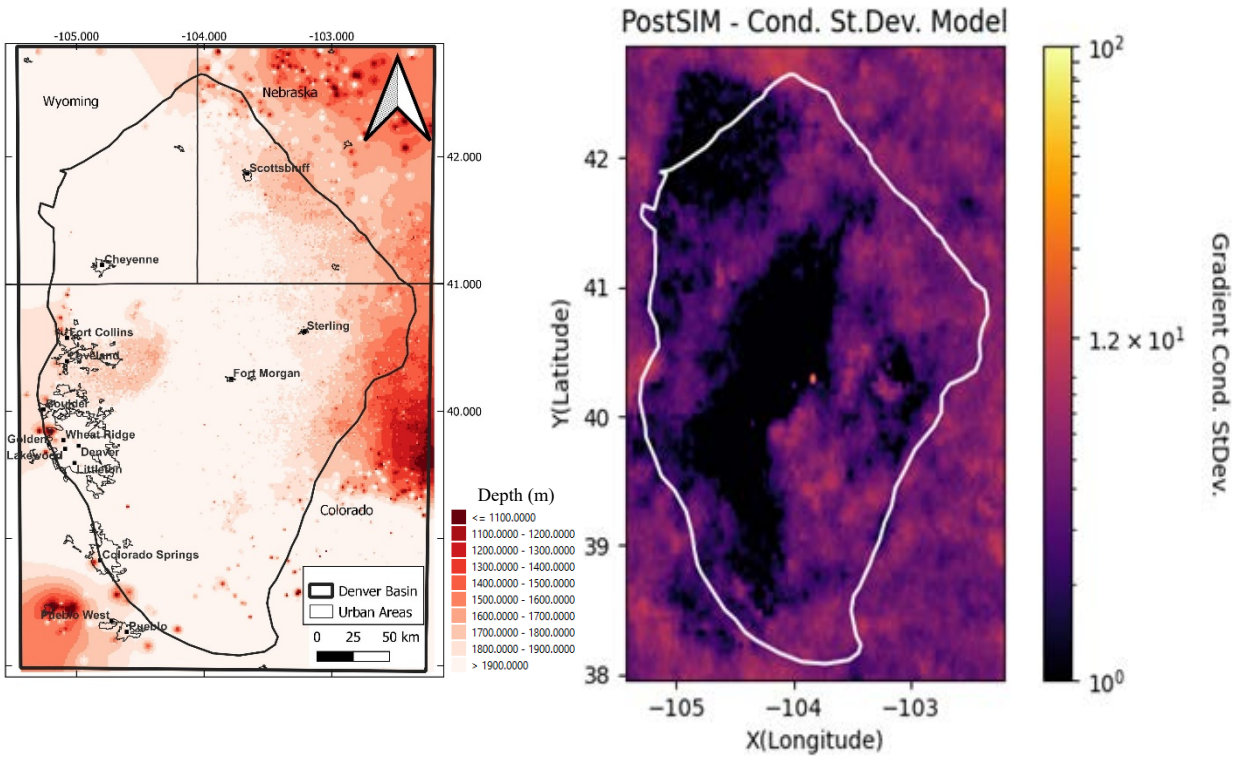

Figure 51. Gradient temperature at 90°C for depths 1–2 km (left). Temperature gradient uncertainty plot for depths 1.5–2 km (right).

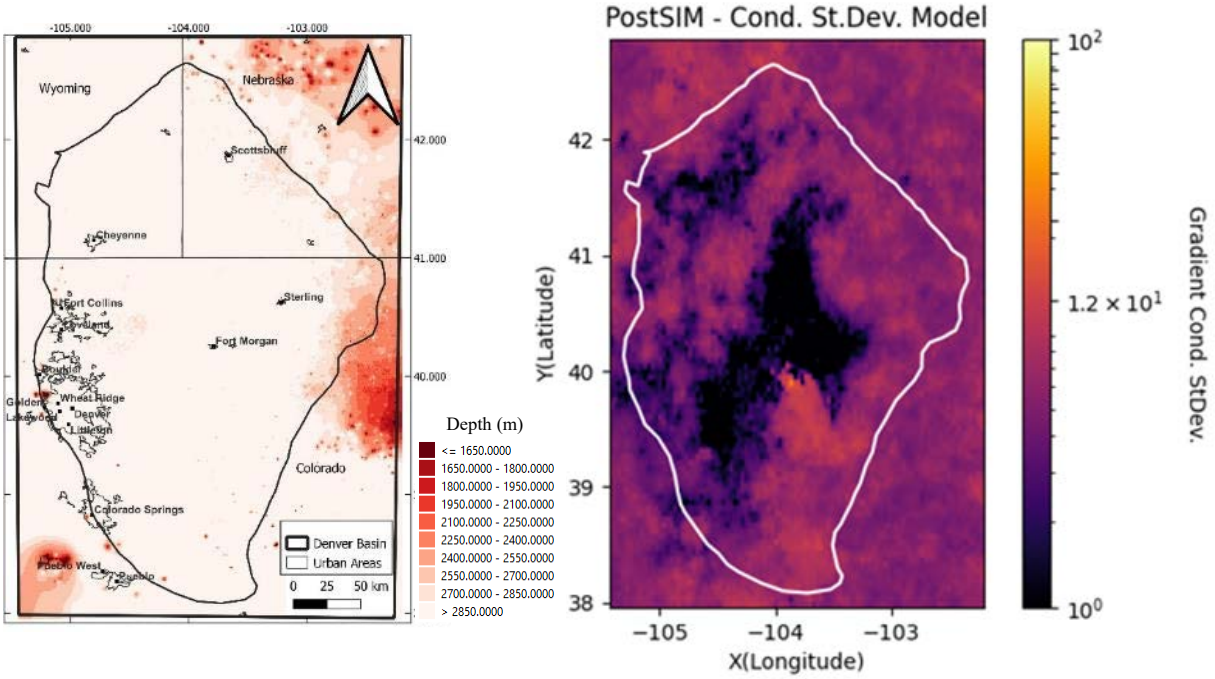

Figure 52. Gradient temperature at 150°C for depths 1.5–3 km (left). Temperature gradient uncertainty plot for depths 2–2.5 km (right).

7 Conclusions

In conclusion, this project aims to accelerate the country's decarbonization efforts by identifying opportunities for utilizing low-temperature geothermal resources (<150°C) in populous sedimentary basins. Considered geothermal applications include geothermal direct use and combined heat and power. The project has provided PFA workflows, data, tools, and favorability maps to support the utilization of low-temperature geothermal resources in the Denver Basin. Future improvements should focus on refining the methodology to ensure accurate and reliable results, ultimately facilitating future assessment of low-temperature geothermal resources in sedimentary basins and supporting the country's transition to a low-carbon economy.

We adapted PFA methodologies from previous studies of SBGPT to assess the potential viability to use low-temperature resources in the Denver Basin. The multi-methodological approach evaluated geological, economic, and risk criteria to identify data gaps and uncertainty quantification to develop favorability and common risk maps. The resulting favorability maps highlight areas with elevated potential for geothermal technology opportunities. The favorability maps also identify potential promising areas for further investigations, particularly in the western part of the Denver Basin, where numerous population centers are situated (e.g., Denver, Colorado Springs).

At the conclusion of this regional geothermal PFA in the Denver Basin, the primary technical needs for future improvement if this study were identified, ranked by their significance:

1. The distribution and capacity of reservoirs
2. The accuracy of thermal resource maps in focused areas
3. Need for additional information on permeability and fluid accessibility components, particularly those that provide information about primary permeability in the geological formations rather than only secondary permeability and flow raters
4. Incorporate additional high-quality data that provide enough information to create confidence layers, not only for the geothermal gradient data, but also for the permeability and fluid accessibility components of the geological criteria
5. Need for additional information on risk and economic criteria such as seismic, wildfire, and landslide risks, and a levelized cost of heat component
6. Refine prior probabilities and weights for each component.

Additionally, to establish a functioning geothermal heat supply and usage system in any part of the study area, further preparatory work related to permitting and public awareness is essential.

Likewise, future directions for the geoPFA library are:

- Improve methodology for fault mapping. In the current method, we see circular anomalies centered at the center of each fault. To be more informative and reflective of faults as a proxy for permeability, the fault evidence layer map should highlight more rectangular anomalies that better follow the faults, and the method should better highlight intersections and dense fault areas. A new and improved version of the

distance_from_lines function, particular for fault distance, density, and intersection mapping, is currently being developed within geoPFA.

- Implement additional/more intelligent transformation methods to better map data values to probability values. The current transformation methods are based on relative relationships between data values and favorability, making them pseudo-probabilities rather than actual probabilities. Because of this, the final probability outputs are normalized onto a favorability scale to improve interpretability. More intelligent transformation methods will enable more realistic and informative probability mapping.
- Improve interpolations in Python code, potentially through implementation of IDW. The current interpolation methods generate maps that are chaotic and not very coherent. More time will be spent in the future investigating other interpolation methods that can be implemented in Python and may give better results.
- Incorporate tools for uncertainty quantification into the geoPFA library. In the workflow presented here, the uncertainty quantification is done outside of the geoPFA workflow. In the future, uncertainty quantification tools will be merged into geoPFA.
- Build in other layer combination methods (e.g. weights of evidence) to allow comparison between these methods. The Voter-Veto method was chosen in this iteration because it is the easiest and most recommended method from the Best Practices Report (Pauling et al. 2023) without having labelled training sites. There are workarounds for applying weights of evidence without training sites, but they are difficult to execute effectively. These workarounds could (with more time) be built into the code (Moghaddam et al., 2013).
- Use parallelization, spatial indexing, vectorization, a more efficient data structure to store the pfa object, and better adherence to software development best practices within geoPFA to make it more efficient, scalable, and transferrable.

Finally, the development of favorability maps for low-temperature geothermal resources serves as a critical tool for pinpointing potential locations for targeted data collection. This study successfully identified five key favorability areas with significant geothermal resource potential, underscoring the importance of these regions for future exploration. We recommend undertaking a Phase I detailed assessment in each of these identified areas, following the workflow established in this research. This approach will enable us to systematically evaluate available datasets, identify data gaps, and develop strategic plans for future data collection in each of these areas. By following these recommendations, stakeholders can enhance their understanding of low-temperature geothermal resources in SBGPT, facilitating informed decision-making and promoting sustainable development in these promising regions.

References

Anderson, T.C., 2013. Geothermal potential of deep sedimentary basins in the United States. In Unconventional resources technology conference. Society of Exploration Geophysicists, American Association of Petroleum Geologists, Society of Petroleum Engineers, pp. 1969-1978.

Arcgis.com. 2021. "Census 202 Redistricting Blocks FGDB." https://www.arcgis.com/home/item.html?id=778bd6d573f54bf188753b0276c11d1c.

Augustine, C. 2014. "Analysis of Sedimentary Geothermal Systems Using an Analytical Reservoir Model." *Geothermal Resources Council Transactions* 38: 641–647. https://www.geothermal-library.org/index.php?mode=pubs&action=view&record=1033602.

Barrett, J.K., and Pearl, R.H., 1978, An appraisal of Colorado's geothermal resources: Colorado Geol. Survey Bull. 39, 224 p.

Blackwell, D. D., M. and Richards. 2004. "Calibration of the AAPG Geothermal Survey of North America BHT Data Base." Presented at American Association of Petroleum Geologists Annual Meeting 2004 Poster session, Dallas, Texas. Paper 87616.

Blackwell, D.D., P.T. Negraru, and M.C. Richards. 2007. "Assessment of the Enhanced Geothermal System Resource Base of the United States." *Natural Resources Research* 15: 283–308. https://doi.org/10.1007/s11053-007-9028-7.

Bryant, B. and Naeser, C.W., 1980. The significance of fission-track ages of apatite in relation to the tectonic history of the Front and Sawatch Ranges, Colorado. Geological Society of America Bulletin, 91(3), pp.156-164.

Coleman Jr, J.L. and Cahan, S.M., 2012. Preliminary catalog of the sedimentary basins of the United States.

Crowell, A.M., A.T. Ochsner, and W. Gosnold. 2012. Correcting bottom-hole temperatures in the Denver Basin: Colorado and Nebraska. GRC Transactions, 36(GRC1030229).

Davalos-Elizondo, E., A. Kolker, N. Taverna, and E. Holt. 2023. *Assessing Low-Temperature Geothermal Play Types: Relevant Data and Play Fairway Analysis Methods.* Golden, CO: National Renewable Energy Laboratory. NREL/TP-5700-87259. https://www.nrel.gov/docs/fy23osti/87259.pdf.

Deutsch, C.V., and A.G. Journel. 1998. *GSLIB: Geostatistical Software Library and User's Guide*. New York: Oxford University Press.

Dixon, J.M. 2002. "OF-02015 Evaluation of Bottom-Hole Temperatures in the Denver and San Juan Basins of Colorado." Denver, CO: Colorado Geological Survey, Division of Minerals and Geology, Department of Natural Resources. https://coloradogeologicalsurvey.org/publications/evaluation-bottom-hole-temperatures-denver-san-juan-basins-colorado/.

Doughty, C., P.F. Dobson, A. Wall, T. McLing, and C. Weiss. 2018. *GeoVision Analysis Supporting Task Force Report: Exploration*. Berkeley, CA: Lawrence Berkeley National Laboratory. LBNL-2001120. https://www.osti.gov/biblio/1457012.

Erslev, E.A., and B. Selvig. 1997. "Thrusts, Backthrusts and Triangle Zones: Laramide Deformation in the Northeastern Margin of the Colorado Front Range." AAPG/Datapages Combined Publications Database. https://archives.datapages.com/data/rmag/geohistfrontrange1997/erslev_b.htm.

Filina, I., M. Searls, K. Guthrie, and C.M. Burberry. 2018. "Seismicity in Nebraska and Adjacent States: The Historical Perspective and Current Trends." University of Nebraska. https://eas.unl.edu/Filina%20et%20al%20MG%20Dec%202018.pdf.

Fishman, N.S., ed. 2005. "Energy Resource Studies, Northern Front Range, Colorado." Denver, CO: U.S. Geological Survey. Professional Paper 1698. https://doi.org/10.3133/pp1698.

Förster, A., Merriam, D.F., and Davis, J.C., 1996, Statistical analysis of some bottom-hole temperature (BHT) correction factors for the Cherokee Basin, southeastern Kansas: Tulsa Geol. Soc. Trans., pp. 3-9.

Harrison W.E., K.V. Luza, M.L. Prater, and P.K. Chueng. 1983. *Geothermal Resource Assessment in Oklahoma*. Norman, OK: Oklahoma Geological Survey. Special Publication 83-1. http://ogs.ou.edu/docs/specialpublications/SP83-1.pdf.

Hartmann, D.J., E.A. Beaumont, and E. Coalson. 2000. "Predicting Sandstone Reservoir System Quality and Example of Petrophysical Evaluation." *Search and Discovery* Article 40005. https://www.searchanddiscovery.com/documents/beaumont/index.htm.

Heidbach, O., M. Rajabi, X. Cui, K. Fuchs, B. Müller, J. Reinecker, K. Reiter, et al. 2018. "The World Stress Map Database Release 2016: Crustal Stress Pattern Across Scales." *Tectonophysics* 744: 484–498. https://doi.org/10.1016/j.tecto.2018.07.007.

Hemborg, T., 1993a, Codell Sandstone and Niobrara Formation (Wattenberg area), in Atlas of major Rocky Mountain gas reservoirs: New Mexico Bureau of Mines and Mineral Resources, p. 107-108.

Hemborg, T., 1993b, Niobrara chalk biogenic gas, in Atlas of major Rocky Mountain gas reservoirs: New Mexico Bureau of Mines and Mineral Resources, p. 109-111.

Hemborg, T., 1993c, D Sand, in Atlas of major Rocky Mountain gas reservoirs: New Mexico Bureau of Mines and Mineral Resources, p. 112-113.

Hemborg, T., 1993d, Muddy (J) Sandstone, in Atlas of major Rocky Mountain gas reservoirs: New Mexico Bureau of Mines and Mineral Resources, p. 113-114.

Higley, D.K., and Cox, D.O., 2007, Oil and gas exploration and development along the Front Range in the Denver Basin of Colorado, Nebraska, and Wyoming, Chap. 2, in Higley, D.K., compiler, Petroleum systems and assessment of undiscovered oil and gas in the Denver Basin Province, Colorado, Kansas, Nebraska, South Dakota, and Wyoming—USGS Province 39: U.S. Geological Survey Digital Data Series 69–P, 40 p., accessed September 2011, at http://pubs.usgs.gov/dds/dds-069/dds-069-p/REPORTS/69_p_CHAP_LIST.pdf

Higley, D.K., and Gautier, D.L., 1988, Burial history reconstruction of the Lower Cretaceous J sandstone in the Wattenberg Field, Colorado, "hot spot", in Carter, L.M.H., ed., U.S. Geological Survey Research on Energy Resources; V.E. McKelvey Forum on Mineral and Energy Resources: U.S.Geological Survey Circular 1025, p. 20.

Higley, D.K., and Schmoker, J.W., 1989, Influence of depositional environment and diagenesis on regional porosity trends in the Lower Cretaceous "J" sandstone, Denver Basin, Colorado, in Coalson, E. B., ed., Petrogenesis and petrophysics of selected sandstone reservoirs in the Rocky Mountain region: Rocky Mountain Association of Geologists, p. 183-196.

Hjellming, C.A., ed., 1993, Stratigraphic correlation chart of major gas-producing basins and uplifts, in Atlas of major Rocky Mountain gas reservoirs: New Mexico Bureau of Mines and Mineral Resources, sheet 2.

Hoyt, J.H., 1963, Permo-Pennsylvanian and Lower Permian of the northern Denver Basin, in Bolvard, D.W., and Katich, P.J., eds., Guidebook to the geology of the northern Denver Basin and adjacent uplifts: 14th Annual Field Conference 1963, Rocky Mountain Association of Geologists, p. 68–83.

Irwin, D., compiler, 1977, Subsurface cross-sections of Colorado: Rocky Mountain Association of Geologists Special Publication No. 2.

Isaac, E., Srivastava, R.M., 1989. An introduction to applied geostatistics. Oxford University Press, New York.

Ito, G., N. Frazer, N. Lautze, D. Thomas, N. Hinz, D. Waller, R. Whittier, E. Wallin. 2017. "Play Fairway Analysis of Geothermal Resources Across the State of Hawaii: 2. Resource Probability Mapping." *Geothermics* 70: 393–405. https://doi.org/10.1016/j.geothermics.2016.11.004.

Johnston, Henry, Amanda Kolker, Greg Rhodes, and Nicole Taverna. 2020. Sedimentary Geothermal Resources in Nevada, Utah, Colorado, and Texas. Golden, CO: National Renewable Energy Laboratory. NREL/TP-5500-76513. https://www.nrel.gov/docs/fy20osti/76513.pdf.

Kolker, A., Young, K.R., Badgett, A. and Bednarek, J., 2019. GeoRePORT Case Study Examples: Reporting Using the Geothermal Resource Portfolio Optimization and Reporting Technique (GeoRePORT) (No. NREL/CP-5500-73922). National Renewable Energy Lab.(NREL), Golden, CO (United States).

Krige DG 1951. A statistical approach to some basic mine valuation problems on the Witwatersrand. Mining Society South Africa 52:119-139.

MacLachlan, M.E., Bryant, W.A., Judkins, T.W., Williams, O.B., Koozmin, E.D., Orndorff, R.C., Hubert, M.I., Murdock, C.R., Starratt, S.W., LeCompte, J.R., and Hubert, M.L., eds., 1996, Stratigraphic nomenclature databases for the United States, its possessions, and Territories: U.S. Geological Survey Digital Data Series DDS–6, release 3, 1 CD-ROM

Meyer, H.J., and McGee, H.W., 1985, Oil and gas fields accompanied by geothermal anomalies in Rocky Mountain region: American Association of Petroleum Geologists Bulletin, v. 69, p. 933-945.

Mibei, G., Gold, A., Kolker, A., Dayo., A., Koenraad., B. 2024, Geothermal Reservoir Characterization at Wattenberg area in Denver Basin. Geothermal Resources Council Transactions: Poster Presentation.

Moeck, I.S. 2014. "Catalog of Geothermal Play Types Based on Geologic Controls." *Renewable and Sustainable Energy Reviews*, 37: 867–882. https://doi.org/10.1016/j.rser.2014.05.032.

Moghaddam, M.K., Y. Noorollahi, F. Samadzadegan, M.A. Sharifi, and R. Itoi. 2013. "Spatial Data Analysis for Exploration of Regional Scale Geothermal Resources." *Journal of Volcanology and Geothermal Research* 266: 69–83. https://doi.org/10.1016/j.jvolgeores.2013.10.003.

Momper, J.A., 1963, Nomenclature, lithofacies and genesis of Permo-Pennsylvanian rocks; northern Denver Basin, in Bolvard, D.W., and Katich, P.J., eds., Guidebook to the geology of the northern Denver Basin and adjacent uplifts: 14th Annual Field Conference, Rocky Mountain Association of Geologists, p. 41–47.

Oh, H. and Beckers, K., 2023. Geospatial Characterization of Low-Temperature Heating and Cooling Demand in the United States (No. NREL/CP-5700-84708). National Renewable Energy Lab.(NREL), Golden, CO (United States).

OpenEI Geothermal Resource Reporting. No date. "GeoRePORT Protocol Documents." https://openei.org/wiki/GeoRePORT/Protocol#top.

OpenEI RAPID. No date. "Geothermal Regulations and Permitting." https://openei.org/wiki/RAPID/Geothermal/Jurisdictions.

Pauling, H., N. Taverna, W. Trainor-Guitton, E. Witter, A. Kolker, I. Warren, J. Robins, and G. Rhodes. 2023. *Geothermal Play Fairway Analysis Best Practices*. Golden, CO: National Renewable Energy Laboratory. NREL/TP-5700- 86139. https://www.nrel.gov/docs/fy23osti/86139.pdf.

Porro, C., Esposito, A., Augustine, C. and Roberts, B., 2012. An estimate of the geothermal energy resource in the major sedimentary basins in the United States. Geothermal Resources Council Transactions, 36, pp.1359-1369.

Pyrcz, M.J. 2024. *Applied Geostatistics in Python: A Hands-on Guide with GeostatsPy*. e-Book: https://geostatsguy.github.io/GeostatsPyDemos_Book.

Pyrcz, M.J., H. Jo, A. Kupenko, W. Liu, A.E. Gigliotti, T. Salomaki, and J. Santos. 2021. "GeostatsPy Python Package, PyPI, Python Package Index." https://pypi.org/project/geostatspy/.

Reber, T., 2013. Evaluating opportunities for enhanced geothermal system-based district heating in New York and Pennsylvania.

Rubin, R., Young, K.R., Badgett, A., Kolker, A., Levine, A., Wall, A., Witter, E. and Dobson, P.F., 2022. GeoRePORT Protocol Volume II: Geological Assessment Tool (No. NREL/TP-5700-81749). National Renewable Energy Lab.(NREL), Golden, CO (United States).

Shervais, J.W., J.M. Glen, D.L. Nielson, S. Garg, L.M. Liberty, D. Siler, P. Dobson, E. Gasperikova, E. Sonnenthal, G. Neupane, and J. DeAngelo. 2017. *Geothermal Play Fairway Analysis of the Snake River Plain: Phase 2*. Idaho Falls, ID: Idaho National Laboratory. INL/CON-17-42832. https://www.osti.gov/biblio/1402043.

Sims, P.K., Finn, C. and Rystrom, V.L., 2001. Preliminary Precambrian basement map showing geologic-geophysical domains, Wyoming (p. 9). The Survey.

Sonnenberg, S.A., and Weimer, R.J., 1981, Tectonics, sedimentation, and petroleum potential, northern Denver Basin, Colorado, Wyoming, and Nebraska: Golden, Colorado School of Mines Quarterly, v. 76, no. 2, 45 p.

Spicer, H.C. 1964. *A Compilation of Deep Earth Temperature Data. U.S.A. 1910–1945*. U.S Geological Survey. Open-File Report 64-167. https://doi.org/10.3133/ofr64147.

Sangwan, N. and Merwade, V., 2015. A faster and economical approach to floodplain mapping using soil information. JAWRA Journal of the American Water Resources Association, 51(5), pp.1286-1304.

Tweto, O., 1979. The Rio Grande rift system in Colorado. Rio Grande rift: Tectonics and magmatism, 14, pp.33-56.

U.S. Geological Survey. 2005. Colorado faults, from the USGS Geologic Map Database (Open-File Report). U.S. Geological Survey. Retrieved April 15, 2024, from https://www.sciencebase.gov/catalog/item/4f4e496be4b07f02db5a0f59

U.S. Census Bureau. 2021. "2021 TIGER/Line® Shapefiles: Roads." https://www.census.gov/cgi-bin/geo/shapefiles/index.php?year=2021&layergroup=Roads.

U.S. Geological Survey. 2022. "USGS CO2Viewer." https://co2public.er.usgs.gov/viewer/%0A.

U.S. Geological Survey. No date. "National Geospatial Program: The National Map." https://www.usgs.gov/programs/national-geospatial-program/national-map.

Weimer, R.J., 1996, Guide to the petroleum geology and Laramide orogeny, Denver Basin and Front Range, Colorado: Colorado Geological Survey Bulletin 51, 127 p.

Weimer, P., and T.L. Davis, eds. 1996. *Applications of 3-D Seismic Data to Exploration and Production (Vol. 5)*. Published jointly by the American Association of Petroleum Geologists and the Society of Exploration Geophysics.

Weimer, R.J., and S.A. Sonnenberg. 1996. *Bulletin 51 – Guide to the Petroleum Geology and Laramide Orogeny, Denver Basin and Front Range, Colorado*. Denver, CO: Colorado Geological Survey, Department of Natural Resources. https://doi.org/10.58783/cgs.b51.bsvl1261.

Whealton, C. 2015. *Statistical Correction of Temperature Data for New York and Pennsylvania Wells*. M.S. thesis, Cornell University. http://hdl.handle.net/1813/40609.

Whealton, C.A. 2016. *Statistical Data Analysis, Global Sensitivity Analysis, and Uncertainty Propagation Applied to Evaluating Geothermal Energy in the Appalachian Basin*. Ph.D. dissertation, Cornell University.

Wolfgramm, M., K. Obst, K. Beichel, J. Brandes, R. Koch, K. Rauppach, and K. Thorwart. 2009. Produktivitätsprognosen geothermischer aquifere in Deutschland. Der Geothermiekongress, pp.17–19.

Wyoming State Geological Survey (WSGS). (2014, June 30). Wyoming faults 500k [Vector digital data]. Wyoming State Geological Survey. http://www.wsgs.wyo.gov/gis-files/faults-500k.zip

Wyoming Water Development Commission. 2024. "WWDC GIS Standards, Tools, and Data." https://water.geospatialhub.org/pages/wwdc-gis-standards.

Yamamoto, J.K. 2005. "Correcting the Smoothing Effect of Ordinary Kriging Estimates." *Mathematical Geology* 37 (1): 69–94. https://doi.org/10.1007/s11004-005-8748-7.

Yuan, H., and B. Romanowicz. 2010. "Lithospheric Layering in the North American Craton." *Nature* 466(7310): 1063–1068. https://doi.org/10.1038/nature09332.

Appendix A. Screenshots of the geoPFA Python Library Configuration and Workflow


```
{
 "criteria": {
  "geologic": {
   "weight": 0.35,
   "components": {
    "heat": {
     "weight": 0.4,
     "layers": {
      "temperature_gradient": {
       "weight": 1,
       "units": "degC/km",
       "data_col": "Gradient",
       "transformation_method": "none",
       "processing_method": "interpolate"
      }
     },
     "pr0": 0.65
    },
    "permeability": {
     "weight": 0.3,
     "layers": {
      "structures": {
       "weight": 0.5,
       "units": "NA",
       "data_col": "None",
       "transformation_method": "negate",
       "processing_method": "distance"
      },
      "earthquakes": {
       "weight": 0.25,
       "units": "NA",
       "data_col": "None",
       "transformation_method": "none",
       "processing_method": "density"
      }
     },
     "pr0": 0.65
    },
    "fluid": {
     "weight": 0.3,
     "layers": {
      "hot_springs": {
       "weight": 0.5,
```

```
      "units": "NA",
      "data_col": "None",
      "transformation_method": "negate",
      "processing_method": "distance"
     },
     "groundwater": {
      "weight": 0.2,
      "units": "NA",
      "data_col": "None",
      "transformation_method": "negate",
      "processing_method": "distance"
     },
     "coproduced_fluid": {
      "weight": 0.3,
      "units": "BBL",
      "data_col": "SUM_WATER_",
      "transformation_method": "none",
      "processing_method": "interpolate"
     }
    },
    "pr0": 0.75
   }
  }
 },
 "economic": {
  "weight": 0.5,
  "components": {
   "demand": {
    "weight": 0.85,
    "layers": {
     "population": {
      "weight": 0.5,
      "units": "Count",
      "data_col": "P0010001",
      "transformation_method": "none",
      "processing_method": "none"
     },
     "infrastructure": {
      "weight": 0.5,
      "units": "None",
      "data_col": "None",
      "transformation_method": "none",
      "processing_method": "distance"
     }
    },
    "pr0": 0.75
   }
  }
```

```
  },
  "safety": {
   "weight": 0.05,
   "components": {
    "natural_disaster": {
     "weight": 1,
     "layers": {
      "flood_plains": {
       "weight": 1,
       "units": "None",
       "data_col": "None",
       "transformation_method": "negate",
       "processing_method": "buffer"
      }
     },
     "pr0": 0.5
    }
   }
  }
 },
 "exclusions": {
  "components": {
   "natual_habitat": {
    "set_to": 0.0,
    "layers": {
     "lepchi": {},
     "padus": {},
     "gpchi": {}
    }
   },
   "park_land": {
    "set_to": 0.0,
    "layers": {
     "NPS": {}
    }
   }
  }
 }
}
```


Figure A.1. Configuration file used to map criteria to components, components to data layers, and additional information to data layers. This configuration file is part of the required setup for geoPFA.

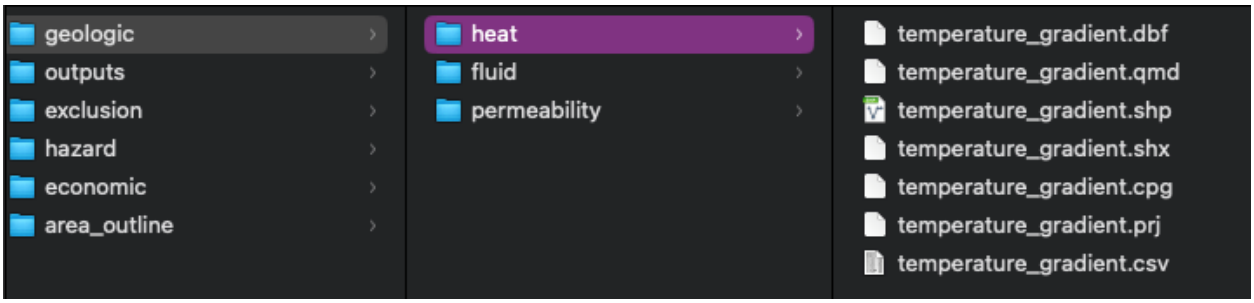

Figure A.2. Configuration file used to map criteria to components, components to data layers, and additional information to data layers. This configuration file is part of the required setup for geoPFA.

Read in Data

```
file_types = ['.shp']
pfa = GeospatialDataReaders.gather_data(DATA_DIR,pfa,file_types)
```

```
criteria: geologic
        component: heat
                reading layer: temperature_gradient
        component: permeability
                reading layer: structures
                reading layer: earthquakes
        component: fluid
                reading layer: hot_springs
                reading layer: groundwater
                reading layer: coproduced_fluid
criteria: economic
        component: demand
                reading layer: population
                reading layer: infrastructure
        component: site_accessibility
                reading layer: roads
criteria: hazard
        component: natural_disaster
                reading layer: flood_plains
```

Figure A.3. Configuration file used to map criteria to components, components to data layers, and additional information to data layers. This configuration file is part of the required setup for geoPFA.

Cleaning

```
pfa = Cleaners.set_crs(pfa, target_crs=3857)

data = pfa['criteria']['geologic']['components']['fluid']['layers']['coproduced_fluid']['data']['SUM_WATER_']
filtered_data = Cleaners.filter(data,quantile=0.9)
pfa['criteria']['geologic']['components']['fluid']['layers']['coproduced_fluid']['data']['SUM_WATER_'] = filtered_data

•••

data = pfa['criteria']['geologic']['components']['heat']['layers']['temperature_gradient']['data']['Gradient']
filtered_data = Cleaners.filter(data,quantile=0.9)
pfa['criteria']['geologic']['components']['heat']['layers']['temperature_gradient']['data']['Gradient'] = filtered_data

•••

gdf = pfa['criteria']['economic']['components']['demand']['layers']['population']['data']
clipped_gdf = Cleaners.set_extent(gdf,extent)
pfa['criteria']['economic']['components']['demand']['layers']['population']['data'] = clipped_gdf

gdf = pfa['criteria']['economic']['components']['demand']['layers']['population']['data']
col = pfa['criteria']['economic']['components']['demand']['layers']['population']['data_col']
filtered_gdf = Cleaners.filter_geodataframe(gdf,col,quantile=0.9)
pfa['criteria']['economic']['components']['demand']['layers']['population']['data'] = filtered_gdf
```

Figure A.4. Screenshot of code to clean data using geoPFA, including setting the coordinate reference system and filtering datasets

Transformation & Layer Combination

Combine layers from each component into component probability maps, and then resource probability maps, using the voter-veto method

```
pfa = VoterVeto.do_voter_veto(pfa,normalize_method='minmax',component_veto=False,criteria_veto=True)
```

```
Normalized a layer using minmax
Transformed a layer using negate
Normalized a layer using minmax
Normalized a layer using minmax
Transformed a layer using negate
Normalized a layer using minmax
Transformed a layer using negate
Normalized a layer using minmax
Normalized a layer using minmax
Normalized a layer using minmax
Normalized a layer using minmax
Transformed a layer using negate
Normalized a layer using minmax
Normalized a layer using minmax
```

Figure A.5. Screenshot showing code to transform and combine data layers in one line of code using geoPFA

Interpolation

```
nx = 100; ny = 100
method = 'linear'
pfa = Processing.interpolate_points(pfa, criteria='geologic', component='heat',
                                    layer='temperature_gradient',
                                    interp_method=method,nx=nx,ny=ny,extent=extent)

method = 'linear'
pfa = Processing.interpolate_points(pfa, criteria='geologic', component='fluid',
                                    layer='coproduced_fluid',
                                    interp_method=method,nx=nx,ny=ny,extent=extent)
```

```
Notice: interpolate_points() function recieved GeoDataFrame with geometry type 'Polygon.' Conv
erting geometry to 'Point' geometry using centroids.
```

Point Representation of Polygons

```
pfa = Processing.polygons_to_points(pfa,criteria='economic',component='demand',
                                    layer='population',extent=extent,nx=nx,ny=ny)
```

```
/Users/ntaverna/Documents/Low Temp PFA/geothermal_pfa/geoPFA/processing.py:407: FutureWarning:
Setting an item of incompatible dtype is deprecated and will raise an error in a future versio
n of pandas. Value '1423980.3668595725' has dtype incompatible with int64, please explicitly c
ast to a compatible dtype first.
  grid_gdf.at[grid_idx, 'count'] += intersection_area
```

Distance Function

```
pfa = Processing.distance_from_lines(pfa,criteria='geologic',component='permeability',
                                     layer='structures',extent=extent,nx=nx,ny=ny)
pfa = Processing.distance_from_points(pfa,criteria='geologic',component='fluid',
                                      layer='hot_springs',extent=extent,nx=nx,ny=ny)
pfa = Processing.distance_from_points(pfa,criteria='geologic',component='fluid',
                                      layer='groundwater',extent=extent,nx=nx,ny=ny)
```

```
pfa = Processing.distance_from_lines(pfa,criteria='economic',component='site_accessibility',
                                     layer='roads',extent=extent,nx=nx,ny=ny)
```

Figure A.6. Screenshot of code to process data using geoPFA, including interpolation, creating point representations of polygon data, distance, density, and buffer functionalities

```
pfa['pr_excl'] = Exclusions.mask_exclusion_areas(gdf_points=gdf_points,
                                                 gdf_exclusion_areas=shp,
                                                 value_col=col, set_to=set_to)
```

Figure A.7. geoPFA code used to mask exclusion areas in the overall combined favorability map

Appendix B. High versus Low Temperature Results

To compare results for a higher-temperature (i.e., power-producing) versus lower-temperature (i.e., direct use) resource, the PFA workflow was repeated twice: once for a lower temperature requirement, generated through using a higher prior probability of 0.85 (i.e., it is more likely to find sufficient temperatures throughout the Denver Basin), and once for a higher temperature requirement, generated through using a lower prior probability of 0.65 (i.e., it is less likely to find sufficient temperatures throughout the Denver Basin). Currently, the geoPFA library does not have specific temperature cutoffs for lower versus higher temperatures, but this could be explored in a future iteration.

Both sets of results were normalized on the same scale to allow visualizations of the different magnitudes. This normalization process masks some of the features in the data, and therefore we keep these results in an appendix rather than in the main text. If the probability mapping functionality is improved, the normalization process will no longer be necessary, and therefore we could better visualize the differences in the low versus high-temperature resource potential.

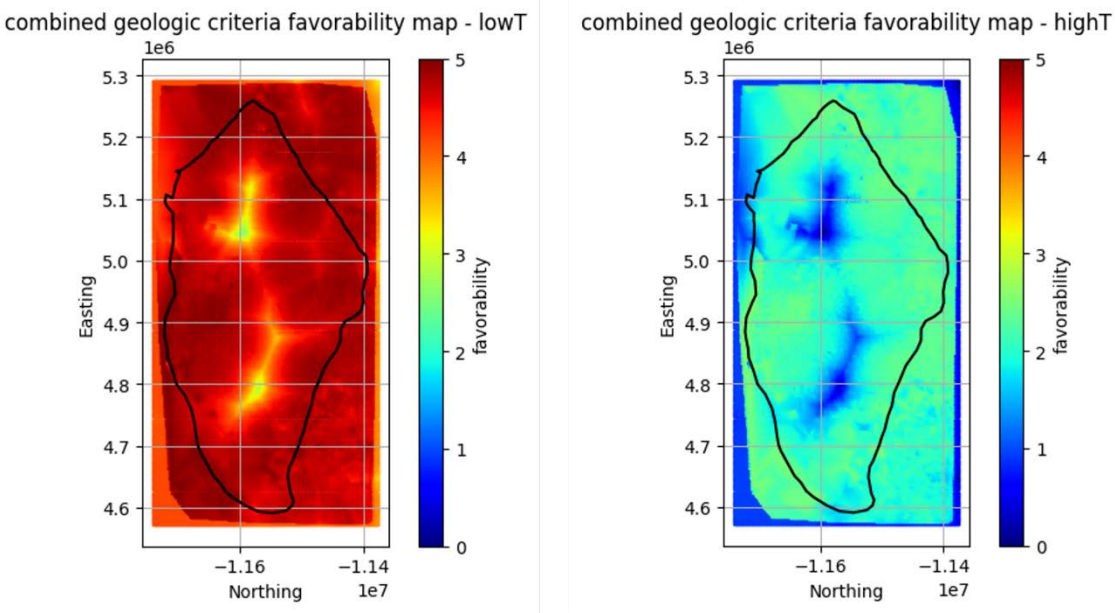

Figure B.1. Geologic criteria favorability maps for lower (left) versus higher (right) temperature requirements

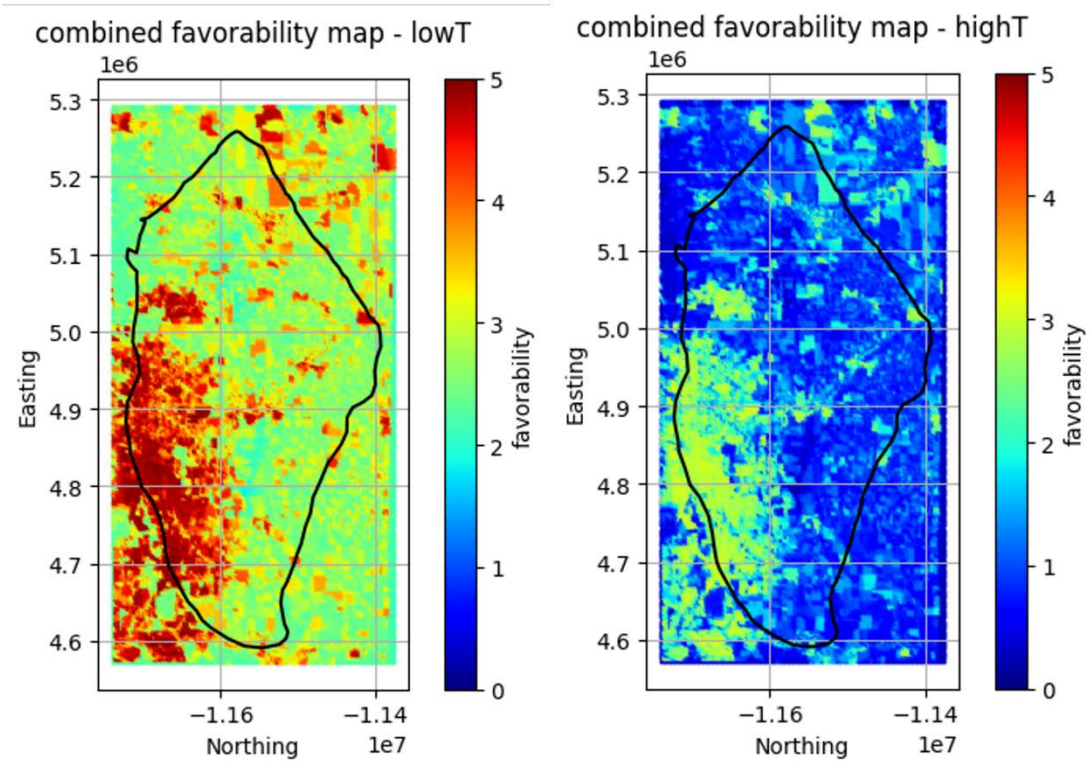

Figure B.2. Combined favorability maps for lower (left) versus higher (right) temperature requirements